1-1-2015

Effects Of Anthropogenic Particles On The Chemical And Geophysical Properties Of Urban Soils, Detroit, Michigan

Katharine Orlicki
Wayne State University,

EFFECTS OF ANTHROPOGENIC PARTICLES ON THE CHEMICAL AND GEOPHYSICAL PROPERTIES OF URBAN SOILS, DETROIT, MICHIGAN

by

KATHARINE M. ORLICKI

THESIS

Submitted to the Graduate School

of Wayne State University,

Detroit, Michigan

in partial fulfillment of the requirements

for the degree of

MASTER OF SCIENCE

2015

MAJOR: GEOLOGY

Approved By:

_____

Advisor Date

DEDICATION

To my family members,

Mike Orlicki, Sue Orlicki, Hannah Orlicki, and Nicki McWhirter

Who have been extremely supportive throughout this whole process and always encouraged me to do my best. Their enthusiasm about my education and research has greatly helped me reach my academic goals and helped keep me in a positive mindset.

ACKNOWLEDGEMENTS

First, I want to thank my advisor, Dr. Jeffrey Howard, for his support and guidance throughout my studies. I have learned from him what it means to work hard and what it means to be passionate about your work. His patience, kindness, and encouragement led me to different projects and achievements throughout my graduate studies that as an undergraduate I never saw myself accomplishing. His continuous excitement about my research made me more motivated about my work and I very much appreciated this, especially on days where I got discouraged.

I would like to thank my committee members, Dr. Sarah Brownlee and Dr. Krysta R, for their contributions to my research as well as all that they have taught me over the course of my studies. Their different backgrounds in research and academia helped me piece together my research into an exciting story.

I want thank my lab companions Mellisa Allen, Phil Backers, and Jenna Hage-Hassan for their encouragement and thoughtfulness. With them, the stressful moments didn't seem so strenuous and the breakthrough moments were even more thrilling.

I also want to thank all the undergraduate students who have helped me out in the field and in the lab: Kevin Seisal, Kalan Briggs, and Guilherme. Their assistance made what seemed like countless amounts of soil samples, be collected and measured in a precise amount of time.

Finally, I want to thank my family and boyfriend Adam Wayne for their endless encouragement and love. Their kindness and motivation will forever be appreciated. I could not have asked for a better support system.

TABLE OF CONTENTS

LIST OF TABLES

LIST OF FIGURES

CHAPTER 1

INTRODUCTION

1.1 Introduction

There has been an increasing need for urban mapping due to the expansion of city growth and population. Urban soil mapping and analysis has been increasing in interest over the years due to the high demand of redevelopment and health concerns. However, efforts to classify urban anthropogenic soils have just begun. Over one fourth of Detroit, Michigan's land is deemed as vacant land, making this city in dire need of new advances. Repurposing vacant land can be done through green infrastructure, urban farming, and building developments.

In order to repurpose Detroit's land, soil content and previous land use history need to be identified. Preliminary mapping of the urban geology of Detroit (Howard, 2013; unpub.) suggested that anthropogenic soils could be distinguished based on different types of artifacts. This study is focused on the microartifact (MA) fraction (artifacts .25 to 2 mm in size) within the soil samples that were collected. A number of different types of demolition debris, industrial waste, and fly ash were located on vacant land sites throughout the city. These different types of debris and waste have the potential to inform users about previous land use history. However, they also have the ability to negatively impact healthy soils and therefore, can also contribute to an unhealthy environment for the public. These MAs can be directly linked to different forms of anthropogenic sources such as factories and the process of deconstruction.

Detroit's zip code 48217 in southwestern Detroit has been listed as Michigan's most polluted area, according to the University of Michigan (Lam, 2010). This zip code is located between I-75 and some of Detroit's largest industrial plants. Unidentified wastes have been taking the form of dust that covers many homes and gardens (Lam, 2010). Families living in this

area have been experiencing serious health issues like asthma and cancer, which is thought to be a result from the dust particles (Lam, 2010). Therefore, knowledge of anthropogenic sources, land use history, and soil composition is vital for human interaction.

In this study, a collection of reference artifacts were gathered in order to determine the composition of selected MA types using optical microscopy, x-ray diffraction (XRD), scanning electron microscope (SEM), and energy dispersive x-ray spectroscopy (EDX) analysis. The reference materials were then used to develop a set of micromorphological criteria for the identification of MAs. Compositional data was collected to formulate an artifact classification system and to discuss the possible implications of microartifact assemblages and compositions for geophysical and chemical mapping.

Mapping an urban area can be very difficult when traditionally using a hand auger. Vacant lots in Detroit contain a lot of debris such as concrete, mortar, and brick, which in turn can cause hand auger refusal quite often. Due to the amount of debris and waste concentrated on selected sites, anthropogenic soils can vary frequently and it becomes unclear if the collected hand auger sample is an overall good representation of the entire vacant lot. Mapping Detroit with a hand auger is time consuming due to the size of the city and as a result can be very daunting and labor intensive. Mapping urban soils by using electrical conductivity (EC) and magnetic susceptibility (MS) can provide a faster, easier, and therefore less expensive way to map urban soils. Previous studies had shown that EC and MS surveying can provide a much more effective approach for mapping soils in agricultural, archaeological and other settings (Moffat et al., 2010; Doolittle et al., 2002, 2013; Nearing et al., 2013; Kapper et al., 2014). It was also well established that anthropogenic soils have elevated levels of MS (Strzyszcz et al., 2006) due in part to anthropogenic microparticles (Lu et al., 2011). Anthropogenic microparticles have

a significant impact on geophysical signals due to their greater surface area. Therefore, in this study microscopic, geophysical, and chemical work was performed in the lab in order to identify the anthropogenic composition of the soil. EC, MS, and pH were measured for each individual microartifact that was identified and also for each soil sample that was collected out in the field. Soil sample sites were studied to determine if they were able to show unique geophysical and chemical properties resulting from their specific MA make-up. These unique signatures may make it possible to map urban soils using EC, MS, and pH.

1.2 Hypotheses Tested

The main goal for this study was to create a more efficient way to map urban soils by using geophysical and chemical properties with the main focus on electrical conductivity and magnetic susceptibility. Three hypotheses were tested in this study:

1. *Artifacts in anthropogenic soils vary as a function of land use history.* Each site has a variable site history. Detroit was founded in 1701 and since then has undergone a number of demolished and rebuilding cycles (Burton, 1922). As a result, the artifacts that are left behind and the anthropogenic soils that have been established can potentially provide an insight on how the land was once used and by whom it was occupied by.
2. *Artifacts have unique geophysical and chemical signatures.* The composition of artifacts can vary greatly from one another resulting in different values when determining geophysical and chemical properties.
3. *Geophysical and chemical methods can facilitate mapping of urban soils in an urban settings.*

   In an urban setting soil samples can vary greatly due to site history, anthropogenic sources, and concentration of artifacts located within the soil. These three things can significantly affect soil composition. Thus, geophysical and chemical properties can be used to identify the soil makeup.

A collection of reference artifacts commonly found throughout Detroit were gathered and analyzed in order to determine their significance towards previous land use history and geophysical and chemical properties. Native and anthropogenic soil samples were collected inside and outside the city boundary lines. Magnetic susceptibility and electrical conductivity

were measured for each soil sample that was collected. Specific artifacts were added to native soil samples and then measured for magnetic susceptibility and electrical conductivity in order to determine their geophysical and chemical signatures on the soils in which they are contained in. Soil transects and profiles were made and analyzed in order to determine on-site soil variability. Magnetic susceptibility and electrical conductivity results were then uploaded into Surfer in order to create contour maps which showed anomalies and similarities throughout the city.

1.3 Terminology

For clarification, the term "artifact" is used for any object that is greater than 2 mm in size that was once produced, modified, or transported from its source by human activity (Dunnell and Stein, 1989; IUSS Working Group, 2006; Soil Survey Staff, 2014ab). "Anthropogenic particles" are artifacts of any size. "Microartifacts" are artifacts that are 0.25 to 2 mm in size (Dunnell and Stein, 1989). "Microparticles" are artifacts < 0.25 mm in size. "Charcoal" refers to the charred remains of wood produced by oxygen combustion. Anthropogenic particles produced by iron smelting are called "metalliferous slag" and "glass slag", whereas those produced by coal combustion are called "cinder" and "ash." The term "concrete" refers to a lime-based material unless otherwise indicated. "Microspheres" are any type of spherical microparticle. "^"Au horizon refers to A horizons with artifacts present.

CHAPTER 2

PREVIOUS STUDIES

2.1 Urban Mapping

Anthropogenic soils on newer soil survey maps are commonly marked as native soil composition or are poorly defined. Further research needs to be done in order to properly identify the makeup and causes of present anthropogenic soils. The pressing need for urban soil mapping is a result from demolition taking place and producing vacant land along large transects throughout urban areas, especially in Detroit. Many of these demolition sites have soils that are in need of revitalization because of extreme compaction, low organic matter content, and large amounts of waste and debris concentrations with in the soil (Howard and Shuster, 2014).

Urban areas have been mapped by the USGS since 1902 (e.g., New York City and Detroit folios). However, older maps created by the USGS do not include urban expansion and are no longer suitable for specific site applications. Urban geologic mapping has been recognized for many years (McGill, 1964; Legget, 1973, 1974) but artificial fill and anthropogenic soils have rarely been defined on earlier USGS maps (e.g., Fleming et al., 1994). Classifications of anthropogenic soils have only recently been endeavored by the British Geological Survey (Rosenbaum et al., 2003) and the NRCS (Soil Survey Staff, 2014). Since methods for urban geologic mapping are not yet recognized, this study will open new doors when it comes to identification of anthropogenic soils and their sources.

In 2014 a hand auger mapping project took place on a vacant lot located in a residential area on the corner of Wisner and Gilbo St. in Detroit, MI. The house that was once on this lot was built around 1989 and was demolished between 1994 and 1998, which could only be determined by aerial photography (Howard and Shuster, 2015). In order to map this vacant lot an

18 m by 16 m grid was made and soil samples were collected every 2 m. The purpose of this project was to test the hypothesis that anthropogenic soils could possible show a special distribution patter when mapped (Howard and Shuster, 2015). Due to demolition that took place, it was apparent that different types of architectural material were concentrated and discarded greatly throughout the soil. As a result, specific concentrations of concrete, glass, brick, and wood were able to be mapped, along with the previous foundation of the house (Fig. 1). These findings made it possible to conclude that it is possible to map architectural artifacts and anthropogenic soils from residential demolition sites (Howard and Shuster, 2015). These artifacts and anthropogenic soils can then reconstruct the history of a site based on their classification and spatial distribution.

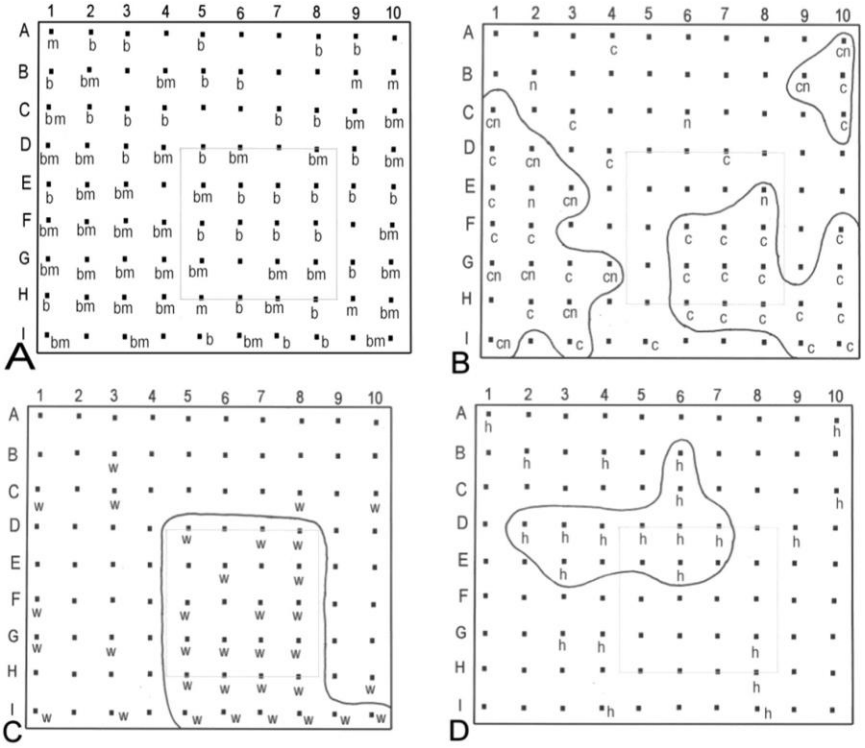

Figure 1: Maps showing distribution of artifacts encountered in borings of the sampling grid at Wisner St.: A, b, brick; m, mortar; B: c, coal; n, coal cinders; C: w,wood; D: h, charcoal (Howard and Shuster, 2015)

2.2 Electrical Conductivity

2.2.1 Background

Electrical conductivity is the ability of a material to conduct an electrical current, which is expressed as mS m^{-1} or μS cm^{-1}. Soil EC was originally used to measure soil salinity, and determined *ex situ* (XEC) properties by using the saturation paste or saturation paste-extract methods (Corwin and Lesch, 2005). Only a few site specific studies are known in which XEC was used to map urban soils (Al-Khashman and Shawabkeh, 2009; Santini et al., 2013).

In contrast to the XEC approach, electromagnetic induction has been widely used to measure soil EC *in situ* (IEC). This technique is also known as apparent electrical conductivity. This method drops a voltage that is measured across one or more pairs of electrodes that may or may not be connected with the soil surface. The probes are connected to a two wheel cart which is then towed behind a truck or tractor, which is seen in most agriculture settings. A GPS-registered system can then produce a map in a quick amount of time based on physical properties that affect the overall connectivity of the soil (texture, porosity, bulk density, structure, aggregation, etc.) (Carroll and Oliver, 2005; Friedman, 2005; Doolittle and Brevik, 2014). More studies have taken place in the laboratory after disturbing the soil than trying to take in-situ measurements in the field. In-situ EC results can be fairly difficult to determine due to methods not being fully developed. For example, equipment is usually not targeted towards shallow soil sampling and measurements need a specific calibration in every study in order to be consistent (Pozdnyakov, 2007).

2.2.2 Agriculture Use

EC has been used greatly in agricultural sciences due to its ability to provide an efficient and inexpensive way to analyze soil characteristics. Farmers are able to use EC sensors in order to make a spatially dense dataset that represents the soil variability over a large area of land (Barbosa, 2009). EC results potentially can correlate with crop yield as long as climatic conditions remain constant (Lund, 1999). Sands, silts, and clays can be identified using EC due to their particle size, soil texture, and therefore their water holding capacity (Barbosa, 2009). Typically EC of different soil types is as follows, clay > silt > sand (Fig. 2).

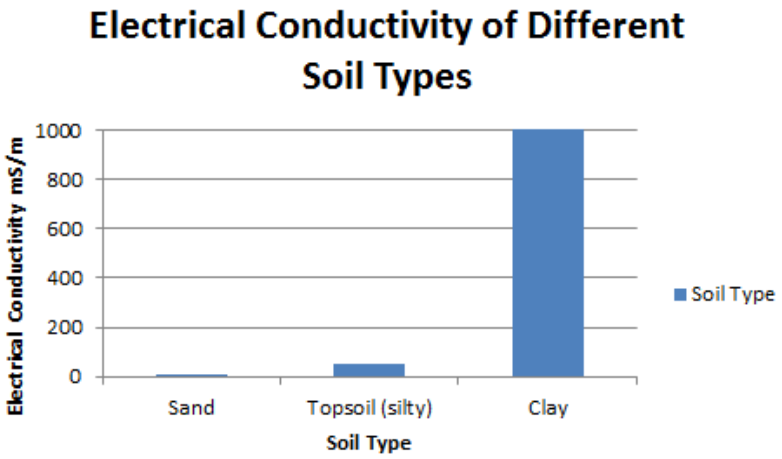

Figure 2: Electrical conductivity for different soil types in µS m^{-1} (Barbosa, 2009)

A soil's capability to hold water directly impacts the amount of crop yield in a field area. There is an enormous potential to use soil EC measurements to outline areas with different yield potentials, organic matter content, and cation exchange capacity (Barbosa, 2009). The most difficult part about using EC is being able to determine what is causing the variations seen in the soil over a given area.

2.3 Magnetic Susceptibility

2.3.1 Background

Magnetic susceptibility (MS) is a measurement of the quantity of magnetism induced in a material (Mi) by an applied magnetic field (H). All matters have magnetic properties and when a magnetic field is induced to a soil or rock the degree of magnetism can be measured as magnetic susceptibility (Pringle, 2015). If Mi is parallel and proportional to H, then: $Mi = \kappa$. The constant κ is given for a material that has the potential to be magnetized. MS is a dimensionless SI unit due to Mi and H sharing the same units of amperes per meter (A m^{-1}). Mass magnetic susceptibility (χ) is defined as: $\chi = \kappa/\rho$, where ρ is density measured in kg m^{-3}, and χ is 10^{-8} m^3 kg^{-1}. Soil MS results are positive for ferromagnetic and paramagnetic materials, and negative for diamagnetic materials (Mullins, 1977).

Soil MS can be measured readily *in situ* (κ) using a device that looks similar to a metal detector (Fig. 3, left). MS can also be measured *ex situ* (κ) using a laboratory sensor (kappameter). The (κ) data is then converted to final MS units (χ) from the mathematical equation $\chi = \kappa/\rho$. The data can be presented as a pixelated map (Fig. 3, right) on which the darkest areas indicate magnetic hot spots.

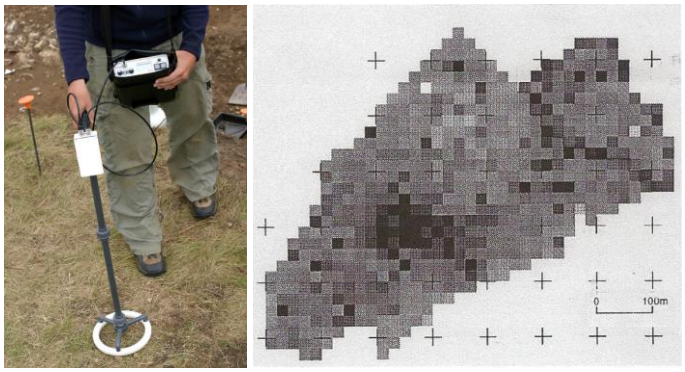

Figure 3: Previous experience mapping anthropogenic soils: left, MS2D surface probe for mapping magnetic susceptibility; right, Pixelated map of magnetic susceptibility

It is well established that anthropogenic soils have elevated MS than native soils (Strzyszcz et al., 2006; Gladysheva et al., 2007). In order to come to this conclusion it is necessary to determine a background level. MS of topsoil is naturally greater in relation to the subsoil. Magnetite or maghemite bearing artifacts greatly contribute to elevated MS of anthropogenic soil. Microparticles, such as ferruginous microspheres, are also known to contribute to the elevated MS signatures of anthropogenic soils (Lu et al., 2011; Yang et al., 2012; El-Baghdadi et al., 2012).

2.3.2 Identifying Pollutants and Heavy Metals

Magnetic susceptibility has been used in many studies to map pollutants in cities that have under gone a rapid population growth. This rapid growth in population then creates an increase of environmental pollutants dispersed through out the city (Huiming Li et. al., 2014). In depth geophysical and chemical analyses can be expensive and time consuming when identifying pollutant within the soil. MS provides a fast and effective alternative method to identify potentially polluted soils. High sensitivity and the speed of magnetic techniques are the major advantages of using MS (Huiming Li et. al, 2014). Pollution of soils can dramatically reduce the environmental quality of any area, especially in an urban setting where there is more risk for exposure. The most common pollutants are heavy metals for which fossil fuels are the main contributor for (Aydin, 2015). MS was used in order to identify the spatial distribution of pollutants throughout different urban areas. Industrial areas showed high values for MS, which came from magnetic particles on study sites (Aydin, 2015). Using MS as a mapping method has commonly been used for identifying contamination, determining the total amount of pollutants, and to trace the pollutants back to its source (Bityukova, 1998).

2.3.3 Archaeology

Sensitive magnetometers have been used for years in order to locate archaeological sites. Sensitive magnetometers were first used to identify pottery kilns and ancient burn pits in the 1950s (Clark, 2005). Previous studies have used MS to successfully identify areas of historic significance, specifically aimed at burned impacted areas. Weakly magnetic charged iron oxide minerals in the soil (hematite and goethite) can transform to highly magnetic minerals (magnetite and maghemite) when a heat that is > 600°C is applied in a reducing atmosphere (Marshell, 1998, Matthews, 1976; Kontny and Dietl, 2002). This overall increases the MS of the soil.

Human interaction with trash pits and fires can further increase the effects of MS located in a specific area and leave an imprint on the soil (Clark, 2005). When using MS to detected buried objects beneath the soil, methods rely on there being a detectable physical contrast between the targeted objected and the host materials (Pringle, 2015). MS should be able to detect previously filled in pits that were once used as privies, trash pits, or other dump sites. The fill substance normally has a higher MS than the subsoil that it was once dug in (Mullins, 1971). However, there can be enhancement between subsoils and anthropogenic fill and therefore can vary widely. Complications can than arise when trying to detect disturbed soils due to this large variation in enhancement. In contrast, if the difference in MS between subsoils and anthropogenic fills are too small then MS may not be able to be detected at all (Mullins, 1971).

2.4 Roosevelt Park Studies

Previous studies and excavation sites have taken place in Roosevelt Park by Wayne State University's Anthropology department. Their studies were focused on identifying the history and cultural significance that once took place in Roosevelt Park. By the late 1830s Corktown began

to transition from an agricultural parcel to an urban settlement (Fig. 4) (Ryzewski, 2012). In the 1908 the first phase of displacement took place in order to plan for the Michigan Central Railroad (MCR) (Ryzewski, 2012). Families were asked to move out of their homes and relocate but many put up a fight. All homes were eventually demolished leaving behind a number of different and extraordinary artifacts. Due to the amount of artifacts and anthropogenic soils left behind, Roosevelt Park became a key spot for analyzing soil profiles and transects in an urban setting.

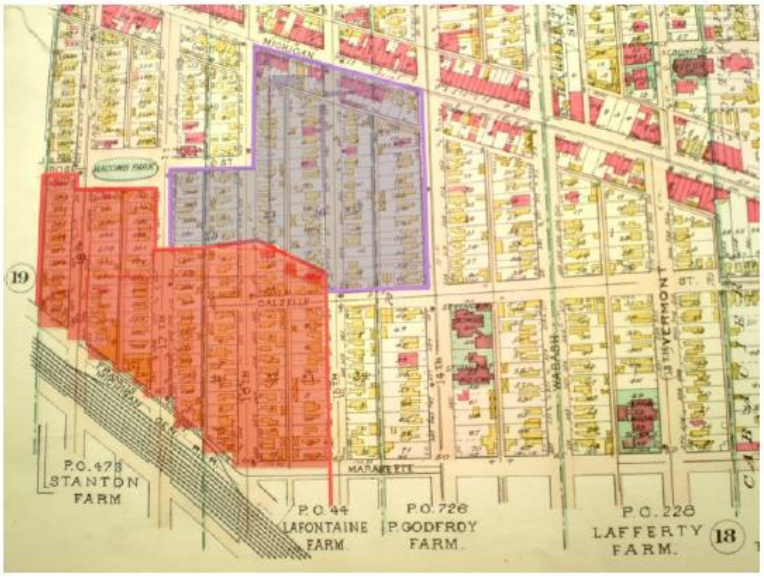

Figure 4: Neighborhood in 1906 before construction of MSC and Roosevelt Park (Baist's Real Estate Atlas). The red box outlines building structures that were demolished in 1911 during the first wave of displacement. The purple outlines building structures that were demolished during the second wave of displacement (Ryzewski, 2012).

Soil samples that were collected from Roosevelt Park looked abnormally dark and it was unclear if this was a result from organic matter or an anthropogenic source. After further microscope work, silicious and ferriginous microspheres were identified and it was then hypothesized that these could potentially be fly ash microparticles. In winter 2015 the DEQ was

able to provide us with two fly ash samples from two different sources, the location of these samples were not able to be disclosed. With further microscope comparison and SEM work, it was concluded that the microsphere particles causing these soil samples to look extremely dark in color were indeed due to the presence of fly ash. This knowledge made it possible to identify fly ash-impacted sites in Detroit, MI.

Other than soil content, the weathering of artifacts was greatly observed as well. It was suggested that due to environmental changes as a result from an increase in anthropogenic activities in urban settings, there has been a significant impact on the preservation of archaeological remains (Howard et al., 2015). The weathering of artifacts can result in an enrichment of elemental compounds in the soil. This has been specifically observed with iron and cement artifacts, resulting in a measureable enrichment of Fe-oxide and carbonate within the soil (Howard and Olszewska, 2011). The presence of any excess soluble salts (road salt, plaster, sulfurous air pollutant) has the potential to accelerate any artifact weathering (Howard, 2010). However, it was concluded that many artifacts located in Roosevelt Park were extraordinarily well preserved. The preservation of artifacts was due to a calcareous soil microenvironment and artificial compaction which limits the weathering effects of water and oxygen (Howard et al., 2015). Artifacts were also well preserved due to an enhanced burial of 23 cm thick created by casting activity of invasive species of earthworm (Howard et al., 2015).

CHAPTER 3

STUDY AREA AND GEOLOGIC SETTING

3.1 Study Area

The study area for this project was located in southeast Michigan, mainly taking place in the city of Detroit. Detroit is located adjacent to Windsor, Ontario, Canada with the Detroit River separating the two (Fig. 5). The oldest part of the city is located Downtown, Corktown, and Midtown where main streets radiate from a central point that essentially mark the place where Antoine de la Mothe Cadillac founded Detroit in 1701 (Burton, 1922). Detroit previously was covered by farmland, but in 1880-1890s downtown Detroit went under an industrial boom (Hyde, 1980). Industries were thriving and brick and mortar buildings were constructed over a wide area. In the 1920-1930s Detroit underwent another rapid development which was fueled by the explosive growth of the automobile industry (Hyde, 1980). Due to constant construction and development over a number of years, the types of MA and anthropogenic soils found in any given location tend to be highly variable.

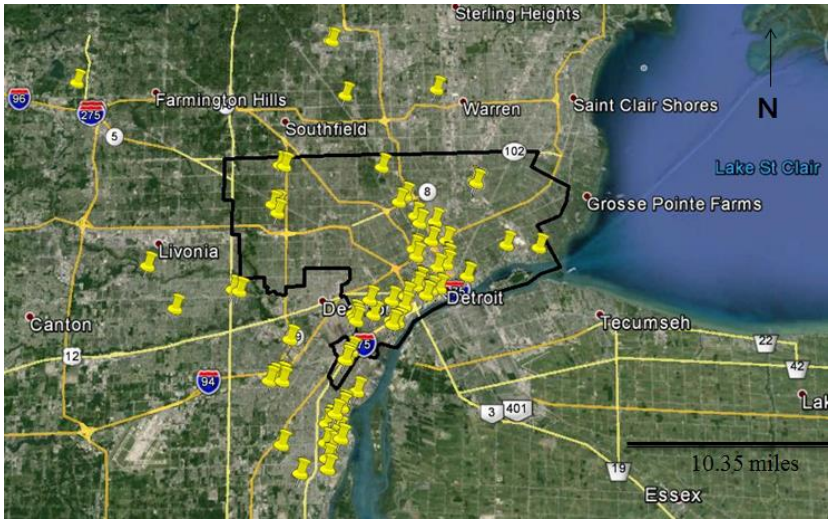

Figure 5: Study site and sample locations in Detroit, MI

Background soil samples were collected from different sites outside of Detroit's boarder. This reassures that the background soil samples were native and not previously disturbed. Anthropogenic soil samples and reference artifacts were collected mostly in mid-Detroit, south Detroit, and a couple miles outside of Detroit's boarder lines (Fig. 5). Overall, the study area is heavily concentrated where much of the older land was occupied by industrial companies, which were mainly located adjacent to the Detroit River. Sample sites were determined by accessibility, location, and if the site was a good representation of the varying types of debris and waste that can be found throughout the city.

Detroit has undergone many years of expansion, demolition, and industrial manufacturing. Different types waste and debris can be identified throughout the city based on location and the type of previous involvement taking place on the land overtime. The different types of debris and waste include, but are not limited to, demolition, steel-making, asphaltic, coal-release, and industrial waste (Fig. 6). Based on land use history and the different types of MAs found at each site, three different urban anthropogenic soil sites (industrial, residential demolition, and fly ash-impacted) were examined in this study.

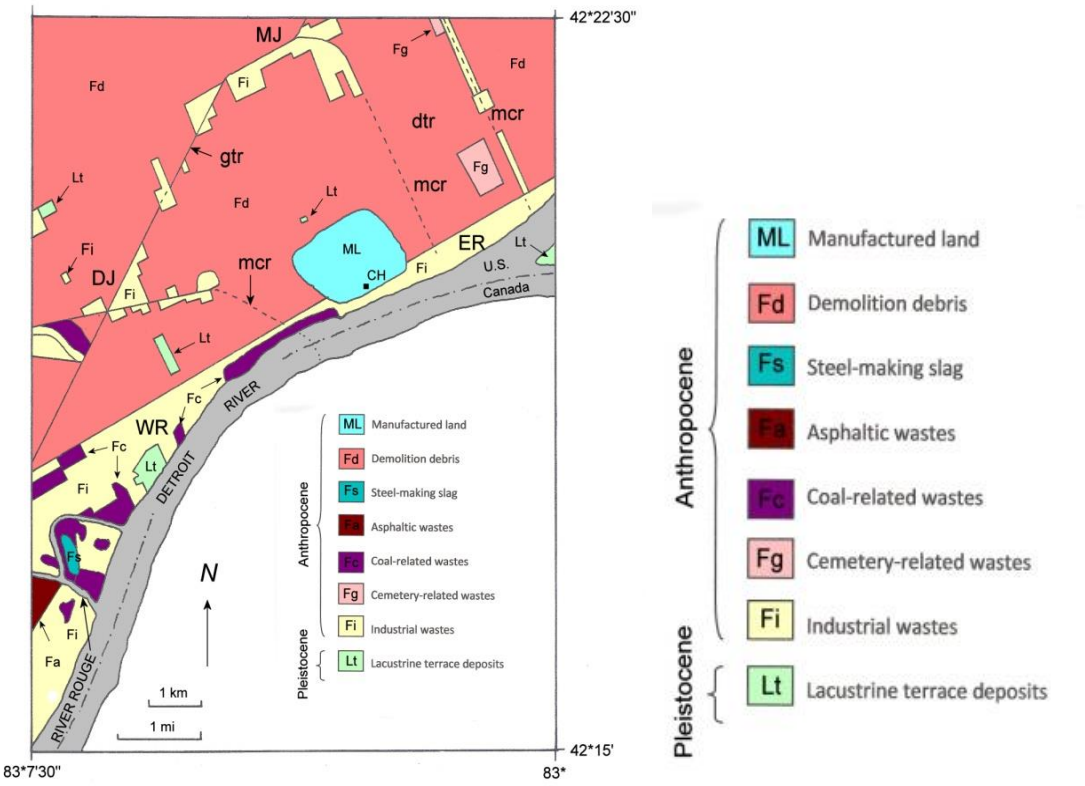

Figure 6: Different types of debris and waste that can be found in urban soils Detroit, MI

3.2 Geologic Setting

Detroit is underlain by Paleozoic sedimentary bedrock capped with a sequence of late Pleistocene glacial sediments 10 to 30 m thick (Mozola, 1969). Detroit is located on the southeastern flank of the Detroit moraine at an elevation of 193 to 203 m. The city lies on the lakebeds plains of paleolakes Grassmere, Elkton, and Rouge (Sherzer, 1916; Bay, 1938). The city is often underlain by a capping of sand 2 to 3 m thick. It rests on weak stratified clay like diamicton 3 to 4 m think, and contains dispersed pebbles and cobbles up to 10 cm in size (Howard, 2010).

Detroit's native soils are slightly poorly drained Metamora Series (Udollic Ochraqualf) and Blount Series (Aeric Ochraqualf) and are established in sandy (Metamora Series) or clay like diamicton (Blount Series) lacustrine sediments with a 70 to 75 cm thick solum (Larson, 1977).

The Metamora soil (Udollic Ochraqualf) has a medium to heavy sandy loam near the surface and is over a gley and mottled subsoil. Depending on thickness of the lacustrine sand capping, the Metamora soil contains a noticeable discontinuity in lithology at variable depths (Larson, 1977). The Blount soil (Aeric Ochraqualf) is loamy near the surface and is located over a gley and mottled silty clay to clay subsoil (Larson, 1977). The climate here is humid-temperate, with a mean annual temperature of 9°C (49°F). The annual precipitation is 99 cm yr^{-1} and acquires a frost line at 107 cm depth.

Anthropogenic soils in Detroit have formed from mixtures of native soils and glacial parent materials, these soils typically being lacustrine sand, clayey, or diamicton (Howard, 2010). Previous demolition sites in Detroit have greatly disturbed parent material and are often comprised of fill material imported from offsite. Previous work indicates that soils located on demolition site have developed an anthropogenic soil horizon containing a number of artifacts usually within 25 years (Howard and Olszewska, 2011; Howard et al., 2013). The anthropogenic soil horizons contain calcareous and ferruginous artifacts that show some evidence of chemical weathering (Howard and Olszewska, 2011; Howard et al., 2013).

Eight types of anthropogenic surface deposits were previously mapped or hypothesized to be present in the Detroit quadrangle (Howard et al., 2013c). These surface deposits were often distinguishable, had a unique artifact assemblage, and could be outlined according to land use history. It was also observed that the inner and outer city urban provinces could be identified from a boundary of anthropogenic surface deposits corresponding to the Detroit city limits around 1919 (Howard et al., 2013c). Older industrial land can be located along the riverfront and major railroad lines. Residential land in the inner city can be characterized by sites where buildings from the 19th century were demolished and have undergone many demolition cycles,

therefore depositing a number of artefactual materials. Outer city residential land is characterized by sites with vacant lots or an abandoned derelict home (undemolished residential sites) building.

CHAPTER 4

MATERIALS AND METHODS

4.1 Studied Sites

Soil samples were first collected near Wayne State University's campus and then gradually sampled outwards into other districts of Detroit. Soil samples were collected from a number of different parklands, residential demolition sites, industrial sites, and fly ash-impacted sites. Soil samples collected in industrial and fly-ash impacted sites were located near or on heavy industrial sites such as the River Rouge Plant and the Packard Plant. Industrial samples were mainly a result of combustion and smelting processes. Soil samples collected from residential demolition sites were located in residential neighborhood parcels that had undergone or expected to undergo demolition. Specific MAs were observed in each studied site in order to further identify their site classifications. Fly ash-impacted sites were later determined after optical microscopy analysis. Previous work in Detroit suggests that demolition soil sites can develop artifact concentrated A horizon under a grass cover within 25 to 30 years. It was also identified that leaching of carbonate from calcareous artifacts into demolition soil sites can be shown in the C horizons (Howard and Olszewska, 2011; Howard et al., 2013). According to Soil Taxonomy, the anthropogenic soils studied from each site are most likely classified as Anthropic or Anthroportic Udorthents (Soil Survey Staff, 2014).

4.2 Field Method

All soil samples were collected with a plastic trowel from surface horizons (0-15 cm depth) of different land use types. Samples were collected in clean polypropylene bags and stored at 4°C until analysis. Soils were described and classified using standard USDA-NRCS

methods (Soil Survey Staff, 2010, 2014a). Soils were air-dried and dried sieved in order to collect the < 2 mm fraction.

All anthropogenic soil samples were collected in the inner city of Detroit and Downriver, MI. Residential and fly ash samples were obtained from vacant lots at former demolition sites and from the front yards of abandoned derelict homes. Industrial soil samples were collected from abandoned industrial lots. Anthropogenic profiles were collected from Roosevelt Park in Corktown, Detroit. Depths of profiles were established once native soil was exposed. Anthropogenic transects were sampled from a residential demolition sites located on the east side of Detroit on Wisner and Kenney St. Transect samples were composed of seven to fourteen topsoil samples and spaced 5 m apart.

Background levels were established by sampling both sandy and clayey native soils in order to assess the effect of texture on geophysical properties. Native soils were collected 20 to 30 km from inner city Detroit, mostly from parklands, farmlands, and backyards. Native soil profiles and linear transects were sampled in Dr. Jeffrey Howard's backyard in Warren, MI. Four or more samples were taken for each native transect and were spaced 2 m apart. Native soil profiles were sampled to a 50 cm to 90 cm depth.

4.3 Laboratory Method

4.3.1 Microartifacts

A list of reference artifacts of known origin were first identified and collected before fieldwork began (Table 1). Many samples were collected from demolition sites, rundown buildings awaiting demolition, and other miscellaneous sources. Their compositions and optical characteristics were identified and described (Table 1, 3, and 4) based on data compiled from the

literature and optical observations. Selected reference artifacts were then crushed to be 0.25 – 2 mm in size (medium to very coarse sand) by using a jaw crusher. Each crushed artifact was then wet sieved to obtain the 90 to 150 μ (very fine to fine sand) fraction. Crushed MAs were checked with a hand magnet in order to recognize that an insignificant amount of metal fragments were artificially produced by crushing.

Table 1: Composition and sources of artifacts commonly found in urban soils, Detroit, MI

Type of Artifact		Description	Source	Composition	Reference
Coal-Related Wastes	Coal	An organic sedimentary rock comprised of carbonized plant fossils and trace amounts of mineral matter	Domestic, commercial fuel source	Organic macerals of various types depending on rank, and minor quartz, illite, kaolinite, feldspar, calcite, dolomite, pyrite, falena	ICCP (1998); Ward (2002)
	Coal cinders	The gravel-sized solid waste material left after coal is burned at 1200° to 1500°C	Incidentally related to coal use	Aluminosilicate glass, mullite, quartz, magnetite, hematite	Ward and French (2005)
	Coal ash	The sand-sized and finer inorganic solid waste material left after coal is burned (fly ash)	Incidentally related to coal use	Aluminosilicate glass, mullite, quartz, magnetite, hematite, calcite, gypsum	Fisher et al, (1976); Ward and French (2005); Lanteigne et a. (2012)
Waste Building Materials	Wood (peat)	The hard fibrous xylem of trees and shrubs	Used in wood-frame construction	A natural composite of cellulose and hemi-cellulose fibers embedded in a matrix of lignin	Singh et al. (2010)
	Charcoal	A residue of mainly black carbon produced by the incomplete combustion of wood	Incidentally related to use of wood as a building material	Aromatic hydrocarbons, black carbon, some remnant lignin	Brodowski et al. (2005); Forbes et al. (2006)
	Asphaltic concrete	Bituminous cement with rock aggregate	Used primarily as road pavement	Bituminous hydrocarbons	Yang et al. (2010)
	Lime concrete	A mixture of lime cement and gravel-sized aggregate	Used for road pavement, sidewalks and building construction	Various mixtures of calcite, portlandite, belite, alite, tobermorite, ettringite, ect. With variable rock and mineral fragment types	Kosmatka et al, (2002); Lane (2004)

	Mortar	A mixture of lime cement and sand-sized aggregate	Used in masonry	Various mixtures of calcite, portlandite, belite, alite, tobermorite, ettringite, etc. with variable rock and mineral fragment types	Kosmatka et al. (2002); Van Oss (2005)
	Cinder block	A lime concrete block containing gravel-sized aggregate	Used to construct walls and foundations	Similar composition to concrete, but containing blast furnace lag and possibly fly ash, etc.	Dubay (2012)
	Soda-lime window glass	A transparent, amorphous mineral-like material formed from silica	Used to make window pane, bottles, ect.	Amorphous silica, usually containing Na, ca, and coloring agents such as Fe, Cu, or Co	Rapp (2009)
	Ceramic brick	Solid, coherent rock-like blocks produced by firing clay at 900 to 1100 degrees C	Used in masonry	Aluminosilicate glass, mullite, wollastonite, cristobalite, sanidine, hematite, quatz	Livingston et al. (1998)
	Ceramic pipe, tile	Solid, coherent rock-like items	Used for water and sewer	Aluminosilicate glass, mullite, wollastonite, cristobalite, sanidine, hematite,	Rapp (2009)
	Corroded iron (nails)	A composite material produced by heating iron ore, limestone and coal to about 1500 degree C	Used in wood-frame construction	Ferrite, ferrihydrite and goethite	Asami and Kikuchi, 2002; Neff et al. (2005); Howard et al. (2013a)
	Drywall	Large sheets of boards comprised of prehardened plaster of Paris (gypsum)	Used for building interior walls and ceilings	gypsum possibly containing plastic fibers	Schaefer, 2010
Industrial Wastes	Coked coal	A hard, dark gray or black carbonaceous fuel produced by heating coal to 300°C	Used as a fuel for smelting iron and in coal-fired power plants	Inertinite macerals and black carbon	Gray (1991)
	Metallifer-ous slag	An inorganic waste produced by smelting iron ore, coked coal and limestone at 1500 to 2000 degree C	Iron- and steel-making	Glass, merwinite, melilite, wollastonite, belite, olivine, wustite, magnetite, hematite, calcite, portlandite	(Yildirim and Prezzi (2011); Piatak and Seal (2012)
	Glass slag	An inorganic, non-crystalline waste produced by smelting iron ore, coked coal and limestone at	Iron- and steel-making	Glass, hematite, magnetite	Fredericci et al. (2000)

		1500 to 2000 degrees C			
Archaeo-logical Materials	Pottery	Household items produced by firing clay at 900 to 1100 degrees C	Domestic use	Aluminosilicate glass, phyllosilicates, mullite, wollastonite, cristobalite, sanidine, hematite	Rapp (2009)
	Bone	An inorganice material comprised primarily of apatite	Primarily the remains of 19th century farm animals	Collagen fibers and hydroxyapatite	Berna et al. (2004)
	Bottle glass	A transparent, non-crystalline mineral-like material	Domeestic and commerical use	Amorphous silica, usually containing Na, ca, and coloring agents such as Fe, Cu, or Co	Rapp (2009)

Specific gravity (SG) of MAs were measured using the standard Jolly balance method (Klein and Dutrow, 2007), and MineraLabs specific gravity kit. Particles 2 to 6 mm in size (n = 5) were measured in air and submerged in water. The equation for specific gravity is shown below:

Specific gravity = weight in air/(weight in air – weight in water)

Abrasion pH and EC (Stevens and Carron, 1948) of artifacts were measured using 5 g of three replicate samples of the < 0.25 mm fraction of crushed artifacts. 10 ml of distilled-deionized water was then added to the 5 g of crushed artifacts. The suspension was stirred for 30 seconds then left to stand for 1 hour. The pH of the supernatant was measured using a Mettler Toledo FEP 20 pH meter. Samples were then stirred again and left to stand overnight to be measured again the following day. The electrical conductivity of the supernatant was then measured using a Mettler Toledo S230 conductivity meter. Electrical resistivity was calculated as the inverse of electrical conductivity. Magnetic susceptibility was measured using two replicate 10 cm^3 samples of the < 0.25 mm fraction of crushed artifacts and a Bartington MS2B dual frequency sensor, using the methodology recommended by the manufacturer.

4.3.2 Soil Samples

The pH of soil samples were measured using three replicates of 25 g samples to which 50 ml of distilled-deionized water was added. The suspension was stirred for 30 seconds and left to stand for 24 hours. The EC of the supernatant was measured with the same sample after the pH was measured, using a Mettler Toledo S230 conductivity meter. Electrical resistivity was calculated as the inverse of electrical conductivity. Magnetic susceptibility was measured using two replicates of 10 cm^3 samples of the less than 2 mm fraction of soils a Bartington MS2B dual frequency sensor, using the methodology recommended by the manufacturer.

The effects of MAs on pH, EC, and MS were studied further using an artificial soil made by adding a known amount (0, 1, 3, 5 and 10 wgt %) of the less than 0.25 mm fraction of a single type of crushed artifact. An artificial soil was made with both sandy and clayey diamicton matrices. Preliminary tests for normality showed that electrical conductivity data was normally distributed, whereas magnetic susceptibility data followed a lognormal distribution. Thus, EC data are reported as arithmetic means and MS data as geometric means. Student's *t*-test was used to test the statistical significance of variations in soil EC as a function of land use type using standard methods (Davis, 1986). Hence, given a mean (X) and standard deviation (S) for *n* measurements, the hypothesis tested was that $X_1 = X_2$, where:

$t = X_1\text{-}X_2/Se$,

$Se = Sp\sqrt{(1/n_1 + 1/n_2)}$, and

$Sp^2 = [(n_1\text{-}1)S_1^2 + (n_2\text{-}1)S_2^2]/n_1 + n_2 - 2$

Magnetic susceptibility data were tested using the same method after lognormal transformation.

4.4 XRD, SEM, and Microscope Analysis

Microscope analysis was done in order to correctly identify the microartifacts in each soil sample. The microscopic characteristics of microartifacts were identified using a binocular microscope, XRD, and EDAX. Reference artifacts were collected and used to classify properties of unknown microartifacts found in urban soils from demolition, industrial, and fly ash-impacted sites. A picture of each reference microartifact was taken and described (Table 4).

Microartifacts in urban soils were obtained after removing soil organic matter by soaking in H_2O_2 for 4 to 7 days and then sieved. Selected uncertain grains comprising the 150 to 250 µ fractions were collected by hand-picking under a binocular microscope. Gold was used as a coating for MAs in order to prevent charging. Carbon was not used as a coating since a majority of the MAs contained carbon in their overall composition. These grains were further analyzed by scanning electron microscopy (SEM) using a JEOL JSM-7600F field-emission instrument. Chemical analyses were done by energy dispersive x-ray spectroscopy (EDAX) using a Pegasus Apex 2 instrument. Identifications were carried out based on the microscopic and geophysical and chemical characteristics of reference artifacts analyzed. X-ray diffraction (XRD) Bruker Phaser II diffractometer equipped with a LYNXEYE detector was used in order to further identify the chemical composition of microartifacts that were still unclear when analyzed under a microscope or had no published data.

4.5 Geophysical and Chemical Mapping

There were 124 topsoil samples collected and analyzed for mapping purposes, profile samples were not included. Surfer was used to create a large scale map of Detroit and small scale transect. The contour maps show a respected representation of EC and MS values that were

measured. Inverse distance weighting (IDW) and kriging were the two interpolation methods being used. After multiple trials and observations, IDW was the preferred interpolation method. IDW was chosen based on how samples were weighted and how space was estimated in-between samples. Overall, IDW showed the best representation of the collected data. Contour maps were then overlaid into Google Earth to further identify the location of anomalies.

CHAPTER 5

ARTIFACT ANALYSES

5.1 Introduction

Microartifact microscopic characteristics and compositions commonly found in anthropogenic soils are poorly known. A better understanding is needed due to their significant and direct impact on soil chemical and physical properties because of their small size, high surface area, and substantial amount of concentration in urban soils. Each reference MA collected was measured for specific gravity, abrasion pH, EC, electrical resistivity (ER), and MS. The mean (X), standard deviation (S), coefficient of variation percent (CV%) were calculated for a selected group of samples (Table 2). The mean represents the average values for EC, MS, and pH for every individual reference microartifact. Standard deviation is often used instead of the variance in order to show relationship between the number of samples and their mean values (Isaaks, 1989). CV% was calculated by S/X x100 and is often used to describe the shape of distribution or variability (Isaaks, 1989). Microartifacts with a CV% less than 30% were considered to show a high reproducibility rate.

Table 2: Chemical and geophysical characteristics of reference artifacts. X, mean; S, standard deviation; CV, coefficient of variation

Sample	Specific Gravity			Abrasion pH			Electrical Conductivity ($\mu S\ cm^{-1}$)			Resistivity (ρ) (Ω m)		Mass Magnetic Susceptibility ($10^{-8}\ m^3\ g^{-1}$)		
	X	S	CV (%)	X	S	CV (%)	X	S	CV (%)	ρ	Corrosivity Index	X	S	CV (%)
Carbonaceous														
Wood (Peat)	< 1	--	--	3.42	0.02	0.6	557.5	6.4	1.1	17.9	Strong	-3.7	-1.6	43.7
Charcoal	< 1	--	--	7.17	0.04	0.6	350.2	28.0	8.0	28.6	Moderate	-4.36	2.14	49.1
Coal	1.19	0.91	7.6	4.53	0.44	9.7	569.0	9.9	1.7	17.6	Strong	-12.0	-0.3	2.3
Coked coal	1.03	0.04	3.9	7.96	0.18	2.2	401.2	3.0	0.7	24.9	Moderate	63.5	1.9	3.0
Coal cinders	2.19	0.08	3.8	8.46	0.35	4.1	149.8	3.2	2.1	66.8	Weak	568.9	40.7	7.1
Coal ash 1	< 1	--	--	6.75	0.15	2.2	478.5	9.2	1.9	20.9	Moderate	880.5	21.5	2.4
Coal ash 2	< 1	--	--	8.24	0.06	0.6	903.8	59.0	6.5	11.1	Strong	344.8	2.9	0.8
Asphaltic concrete	2.31	0.18	7.9	7.52	0.22	2.9	436.3	20.6	4.7	22.9	Moderate	226.2	--	--
Calcareous														
Concrete 1	2.48	0.11	4.5	11.86	0.05	0.4	3238.3	11.8	0.4	3.1	Very strong	54.0	0.9	1.6
Concrete 2	2.36	0.14	5.7	12.11	0.08	0.6	7846.7	433.7	5.5	1.3	Very strong	33.8	1.2	3.6
Concrete 3	2.77	0.14	5.0	12.15	0.05	0.4	10341.7	426.6	4.1	1.0	Very strong	42.7	14.6	34.1
Pink Mortar	2.32	0.10	4.5	8.80	0.02	0.2	5210.0	1160	22.3	1.92	Very strong	78.0	11.9	15.2
White mortar	2.25	0.06	2.8	11.62	0.01	0.1	2106.7	42.4	13.8	4.7	Very strong	29.1	4.1	14.2
Cinder block	1.64	0.12	7.4	9.72	0.05	0.5	946.0	69.3	7.3	10.6	Strong	356.9	2.0	0.6
Lime brick	2.42	0.16	6.7	8.92	0.7	0.1	1046.0	12.7	1.2	9.6	Strong	54.4	1.4	2.5
Siliceous														
Window glass	2.43	0.05	2.2	9.87	0.17	1.7	262.5	61.5	23.4	38.1	Moderate	-1.0	0	0
Bottle glass	2.50	0.03	1.2	10.60	0.12	1.2	660.6	225.3	34.1	15.1	Strong	3.5	1.7	49.5
Glass slag	2.73	0.04	1.3	9.80	0.11	1.1	103.4	18.2	17.6	96.7	Weak	186.4	2.0	1.1
Red brick 1	2.28	0.05	2.3	8.48	0.08	0.9	883.5	135.1	15.3	11.3	Strong	68.6	0.6	0.87
Red brick 2	2.24	0.06	2.5	9.44	0.02	0.2	537.8	27.2	5.1	18.6	Strong	280.0	0.8	0.3
Red brick 3	2.37	0.05	2.0	9.11	0.01	0.1	439.2	41.4	9.4	22.8	Moderate	121.0	1.0	0.8
Red brick 4	2.50	0.12	4.8	8.83	0.11	0.1	701.0	65.1	9.3	14.2	Strong	28.7	0.9	3.1
Orange brick	2.25	0.07	3.1	8.31	0.15	1.8	5082.3	170.4	3.4	2.0	Strong	256.8	4.2	1.6
Yellow brick	2.58	0.07	2.6	8.80	0.05	0.5	183.8	10.2	5.6	2.0	Very strong	87.3	1.0	1.1
Terracotta	2.42	0.04	1.8	10.02	0.58	5.8	557.5	71.0	12.7	17.9	Strong	24.7	1.0	4.1
Glazed ceramic pipe	2.07	0.13	6.1	5.51	0.11	1.9	177.4	14.2	8.0	56.4	Weak	89.4	--	--
Ferruginous														
Metalliferous slag	3.66	0.18	4.8	11.50	0.04	0.3	1747.5	296.3	16.9	5.7	Very strong	2010.9	186.7	9.3
Corroded iron	3.44	1.6	45.5	7.69	0.08	0.1	1474.1	203.1	13.8	21.1	Moderate	2786.2	2537	91.0
Miscellaneous														
Bone	1.66	0.02	1.1	7.93	0.43	5.4	615.5	34.6	5.6	16.2	Strong	1.0	0.1	1.9
Drywall	1.07	0.01	1.3	7.13	0.74	10.3	2335.0	35.4	1.5	4.3	Very strong	-8.1	1.9	23.7

5.2 Specific Gravity

Measured specific gravity (SG) of artifacts may be generally categorized as ferruginous > calcareous ≥ siliceous > carbonaceous (Table 2). The measured results were mostly expected and had a good overall agreement between SG and the mineralogical composition of MAs. Metalliferous slag had a greater SG value than its common ferromagnesian mineral components (~3.3). This is most likely due to steel slag containing denser mineral phases such as hematite and magnetite with SGs (~5.2) (Klein and Dutrow, 2007). The corroded nails had inconstant SG results due to their variation in the amounts of remaining ferrite (SG = 4.9) contained in their cores. Glass slag was much denser than typical soda-lime window and bottle glass due to the concentration of Fe from iron smelting. Concrete, mortar, and other calcareous artifacts were often denser than siliceous ceramics, most likely due to the presence of quartzose aggregate. Concrete may have had a greater value of SG than mortar because of it containing gravel-sized aggregate, whereas mortar contained sand-sized aggregate.

Terracotta had a higher SG than the other ceramics studied as a result from it being fired at a lower temperature. The lower temperatures of burning allowed terracotta to contain somewhat intact clay minerals. Carbonaceous artifacts had the lowest SGs which can be credited to the low density of bitumen (~1.0). Coal cinders had a much greater SG than other carbonaceous artifacts because they are characteristically comprised of glass and high density phases such as magnetite (Ward and French, 2005).

Overall, there was a general normal averaging of SG in artifacts comprised of compound materials. The SG of artifacts is expected to contribute to the overall elevated bulk density typical of urban soils. This relates to this study because previous work suggests that EC

surveying is occasionally useful for mapping soils on the foundation of bulk density (Brevik and Fenton, 2004).

5.3 Abrasion pH of Microartifacts

MA surfaces were obviously severely abraded during the crushing process. Abrasion pH results in the release of cations from the abraded surfaces of minerals (Stevens and Carron, 1948; Grant, 1969). Measured abrasion pH values ranged from 3.42 to 10.02 and were overall in the order of calcareous > siliceous > ferruginous > carbonaceous (Table 2).

The pH values for fresh mortar and concrete were usually around 12.0. Mortar samples had a pH around 8.0 which can be seen in both mortar and concrete MAs after it has aged and settled through carbonation (Wilimzig and Bock, 1996). High pH for metalliferous steel slag (11.5) can be from the use of limestone or dolostone being a fluxing agent during the iron smelting process. The carbonaceous pH was usually around 6.0 the highest being for coal ash around 8.0. Acidity of wood, charcoal, and coal can possibly explained by dissociation of carboxyl or other organic functional groups. Siliceous MA pH was usually around 8.0, brick having the highest value around 10.0. Glass and some ceramic MAs had high pH values and can be explained by hydrolysis of basic cations due to abrasion (particularly Na^{+} and K^{+}) (Stevens and Carron, 1948; Grant, 1969). Artifacts composed of calcite or portlandite (limey cement) may have hydrolyzed and generated an alkalinity from bicarbonate production. Some of the ceramic MAs had a slight acidic pH from abraded edges of phyllosilicates due to hydrolysis of Al^{3+} (or Fe^{3+}).

5.4 Electrical Conductivity

Measured EC values of MAs had a wide ranged from 103 µS cm^{-1} to 10,342 µS cm^{-1} (Table 2). Corresponding values of ER ranged from 1.0 to 96.7 Ωm (Table 2). Once measured, microartifacts showed a notable pattern and were classified into subgroups based on their composition, the results being, calcareous > ferruginous > silicious > carbonaceous. Silicates, non-metallic non-silicates, and glass are poor electrical conductors. When these materials (along with any other MAs from a different subgroup) are in contact with water an electrical current can transmit and be measured as a result of ionic conduction. EC and ER of soils and rocks are mostly dependent on the electrolytic characteristics related to porosity and fluids (Rhoades et al., 1989; Telford and Geldert, 1990; Corwin and Lesch, 2005). Ionic conduction may be affected by electrically charged particle surfaces associated with phyllosilicates (Kriaa et al., 2014) and calcite (Wu et al., 2010). This is because the minerals themselves contain a diffused double layer which causes a higher conductivity (Telford and Geldert, 1990; Wightman et al., 2003). EC can also occur by electron transfer resulting from hydrogen and transition metal impurities. EC measurements are normally proportional to ferric iron content within the sample (Schaefer, 2010; Karato and Wang, 2013).

Calcareous artifacts were found in Detroit neighborhoods that were classified as residential demolition sites. They are mostly a result from left over architectural debris such as, mortar, concrete, cinder blocks, etc. EC of this subcategory ranged between 946.0 to 7,846.7 µS cm^{-1}. The pink mortar collected most likely got its color from adding brick dust to its mix. As a result, the EC for pink mortar was approximately as high as the orange brick. High EC of cinder block may be the result of electron transfer reactions involving elemental iron and Fe-oxides; this can also be seen for red brick.

Ferruginous artifacts were found at industrial and fly ash-impacted sites and had an EC range of 1,474.1 µS cm^{-1} to 1,747.5 µS cm^{-1}. These artifacts are a result from the combustion and smelting process and therefore produce MAs such as steel slag, ferruginous microsphere, etc. Like red brick and cinder block, the relatively high EC of metalliferous slag may be the result of electron transfer.

Siliceous artifacts were mostly found on residential demolition sites. EC of siliceous MAs ranged from 103.0 µS cm^{-1} to 5,082.0 µS cm-1. High EC for orange brick (commonly used in the 19th century) are a result from techniques and methods that were used when firing clays at 900°C which left the clay minerals reasonably intact. When firing above 900°C phyllosilicates decompose into glass. This can explain the lower EC of red brick that dated from the 20th century is attributed to higher glass content resulting from improved technology and firing at a temperature greater than 900°C (Cultrone et al., 2004, 2005; Reedy, 2008).

Carbonaceous artifacts were observed mostly at industrial sites and had an EC range of 149.8 µS cm^{-1} to 903.8 µS cm^{-1}. EC of carbonaceous artifacts can be accredited to electron transfer reactions involving hydrogen impurities. High EC measurements of drywall can be a result to its high porosity and greater electrolytic conduction. This is caused by a release of Ca and SO_4 from the abraded surfaces of gypsum particles (Schaefer, 2010). Bone had a much lower EC, likely due to the lower solubility of apatite.

Once ECs were measured electrical resistivity values (ER) were able to be calculated. Values of electrical resistivity (ER) ranged from 1.0 to 96.7 Ωm (Table 2). Corrosive artifacts were determined by ER calculations and the corrosive index used for metals buried in soils (Elias, 2000). Crushed artifacts comprised of waste building materials were found to be strongly corrosive (concrete, mortar, brick, ect.). Coal related artifacts (charcoal, coked coal, ect.) were

found to be moderately corrosive. Artifacts that had a weak corrosive index were coal cinders, slag glass, and ceramic.

5.5 Magnetic Susceptibility

Measured magnetic susceptibility of microartifacts ranged from negative values to in the thousands, results showing ferruginous > carbonations > siliceous > calcareous. It has been known that the degree of magnetization in response to an applied magnetic field is generally a function of the amount of magnetite, maghemite, elemental iron and heavy metals present in an earth material (Oldfield, 1991; Verosub and Roberts, 1995; Schmidt et al., 2005; Magiera et al., 2006). Measured values of MS were highest for corroded iron nail, metalliferous slag, coal cinder, coal ash, and cinder block MAs (Table 2). These MAs all reacted to a hand magnet which indicating the presence of ferrimagnetic material.

Ferruginous artifacts resulted in the highest MS values. Specifically, these artifacts were corroded metal which had an MS value of 2,786.2 x 10^{-8} m^3g^{-1} and steel slag with a value of 2,010.9 x 10^{-8} m^3g^{-1}. The high MS of corroded nails was due to the occurrence of inconstant amounts of non-corroded fragments of a ferrite (elemental Fe) nail core. High MS for metalliferous slag is from hematite altering into magnetite by oxidation at 900°C to 1000°C (Hu et al., 2006).

The carbonaceous group had MS values that ranged between 63.5 x 10^{-8} m^3g^{-1} and 880.5 x 10^{-8} m^3g^{-1}. This category had mostly the lowest MS values. Negative MS values are due to diamagnetic minerals having a negative susceptibility (Burger, 2006). High MS values are obtained due to coal often containing pyrite that decomposes into hematite or magnetite at temperatures of 200 to 1000°C (Waanders et al., 2003; Hu et al., 2006). Therefore, the high MS

values for coal cinders and ash are explained by magnetite formed as a by-product of coal combustion.

Siliceous and calcareous microartifacts had MS values ranging between 3.5 x 10^{-8} m^3g^{-1} and 356.9 x 10^{-8} m^3g^{-1}. MS values for these MAs were neither the highest or lowest measured subgroup. The MS value for cinder block MAs was much greater than any other MA in the calcareous group. It is most likely attributed to the presence of magnetite bearing blast furnace slag as aggregate during the process of production.

5.6 Artificial Soil

An artificial soil was made in the lab where a weight percent of a known microartifact was gradually added to a clay or sandy native soil. The pH, EC, and MS, were measured after each weight percent increase (Fig. 7). The MAs that were measured were fly ash, coal cinders, concrete, and red brick. These results suggest that artifacts can directly affect chemical and geophysical properties in sandy soils with only a 1 weight (wgt) % present increase.

It is apparent that as the weight % of microartifacts increases so do the geophysical and chemical property values. Most EC and MS values of the artificial soil doubled in value once there was an increase of microartifact of 10%. The pH values typically increase by one value. It can also be noted that although most pH, MS, and EC values do increase there are a few samples that stay relatively the same as weight percentages are added. For example, the pH of the artificial soil fly ash increased from a pH of 4 to a pH of 5.5 after 1% of fly ash was added. However, the pH then stayed constant at 6.5 for the following added weight percent.

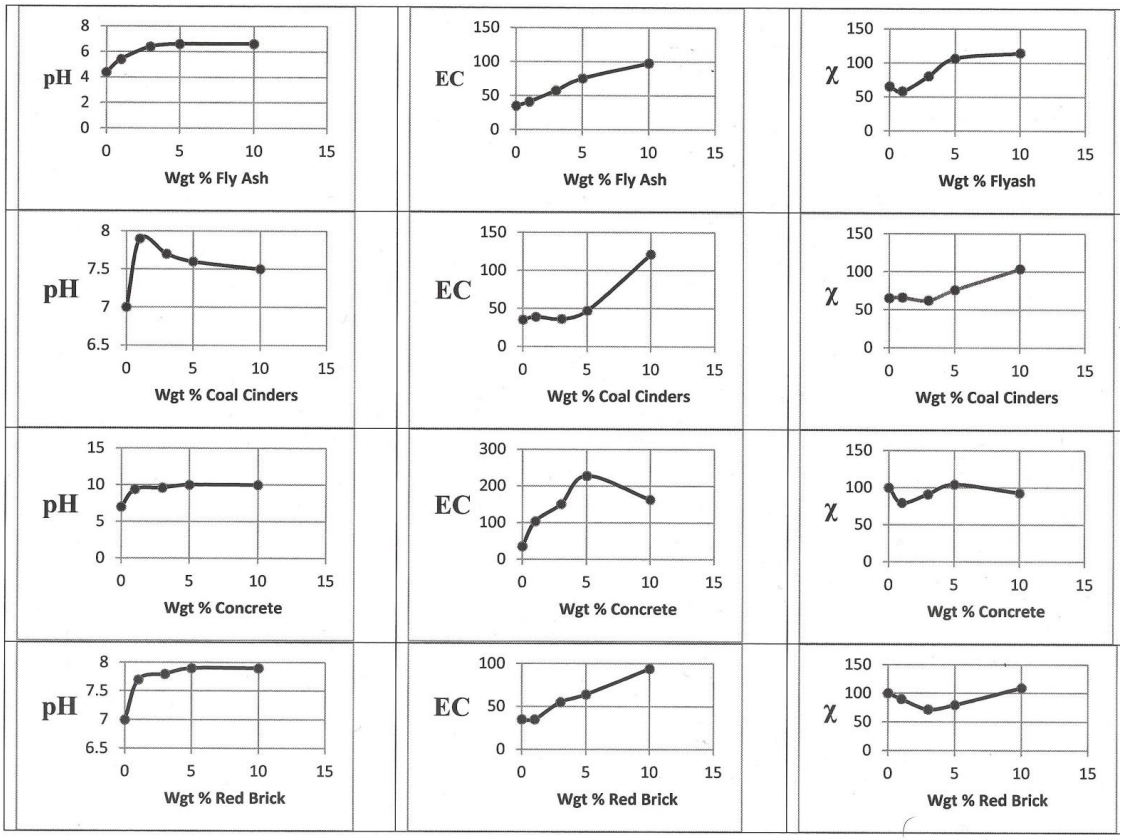

Figure 7: Effects of anthropogenic MA on pH, EC, and MS in artifact-sand mixtures

Native clay and sand play different roles on EC, MS and pH results. EC is heavily impacted by the soil matrices where MS is not. Soil conductivity is greater in clays, intermediate in silts, and low in sands (Lund, 1999). This is due to conductivity having a strong correlation to soil grain size and texture. In the lab an artificial soil was made with clay and sand matrices. The native clay and sand were measured first with a 0 weight % increase of corroded iron and then measured again after a weight % increase of corroded iron was added. Only one microartifact (corroded iron) was observed in the clay and sand matrices in order to less complicate the results. Corroded iron was selected as the microartifact because it highly impacts the EC and MS, therefore making an evident geophysical and chemical change to the soil (Fig. 8).

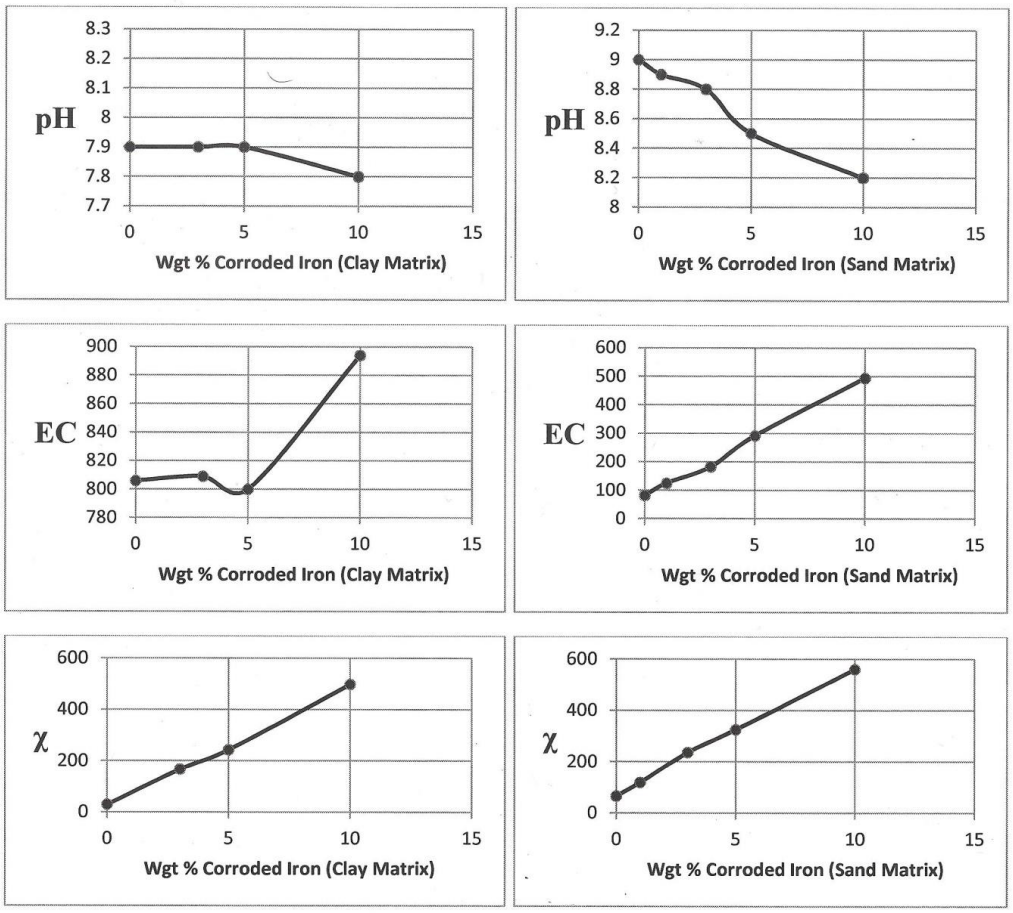

Figure 8: Effects of corroded iron nail MAs on pH, EC, and MS in artifact-sand and artifact-clay mixtures

The abrasion pH of corroded iron is less than the clay or sand matrices. Therefore, once a weight percent of the corroded nail was added to the clay or sand matrix there was a decline in pH. The pH for the clay matrix was 7.9 and 9 for sand. Once the corroded iron was added to the clay matric the pH decreased from 7.9 to 7.69. When the corroded iron was added to the sand matric the pH decreased from a pH of 9 to 8.2. The strongly buffered clay matrix results in a greater change in pH than the sand matrix.

The EC for the clay and sand matrix with a 0 % of artifact weight added was about 805 $\mu S\ cm^{-1}$ for the clay matrix and just under 100 $\mu S\ cm^{-1}$ for the sand matrix. Similarly to pH, there was an increase in EC with increasing weight % of MA. Increases of EC in the sand matrix could

be seen about 1% MA weight increase. The more strongly buffered clay matrix did not have a noticeable increase in EC until about 5% of MA weight was added.

Both clay and sand matrices had a MS close to 0 x 10^{-8} m^3 kg^{-1} when there was a 0 % weight of corroded iron added. Once the weight % of corroded iron was added to both matrices there is a substantial increase in MS values. At 10% weight increase of corroded iron the clay matrix had an increased MS value from 0 x 10^{-8} m^3 kg^{-1} to roughly 500 x 10^{-8} m^3 kg^{-1}. The sand matrix had an increased MS value from 0 to 600 x 10^{-8} m^3 kg^{-1}at at 10 % weight increase of artifact. MS is unaffected by buffering capacity and showed a sudden increase in MS in both clay and sand matrices.

Overall, pH, EC, and MS values started to dramatically increase with only 1% weight increase of MAs. This shows that MAs have a direct and strong influence on soil geophysical and chemical properties. MA effects on pH and EC are more unresponsive in the clay matrix because of its high buffering capacity but have a gradual increase once there is greater than a 5 % increase in artifact concentration. MA effect on MS was very responsive for both clay and sand matrices making the clay buffering capacity not prevalent.

5.7 Microartifact Description

The composition of artifacts reflects highly on related heating and combustion processes as a result of human activity. For instance, wood (comprised of cellulose and lignin) is converted into highly condensed aromatic hydrocarbons and black carbon when undergoing thermal decomposition at 250° to 400°C (Rutherford et al., 2004; Brodowski et al., 2005). As a result, charcoal is composed of combustion byproducts and remnant structures from parent plant materials (Cornelissen et al., 2005; Forbes et al., 2006).

Coal is made of macerals which is the primarily component of vitrinite. Vitrinite is what preserves the observed microstructure of the wood (Petrakis and Grandy, 1980; ICCP, 1998; Suarez-Ruiz, 2012). The coking process comprises of heating coal to 1100°C (or more) and creating a depleted oxygen environment to form a hard flexible mass made of nearly pure carbon (Suarez-Ruiz, 2012). The coal then takes a form of a soften plastic mass after being heated at 350°C to 450°C and volatiles are removed. This process often results in considerable amount of foaming. Coal is then further heated to a temperature of 450°C to 550°C. At this temperature the coal begins to solidify into coke (Gray, 1991). Coked coal is mainly used as a type of fuel for smelting iron. It is an ideal fuel for coal-firing power plants. Coked coal was observed at a number of industrial sites but large amounts were specifically seen at the River Rouge Plant.

Siliceous artifacts are generally made of silicate minerals such as carbonates and oxides. These minerals have the likelihood to be able to be altered by a heating process in order to form glass. Coal cinders are made by coal combustion at temperatures of 1200°C to 1500°C. Coal cinders are composed of ash particles made from inorganic components of coal fused together. Coal ash is similar to coal cinders in composition, but coal ash normally contains pieces of unburnt coal or soot (Ward and French, 2005). Coal cinders and coal ash are often magnetic due to their high burning temperatures which cause the concentration of hematite to be converted into magnetite. This takes place at temperatures of 900°C to 1000°C (Matthews, 1976; Kontny and Dietl, 2002; Wagner et al., 2006; Hu et al., 2006; Bhargava et al., 2009). Many coal related products were commonly found in both industrial and residential demolition sites.

Coal ash is a mixture of inorganic and organic particulate matter. They are usually 15 to 150 µ in size and sometimes smaller and therefore are prone to eolian transport. Coal ash microparticles are morphologically complex but it has pronounced characteristics. For instance,

various types of microspheres within the coal ash are distinct. Previous work suggests that the clear microspheres studied are siliceous and opaque black microspheres are ferruginous or carbonaceous (Howard et al., 2013a, 2015). Microspheres are made when coal is heated up to 350° to 450°C, this temperature creates a plastic phase. Degassing at a high temperature during coking, gasification, or combustion produces small bubble shaped spheres made up of glass, mineral, or carbonaceous materials (Fisher et al., 1976; Smith et al., 1979; Gray, 1991). The bubble like sphere escape from the furnace with the hot gases and are carried deposited in the environment as fly ash. Coal ash can also be observed as non-spherical or agglomerates microparticles. It can also be comprised of a mixture of spherical and non-spherical types (Fisher et al., 1976, 1978; Smith et al., 1979). Types of microspheres and agglomerates were also found to be magnetic as a result from coal combustion. Coal ash was found at all three urban sites but was heavily concentrated at industrial and fly ash sites.

Another common siliceous artifact found on residential demolition sites is ceramic brick. Ceramic brick is made by firing clay at 800°C to 1200°C. Other bricks that lack glass and high temperature phases are usually fired at <1000°C. This tends to me the brick more porous and weak (Ahmad et al., 2008). As the temperature rises during the firing process to 820° and above 1000°C, carbonates and phyllosilicates decompose to form aluminosilicate glass and hematite (Livingston et al., 1998; Cultrone et al., 2004, 2005). Bricks that are red and very solid are usually of the 20th century and often have a coated exterior of glass. Burnt shale was a byproduct of coal combustion and contained glass and mullite. Soda-lime glass is a siliceous non-crystalline material used to make window pane. Sodium (Na_2O) and lime (CaO) are added as fluxing agents to reduce the melting temperature of quartz (Mukherjee, 2011). Glass slag is also siliceous and is produced by iron smelting. It has a distinct green color due to the presence of chlorite. Many

of the siliceous MAs were found in demolition residential sites. However, glass slag was only observed in industrial sites.

Calcareous artifacts observed at different urban sites were rock-like materials made of sand-sized (mortar) or gravel-sized (concrete, cinder block) aggregate (rock and mineral fragments) held together by a lime-based cement. Most concretes are mixtures of gravel, sand, and cement (Kosmatka et al., 2002). Once water is added to the mixture it hardens over a period of time (Van Oss, 2005). A more modern type of cement that is used is called Portland cements. Portland cements are blends of lime, gypsum, and perhaps other raw materials (Van Oss, 2005). Natural cement is comprised primarily of portlandite, belite, and calcite. Earlier types of cement had high clay content and were produced by calcination of clay-rich limestone. Cinder block artifacts contained aggregate made of blast furnace cinders. Many of these calcareous microartifacts were found in residential demolition neighborhoods due to the use of different types of cements for architectural home foundations.

Metalliferous (ferruginous) slag is produced by iron smelting and has a similar appearance to basaltic cinders. It is made by the process of heating a mixture of iron ore, coked coal, and a fluxing agent (limestone or dolostone) at 2000°C. This mixture is heated in a brick-lined heat-resistant blast furnace (Proctor et al., 2000). Metalliferous slag is easy to identify based on its density, highly vesicular texture, and by a high temperature mineral group including olivine, merwinite and wollastonite. Wrought iron nails were commonly found in soils where buildings from the 19th century were demolished (Howard et al., 2013, 2015). These nails were usually corroded and had a remnant ferrite nail core encased in a ferrihydrite- and goethite-cemented soil crust. Most metalliferous MAs were observed at industrial sites. Corroded nails were observed in both industrial and residential demolition sites.

Other miscellaneous artifacts found in Detroit soils include bone, pottery, bottle glass, plaster, and paint. Apatite is known to be a major component of bone. The characteristics of pottery and bottle glass are similar to ceramic brick and soda-lime glass that were previously described. Drywall showed that it was comprised of mostly gypsum and paint had inconclusive data results.

Table 3: Description of reference microartifacts

Microartifact	Color	Clarity	Luster	Fracture	Texture	Shape
Carbonaceous						
Peat	light to dark brown and black	opaque	earthy	splintery to fibrous	agranular	angular platy to rod-like and fibrous
Charcoal	black	opaque	bright vitreous	splintery to fibrous	agranular	angular blocky to prismatic
Coal	black	opaque	bright vitreous	splintery to hacky jagged and conchoidal	agranular, possible microlamination	angular to very angular blocky
Coked coal	black	opaque	dull to bright vitreous; some iridescence	jagged hacky	agranular vesicular	very angular blocky
Asphaltic concrete	black	opaque	earthy to resinous	smooth hacky	polymictic granular, aggregatic	subangular to subrounded equant
Calcareous						
Lime concrete	white	opaque	earthy	smooth hacky	polymictic granular aggregatic	subangular to subrounded equant
Lime brick	grayish-white	opaque	earthy	smooth hacky	polymictic granular aggregatic	subangular to subrounded equant
Mortar 1	white	opaque	earthy	smooth hacky	polymictic granular aggregatic	subangular to subrounded equant
Mortar 2	pinkish white	opaque	earthy	smooth hacky	polymictic granular aggregatic	subangular to subrounded equant
Cinder block	grayish-white to dark gray	opaque	earthy	jagged hacky	polymictic granular aggregatic vesicular	angular blocky
Siliceous						
Coal cinders	black to pale brown	opaque to semi-translucent	dull to bright vitreous	conchoidal to jagged hacky	agranular vesicular	angular to very angular blocky
Coal ash (microspheres)	gray	translucent	bright vitreous	none	granular	Very well rounded
Coal ash (agglomerate)	gray to grayish-brown	semi-translucent	dull vitreous	none	granular aggregatic	Well-rounded to subangular

Burnt shale	pale pinkish gray to pinkish brown	opaque	Dull vitreous	platy	agranular	subangular to very angular
Red brick	dark brownish orange to reddish brown	opaque	earthy	smooth hacky	polymictic granular aggregatic	subrounded equant to blocky
Orange brick	brownish orange	opaque	earthy	smooth hacky	polymictic granular aggregatic	subangular to subrounded equant
Yellow brick	pale yellowish brown	opaque	earthy	smooth hacky	polymictic granular aggregatic	subangular to subrounded
Terracotta	reddish orange	opaque	earthy	jagged hacky	polymictic granular aggregatic	very angular to subangular blocky
Glazed ceramic	light grayish brown to brownish orange	opaque	earthy to vitreous	Smooth hacky	polymictic granular aggregatic	angular to subrounded blocky
Glass slag	dark to pale green	opaque to translucent	bright vitreous	conchoidal	agranular	very angular blocky
Ferruginous						
Wrought iron (corroded)	orange to dark brown	opaque	earthy	none	none	none
Ferruginous slag	very dark gray	opaque	Dull resinous to bright metallic	jagged hacky	agranular vesicular	angular to very angular blocky
Coal ash (microspheres)	brown, red and black	opaque	metallic	none	granular	Very well rounded
Miscellaneous						
Bone	light brownish yellow to yellowish brown	opaque	earthy	jagged to smooth hacky	agranular porous	angular to very angular blocky to platy
Drywall	white	opaque	earthy	smooth hacky	agranular vesicular	subrounded equant

Table 4: Pictures and descriptions of microartifacts commonly found in different sites in Detroit, MI

Microartifacts	Site Found	Description
Ferruginous Spheres: 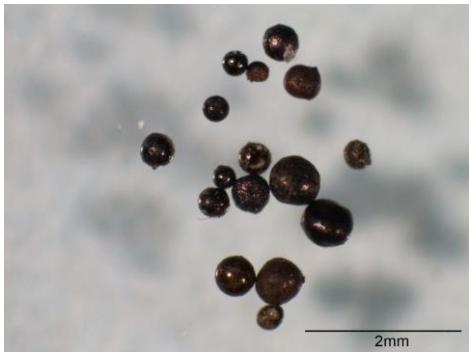	• Fly ash-impacted • Industrial • Residential demolition	• Typically spherical • Irregularly shaped • Dark in color • opaque • Commonly comprised of magnetite
Siliceous Spheres: 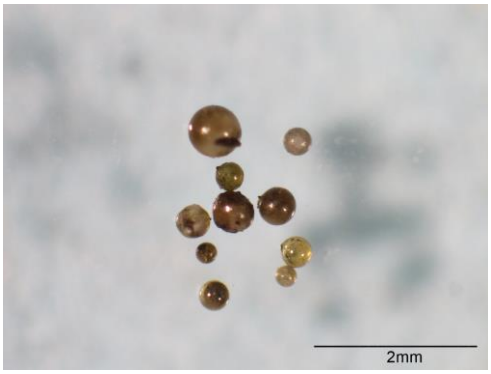	• Fly ash-impacted • Industrial • Residential demolition	• Typically spherical • Irregularly shaped • Microspheres tend to be translucent • Sometimes present as in inclusions in siliceous grains
Ferruginous Non- spherical: 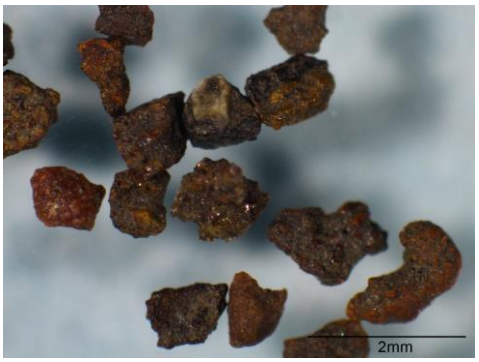	• Fly ash-impacted • Industrial • Residential demolition	• Angular • Serrated edges • Dark in color • Opaque • Highly magnetic

Agglomerate: 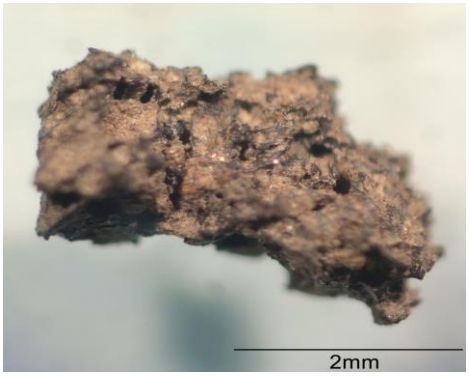	• Fly ash-impacted • Industrial • Residential demolition	• Black or brown in color • Angular • Vesicular microtexter • Magnetic
Charcoal: 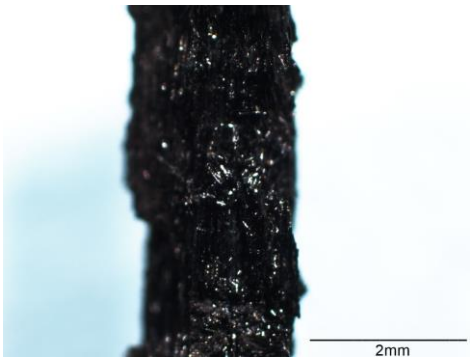	• Industrial • Residential demolition	• Fibrous or platy shape • Splintery cleavage of wood • Black • Bright vitreous luster lamellar • Microstructure of wood is partially retained by coal
Coal: 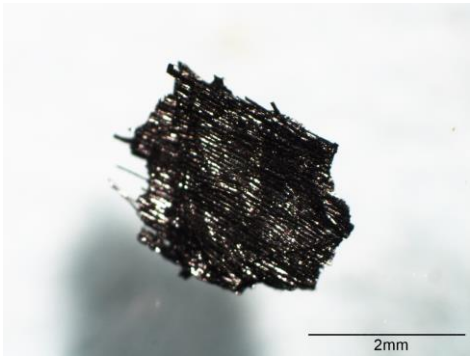	• Industrial • Residential Demolition	• Angular blocky grains • Well-developed conchoidal fracture, and may be distinguished by microlamination not seen in charcoal. • Vitreous luster

Coal Cinders: 	• Industrial	• Moderately to strongly magnetic • Distinguishable from coal by their vesicular microtexture • Multicolored black and pale brown to greenish-brown • Dull vitreous luster • Conchoidal fracture
Coked Coal: 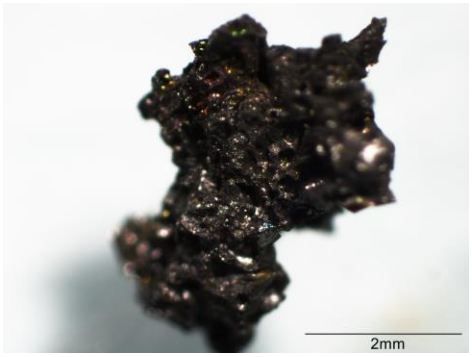	• Industrial	• Highly vesicular morphology • Black and gray colored • Some coke grains are iridescent, possibly due to thin microlamellar coatings of glass or an unknown crystalline
Glass Slag: 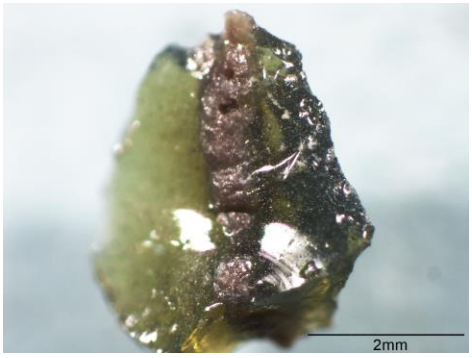	• Industrial	• Conchoidal fracture like manufactured glass shards, but tended to be less transparent • They ranged from darker green and opaque grains to pale green translucent grains • Sometimes a dull vitreous or resinous luster • Sometimes a bright vitreous luster.

Steel Slag: 	• Industrial	• Strongly magnetic • Granular vesicular texture • Distinguishable from coal cinders by a jagged hacky fracture and a metallic luster
Iron Nails: 	• Industrial • Residential Demolition	• Associated with ferrite, goethite and ferrihydrite • Brown, orange, reddish in color • Corroded iron MAs can be very similar in appearance to non-spherical ferruginous fly ash microparticles but the later generally have an upper size limit of < 150 µ
Cinder Block: 	• Residential Demolition	• Gray color • Granular vesicular texture • Presence of highly vesicular pumice-like pieces of blast furnace slag

Asphalt: 	• Residential Demolition	• Black and opaque • Equant and subrounded • Dull earthy or resinous luster • Granular, polymictic, aggregatic microtexture.
Concrete: 	• Residential Demolition	• Granular • Coalescence of particles • Pieces of aggregate
Mortar: 	• Residential Demolition	• Granular • Coalescence of particles • Smaller pieces of aggregate than concrete

Drywall: 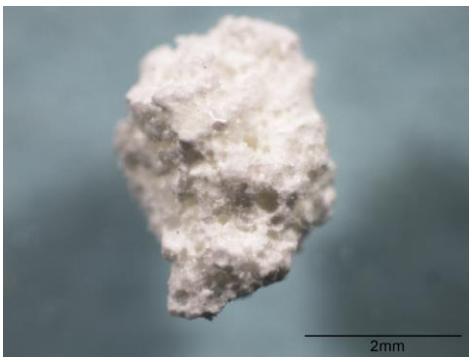	• Residential Demolition	• Plaster and paint are laminated and platy • Very soft due to being highly composed of gypsum • Fine pores • Contained plastic fibers
Brick: 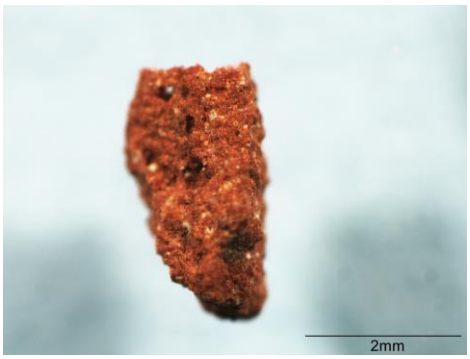	• Residential Demolition	• Earthy luster • Granular microaggregatic texture • Generally reddish or orangish brown in color • Contain finer grained aggregate than mortar
Wood: 	• Residential Demolition	• Brown • Fibrous or platy • Splintery cleavage • Lack luster

Glazed Ceramic: 	• Residential Demolition	• Vitreous luster • Characterized by an association of gray and reddish brown particles • The later often coated with a conspicuous glassy glaze
Terracotta: 	• Residential Demolition	• Earthy red/brown color • Composed of a finer grain (clay) with larger aggregate material
Window Glass: 	• Residential Demolition	• Extreme angularity • Conchoidal fracture • Differentiated from quartz by their characteristic transparency

Bone:  	• Residential Demolition	• Biofact • Light tan in color • Brittle • Irregular or angular shaped • Very coarse cavities and pores
Burnt Shale: 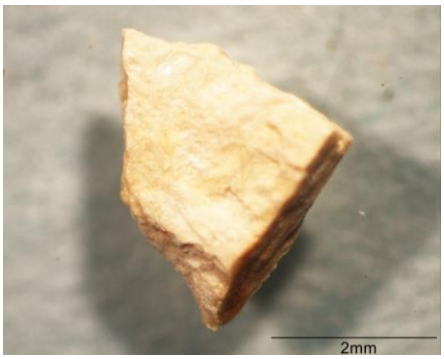 	• Residential Demolition	• White to tan color • Fine grain • Flakey

5.8 XRD, SEM, and EDAX Results

5.8.1 XRD Results

Some MA compositions were determined based on optical microscope work and previous text references, if compositions were still uncertain samples were ran though the XRD for further analysis. Based from optical microscopy, coal MAs were commonly comprised of macerals, primarily vitrinite. Asphaltic concrete was made up mainly of aggregate and contained about 5% asphaltic binder. Mortar and concrete were comprised of sand-sized or gravel-sized aggregate and were bound together mainly by calcite and/or portlandite. Cinder block artifacts contained blast furnace cinders as aggregate and were characteristically large voids. Coal cinders were characterized by their glassy vesicular microtexture with a variable structure. Wrought iron nails were usually corroded and consisted of a remnant ferrite nail core encased in a ferrihydrite- and goethite-cemented soil crust.

XRD analyses were chosen for coal cinders, orange brick, burnt shale, slag and glass slag (Fig. 9). XRD analysis revealed that the sampled coal cinders contained glass and crystalline components, this included magnetite and wustite. XRD analysis for orange brick showed it was primarily comprised of silicate and carbonates minerals and had some glass present. For burnt shale the XRD was able to identify glass and mullite present, which is also a produced byproduct of coal combustion and contained glass and mullite. XRD of metalliferous slag showed presence of high temperature dependent mineral group such as olivine, merwinite and wollastonite. Glass slag XRD results found to contain some silicate minerals including chlorite, which explains its distinct green color.

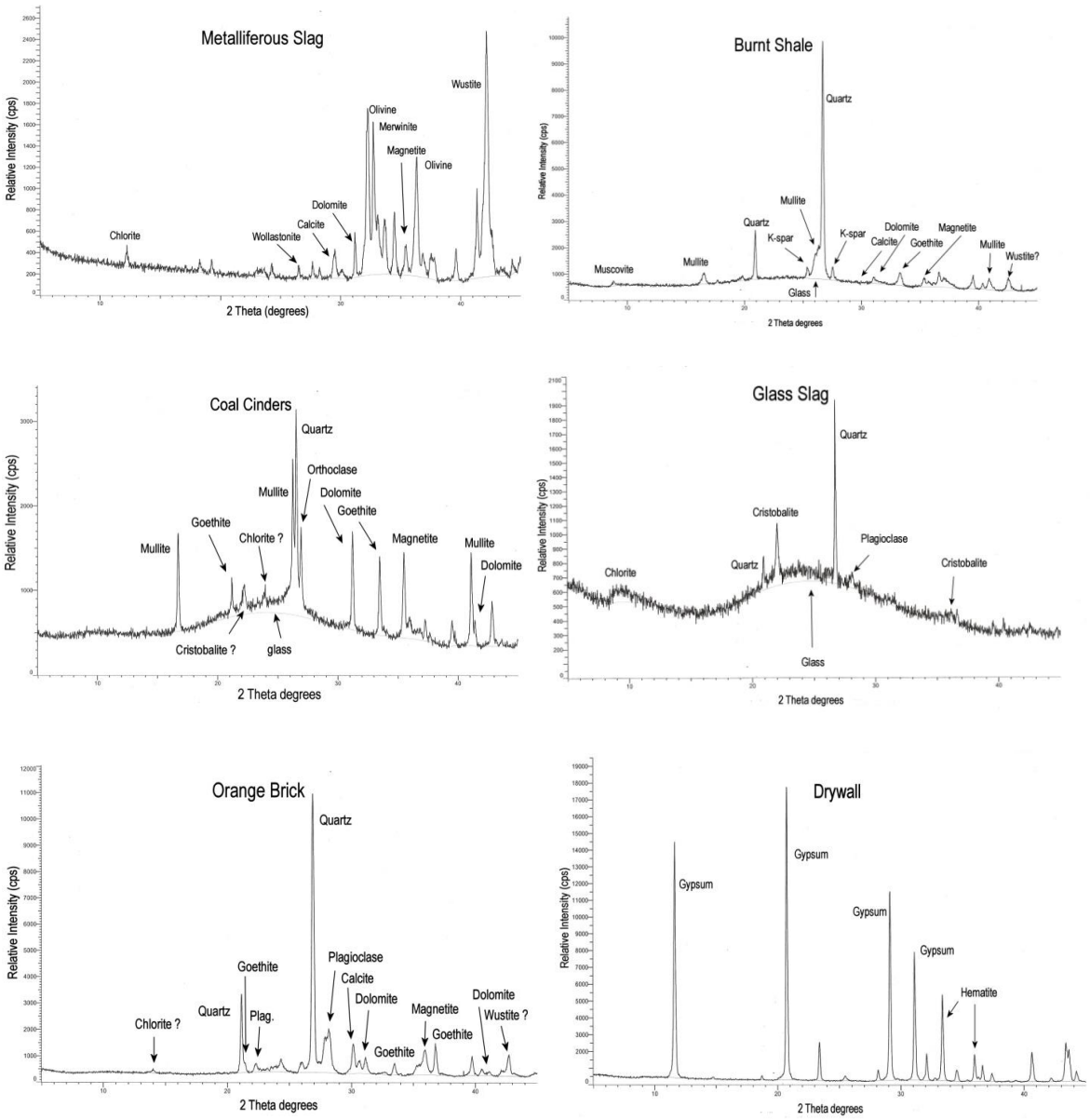

Figure 9: XRD results from selected microartifacts metalliferous slag, burnt shale, coal cinders, glass slag, orange brick, and drywall

5.8.2 SEM and EDAX

The characteristics of the frequently observed microparticles found in soils were then determined by SEM and EDAX. Their results helped to solidify that artifacts can be classified into subgroups of carbonaceous, calcareous, siliceous, ferruginous, and miscellaneous. Additional observations were made with optical microscopy. Microparticles that were collected for analysis were thought to similar to slag, coal, or fly ash.

It was unclear what the magnetic fraction from undemolished residential soils contained in the collected soil samples. SEM and EDAX analysis showed that the magnetic fraction was comprised of microsphere and microagglomerate grains resembling the reference fly ash samples (Fig. 10A and B). EDAX analyses showed that the black opaque microspheres were comprised Fe and O and are in the form of magnetite. This is consistent with the optical microscopy observations. Two types of microagglomerate MAs were distinguished by SEM (Fig. 10C-F). Type A (Fig. 10C) was made of microspheres with embedded agglutinated matrix of non-spherical microparticles. The EDAX analysis helped specify that the microspheres were magnetite and comprised of Fe, unlike the matrix of non-spherical grains which was made of aluminosilicate glass. Type B (Fig. 10E), microagglomerates, was comprised of completely non-spherical grains. These grains were the main type of microagglomerate in the fly ash-impacted soils. The EDAX analyses showed that type B grains had a very similar composition in each of the five soil samples that were tested and were also similar to the reference fly ash. Type B grains were comprised of Ca- and Fe-bearing aluminosilicate glass containing trace amounts of Cu, Ti, and Zn. Sulfur was detected in the reference fly ash, but was not seen in type B grains from the soils.

Industrial soil sites have complex arrangement of microparticles. Some of the grains were hard to distinguish when only using optical microscopy. A bulk group of microparticles

commonly found on industrial sites were gathered and compared with coal, metalliferous slag, and other reference microparticles in order to identify chemical compositions of the bulk sample. Selected industrial microparticles had similar compositions related to coal, fly ash, and steel slag (Fig. 10G-L). Industrial microparticles were easily observed to be similar to fly ash based on presences of trace elements Cu, Ti, and Zn. Fly ash can also be distinguished by having a high Si and a higher O/C ratio. Coal and slag also have distinct compositions. Slag has very high values of Ca and Fe with very low values of C and Si. Coal was distinguishable by its high C and low O/C ratio. It also often has the presence of S and P. Overall, SEM and EDAX results show that the general chemical composition of the industrial soil seems to be a mixture of microparticle types. This is consistent with observations made using optical and scanning electron microscopy.

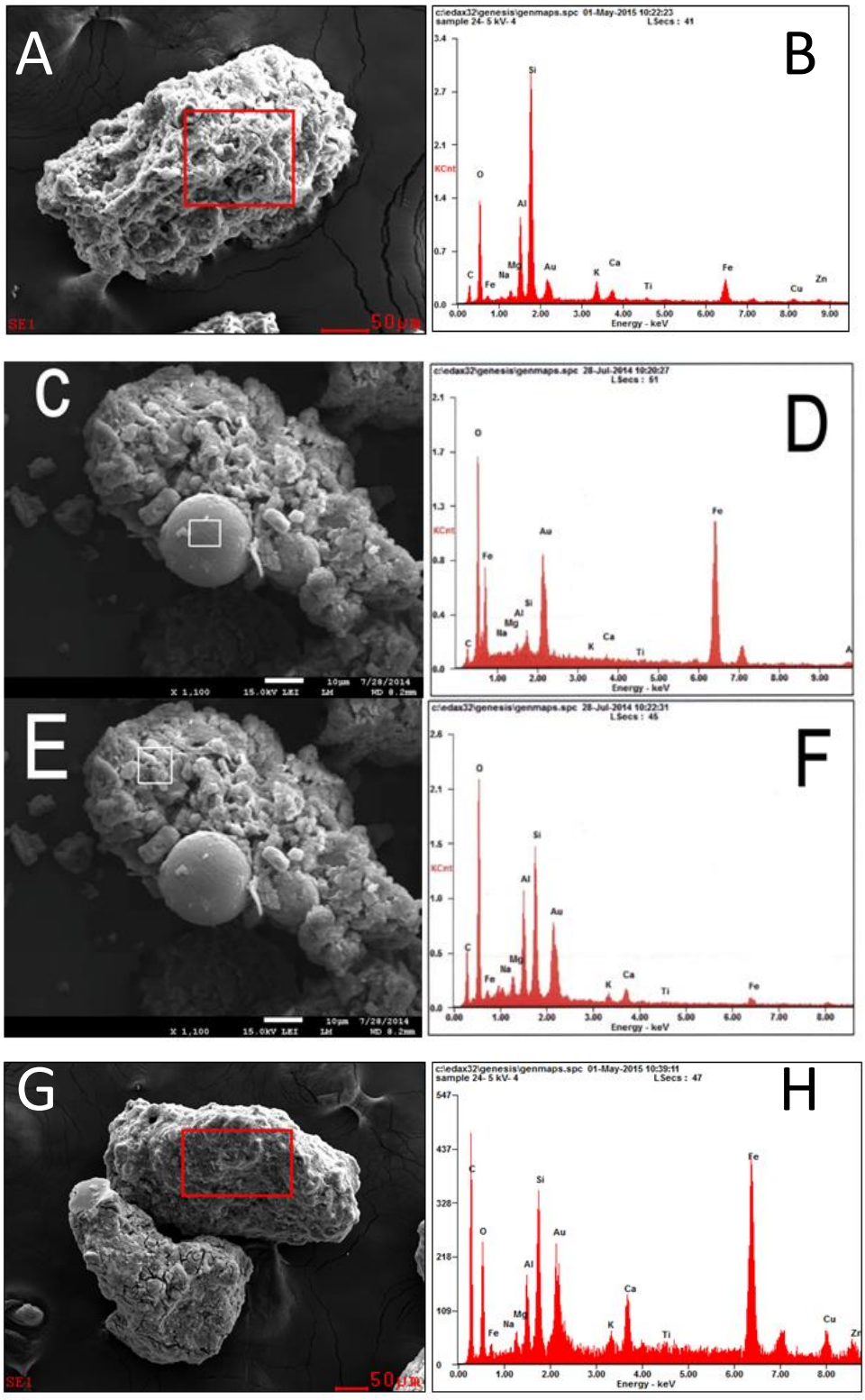
A
B
C
D
E
F
G
H
Energy - keV
SE1
50µm

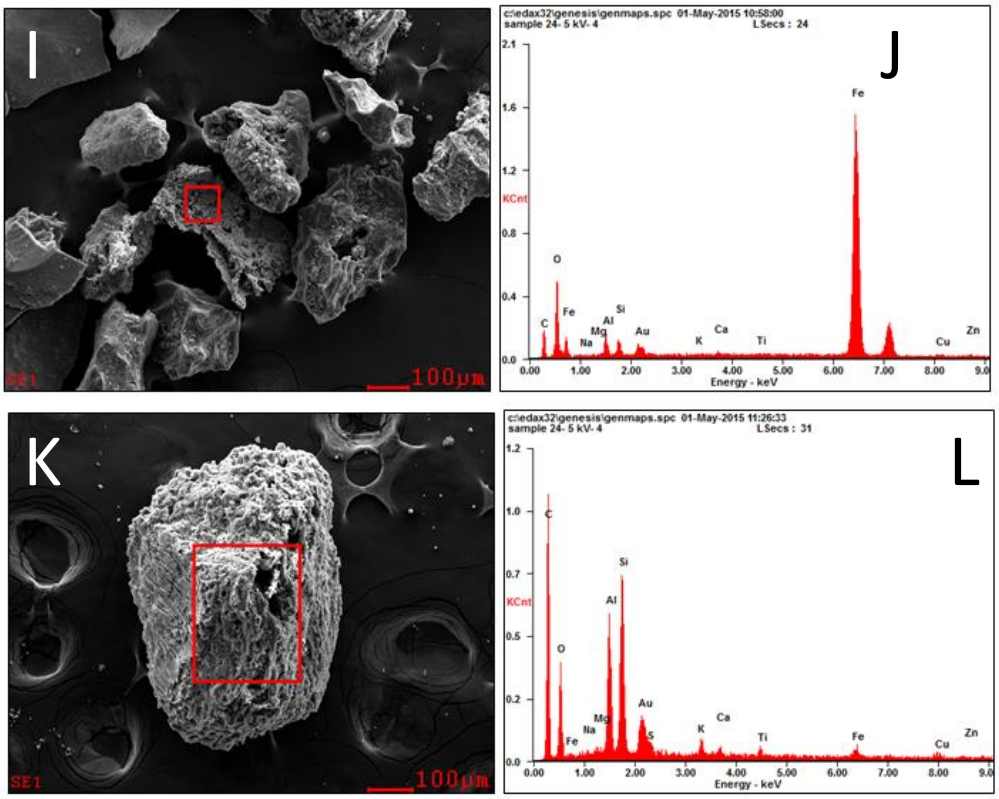

Figure 10: SEM (left) and EDAX (right) results of different microparticles. A, microagglomerate grain; B, elemental composition suggesting that the microparticles are aluminosilicate glass; C, fly ash microsphere grain; D, elemental composition suggesting that microsphere is magnetite; E, fly ash grain; F, elemental composition suggesting that other microparticles are aluminosilicate glass; G, metal microparticle collected form Orleans St.; H, elemental composition showing high concentrations of Fe, C, O, and Si; I, black microparticles collected at Orlean St.; J, elemental composition showing high concentrations of Fe with trace elements common in fly ash. K, fly ash microagglomerate grain; L, elemental composition showing typical fly ash elemental composition.

5.9 Micromorphology of Reference Artifacts

Artifacts can be classified into five basic compositional types, these types being carbonaceous, calcareous, siliceous, ferruginous, and miscellaneous. Carbonaceous MAs mainly encompassed organic compounds, calcareous types of calcite, siliceous types of silicate minerals and glass, ferruginous types of Fe-oxides, and miscellaneous types of sulfate and phosphate minerals. Heating or combustion as a result of human activity can account for the many observed compositional and micromorphological characteristics.

Reflected light microscopy was used in order to determine the micromorphological characteristics of MAs (Table 4). Results indicate that some MAs are more difficult to distinguish than others. Coal MAs were often angular and blocky with a well-developed conchoidal fracture that also may be identified by its microlamination which is not seen in charcoal. Coked coal MAs differ from charcoal and coal by their extremely vesicular morphology. This is greatly dissimilar when compared to coal and charred wood which have a splintery fracture. Some coke grains were also observed to be lustrous which could be due to thin microlamellar coatings of glass, or an unknown crystalline organic compound. Microspheres were observed in coal ash samples and can be identified by their range in color from translucent to opaque in color, non-spherical shape, and agglomeratic grains comprised of an agglutination of non-spherical or spherical microparticles. Asphaltic MAs were similar in color to coal and coke, but obtain equant and subrounded surface with a dull earthy or resinous luster. Asphaltic MAs also had a granular, polymictic, aggregatic microtexture. Indistinguishable aggregate remains to be unknown from natural origin as a result from asphaltic concrete crushing. However, they can still be classified as anthropogenic because of the presence of bitumen.

Metalliferous slag MAs agranular with a vesicular texture and were strongly magnetic. They can be distinguished from coal cinders by their serrated fracture and metallic luster. Glass slag MAs are similar to manufactured glass shards based on their conchoidal fracture but glass slag is commonly less transparent than manufactured glass. Glass slag MAs observed ranged from dark opaque green grains with dull luster to pale translucent grains with bright luster. Corroded iron nail MAs can be distinguished by the presence of ferrite, goethite and ferrihydrite. Some corroded iron MAs were very similar in appearance to non-spherical ferruginous fly ash microparticles, but corroded iron MAs generally take a larger shape than the fly ash microparticles.

Lime-based concrete and mortar reference artifacts were crushed resulting in indistinguishable aggregate MAs from natural rock and mineral particles, similarly to the crushing of the asphalt MAs. It can be identified that MAs that contain an anthropogenic cement factor differ from most carbonaceous MAs in being lighter in colored and having a polymictic granular texture. Asphaltic concrete MAs also had a granular aggregatic texture but were darker in color and were more rounded in shape than the lime-based MAs. Cinder block MAs were identified by their common gray color, granular vesicular texture, and the high vesicular pumice-like pieces of blast furnace slag.

Terracotta MAs that were studied were difficult to distinguish from brick MAs. Brick also looked similar to glazed ceramic pipe MAs but the ceramic had a slightly more vitreous luster. The glazed ceramic could also be identified by its gray and reddish brown particles which were often coated with a noticeable glassy glaze.

Wood MAs that were studied were comprised of cellulose and lignin and underwent partial thermal decomposition at ~250° to 400°C. Therefore, charcoal MAs are comprised of

hydrocarbons and black carbon (Rutherford et al., 2004; Brodowski et al., 2005). Charcoal also has remainder laminar structures from the parent plant materials (Cornelissen et al., 2005; Forbes et al., 2006) which can similarly be seen in coal as well (ICCP, 1998; Suarez-Ruiz, 2012). As a result charcoal and coal obtain a splintery fracture of wood.

The coked coal is made by heating bituminous coal to ~1100°C or more (Suarez-Ruiz, 2012). As the coal increases in heat it becomes softer and turns into a plastic form. This form can then devolatilize and vesiculate, often associated with a considerable amount of foaming. This then explains the vesicular microtexture of the coked coal MAs. When coal burns at ~1200° to 1500°C coal cinders are formed (Ward and French, 2005) once ash particles from inorganic compounds of coal fuse together. The vesicularity of a typical coal cinder can be determined based on the degassing from the liquefied state created by the rise in temperature. Metalliferous slag obtains its vesicularity similarly to coal cinders. As the heated iron ore and additives reach a temperature of ~2000°C in a blast furnace a liquefied ferruginous inorganic waste is left over and vesicularity is determined by degassing that takes place (Proctor et al., 2000). Cinders and certain ceramic obtain a vitreous luster which can be attributed to the occurrence of glass formed by the decay of phyllosilicates when they reach a heart temperature above ~1000°C (Livingston et al., 1998; Cultrone et al., 2004, 2005).

CHAPER 6

SOIL ANALYSES

6.1 Introduction

Soil background levels were established and assessed based on texture on geophysical properties. In order to observe textural differences both sandy and clayey native soils were studied. Native soils were obtained from parkland, farmland, and backyards located outside of Detroit. These locations include Warren, Royal Oak, and Novi. Anthropogenic soils were collected at abandoned industrial sites, demolition residential sites, and undemolished residential sites within 10 to 15 km of the inner city in Detroit. Some residential samples were obtained from vacant lots at former demolition sites. Others were obtained from front yards of abandoned derelict homes. These samples were then reassigned to the fly ash-impacted site category after microscopic analysis was performed.

Within-site variability of geophysical properties were assessed by measuring seven linear transects across native soils in a wooded parkland and anthropogenic soils in urban grassland settings. Four to fourteen topsoil samples (0 to 15 cm depth) were collected for each transect with borings spaced two to 5 m apart. Soil profile variability was also assessed in a suburban area for native soils and in Roosevelt Park for anthropogenic soils.

Each soil sample was measured for pH, EC, and MS. Figure 11 shows locations for 25 soil samples that were specifically chosen to represent the best of each land use type (residential demolition, industrial, and fly ash-impacted). Table 6 shows EC and MS results for samples shown in figure 11 along with the mean (X), standard deviation (S), correlation of variation percent (CV %), and electrical resistivity (ER). The full data set can be seen in Appendix A.

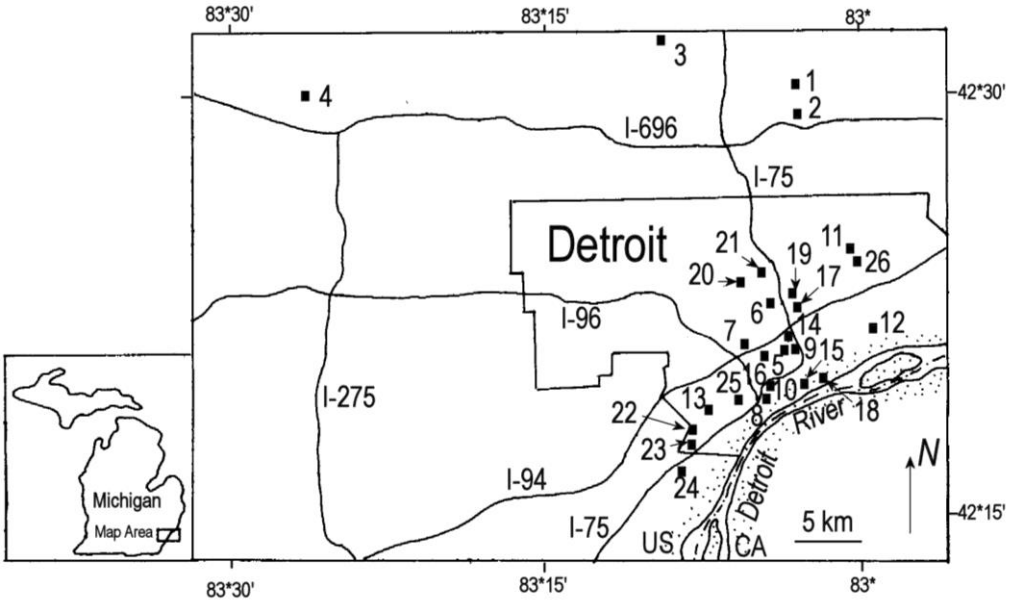

Figure 11: Study area in the Detroit, Michigan showing locations of 25 anthropogenic soils sampled for geophysical and chemical analysis

6.2 Microartifacts in Urban Soils

Generally 5 to 15% of the sand fraction was comprised of MAs in soils located at residential demolition sites. Few soil samples from residential demolition sites contained 30 to 40% MAs in the sand fraction, but 5 to 15% was more common. Soil samples containing 20 to 40% MAs were found at undemolished residential sites. MAs that comprised of 80 to 95% of the sand fraction were found in soil sampled collected at industrial sites. Most common type of MAs found in the soil samples were coal related wastes and were seen in all three of the urban sites that were studied. The common coal related wastes includes unspent coal, ash (microspheres/microagglomerate), cinders, and burnt shale. While coal and charcoal MAs were indistinguishable from one another, coal MAs appeared with cinders, microspheres and microagglomerate.

Residential demolition soil sites typically had a mixed group of MAs representing building waste materials such as brick, mortar, glass, and coal related waste (Fig. 12A and Table 5). Most common residential demolition MAs that were observed on site and in soils were glass, brick, mortar, and cinder. Undemolished residential soils had only microspheres and microagglomerate grains contained in the soil and were most likely airborne deposited (Fig. 12C and Table 5). These sites were later categorized as fly ash-impacted sites. These soils were mostly associated with abandoned derelict homes that were mainly located near railroads or other areas of heavy industrial activity. Industrial soil sites mostly contained coal related waste MAs such as coal, cinder, and ash (Fig. 12B and Table 5). These MAs were often mixed with other MAs unique to manufacturing operations such as coked coal and metalliferous slag. Figure 12 below shows MA assemblages correspond to differences in land use history that were observed at each site.

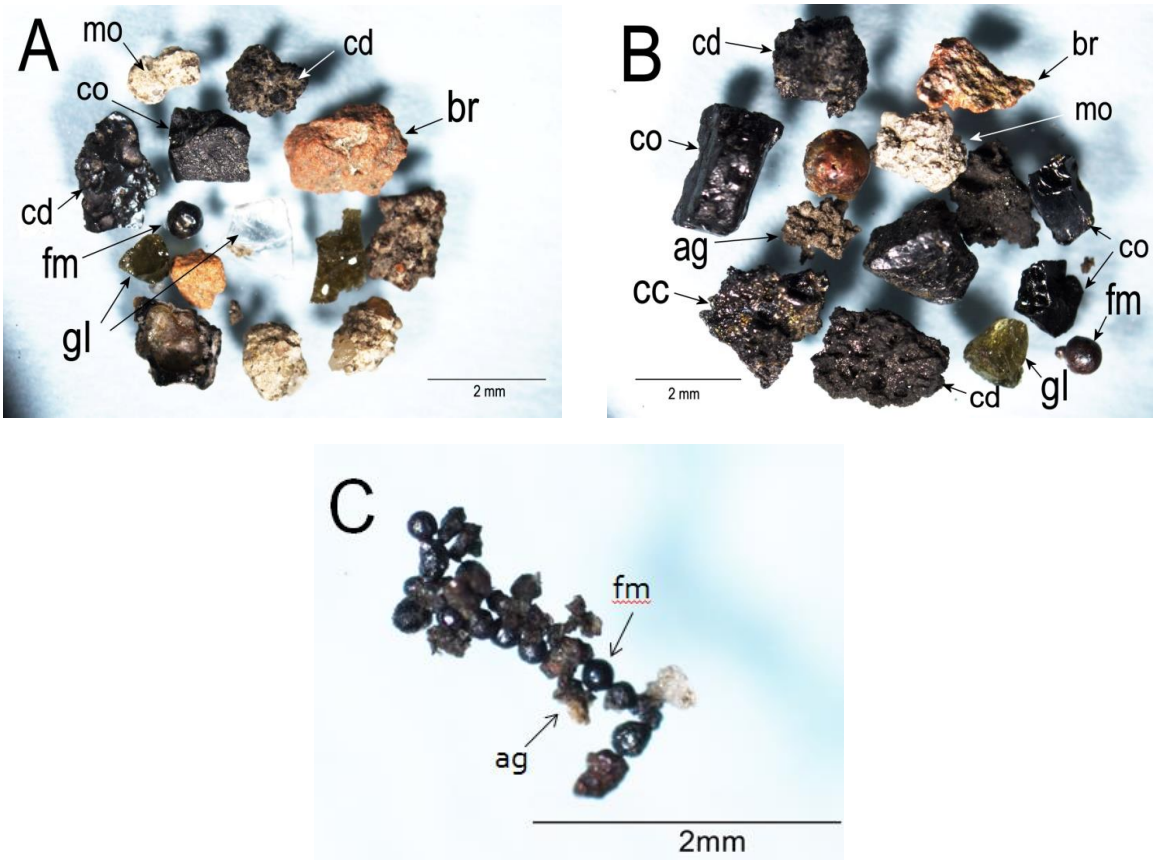

Figure 12: Characteristics of MAs in anthropogenic topsoils, Detroit, MI: A, microartifact assemblage in demolition site soil; B, microartifact assemblage in an industrial site soil; C, microartifact assemblage in fly ash-impacted sites. Symbols are as followed, mo – mortar, cd – coal cinder, br – brick, gl – glass, fm – ferruginous microsphere, cc – coked coal, co – coal, ag – agglomerate.

Table 5: Types of microartifacts found in residential demolition, industrial, and fly ash-impacted sites

Type of Microartifact	Type of Site																			
	Residential Demolition											Industrial				Non-Demolished Residential				
	1	2	3	4	5	6	7	8	9	10	11	12	13	14	15	16	17	18	19	20
Wood	o	o	o	o	o	o	o	o	o	●	o	o	o	o	o	o	o	o	o	o
Charcoal	o	o	o	o	●	o	o	o	o	●	o	o	o	o	o	o	o	o	o	o
Coal	●	o	■	o	●	o	●	●	●	■	●	■	●	■	■	o	o	o	o	o
Coked coal	o	o	o	o	o	o	o	o	o	o	o	o	●	●	●	o	o	o	o	o
Coal cinders	●	■	●	●	●	●	●	■	■	■	●	■	●	●	■	o	o	o	o	o
As. Concrete	●	o	o	o	o	o	o	o	o	o	o	●	o	o	o	o	o	o	o	o
Brick	●	●	●	■	o	■	●	o	■	●	■	●	●	●	●	o	o	o	o	o
Mortar	●	■	●	■	■	■	●	●	●	o	■	●	●	●	o	o	o	o	o	o
Bone	o	o	●	o	o	o	o	o	o	o	o	●	o	o	o	o	o	o	o	o
Glass	■	o	o	●	o	●	●	●	o	●	o	o	o	●	o	o	o	o	o	o
Glass-slag	o	o	o	o	o	o	o	o	o	o	o	o	o	●	o	o	o	o	o	o
Metal. slag	o	o	o	o	o	o	o	o	●	●	o	o	●	●	■	o	o	o	o	o
Corroded iron	o	o	●	●	o	o	o	o	o	o	o	o	o	●	o	o	o	o	o	o
Microspheres	●	●	●	●	●	●	●	o	●	●	o	o	●	●	■	●	■	●	■	●
Microagglomerate	●	■	■	●	o	●	o	■	■	■	o	o	o	●	o	■	■	■	■	■
Wgt. % Magnetic	4.3	4.0	15.3	3.2	0.2	0.5	0.6	1.1	1.5	2.6	2.7	33.7	19.1	12.3	22.2	3.0	3.2	2.9	1.4	1.4

Observations were made between urban sits, topsoil color, and weight % of magnetic microparticles in the study area. Topsoil at residential demolition sites ranged from brown (10YR5/4) to black (10YR3/1) with an increase in soil age. The fine sand fraction at these sites tended to have a concentration of magnetic microparticles of 1 to 4%. In contrast, industrial site topsoil were all very black in color (10YR2/1), and the fine sand fraction had a concentration of magnetic microparticles of 25 to 35%. Fly ash-impacted, undemolished residential topsoil was also black (10YR3/1) but only a 1 to 4% magnetic fine sand fraction.

Overall, the types of MAs found at each urban site were a good representation of previous land use history. Residential demolition sites mainly contained siliceous and calcareous MAs with small amounts of coal related waste. Soils at residential demolition sites varied in color from brown (10YR5/4) to black (10YR3/1) with an increase in soil age and had a low magnetic fine sand fraction. In contrast, MAs found in industrial site soils are dominantly coal-related wastes mixed with other MAs unique to previous manufacturing operations that once took place on the site. Industrial topsoil was consistently very black (10YR2/1) and had a greater amount of magnetic microparticles in the fine sand fraction (25 to 35%) than residential

demolition sites. Fly ash-impacted soils contain only microspheres and microagglomerate grains and were located near the city's railroad and other industrial factories. Fly ash-impacted topsoil was typically black (10YR3/1) similar to industrial sites but only had a 1 to 4% of the fine sand fraction is magnetic similar to residential demolition sites.

6.3 Soil pH

The pH of native soils was found to range from 4.6 to 7.0, and the average being 6.6 (Table 6). Slightly poorly drained soils that were formed from clayey diamicton parent materials were noticeably more acidic than well drained soils developed by glaciolacustrine sand. This is typical of the soils in this study area (Larson, 1977). It can be a result due to dissolution of calcite under low redox conditions. In contrast, the pH of anthropogenic soils ranged from 7.1 to 8.8, the higher basic values being from industrial urban sites and the lower values being samples being from residential demolition sites.

The data in Table 6 suggest that the elevated pH values of anthropogenic soils at residential demolition are a result of the high concentration of calcareous building materials (mortar and brick) contained in the soil. These MAs get deposited by equipment during the demolition process. Previous work indicated that portlandite can leach from mortar and build up its concentration significantly over a course of 30 years or less (Howard et al., 2013). Gypsum ($Ksp = 10^{-4.7}$) and cerrusite ($Ksp = 10^{-4.7}$) are more soluble than portlandite ($Ksp = 10^{-5.2}$). As a result, the time of weathering of plaster and paint may be faster and produced basic cations (Howard et al., 2013, 2015). The pH may have also increased because of the weathering of soda-lime glass from demolition site soils. Ash and cinder wastes from domestic coal-burning era in Detroit may have had an increase effect on the pH as well. Fly ash-impacted sites most likely had

an elevated pH due to concentrations of coal-ash. The contributed factor for elevated pH values for industrial sites is most likely from concentrations of metalliferous slag. Overall, the elevated pH levels that were measured from anthropogenic soils were expected, previous studies have reported similar (Howard and Olszewska, 2011; Howard et al., 2013).

Table 6: Geophysical characteristics of soil surface horizons as a function in land use type. Xm, mean; S, standard deviation; CV, coefficient of variation

Site	pH			Electrical Conductivity ($\mu S\ cm^{-1}$)			Electrical Resistivity(ρ) (Ωm)		Magnetic Susceptibility ($10^{-8}\ m^3\ kg^{-1}$)			Sample
	X	S	CV (%)	X	S	CV (%)	ρ	Corrosivity Index	X	S	CV (%)	
Native Soils												
1	6.96	0.08	1.2	109.5	9.7	8.9	91.3	weak	83.2	5.3	6.4	PM1a
2	7.24	0.06	0.9	189.5	30.1	15.9	52.7	weak	17.2	0.4	2.2	PM5a
3	4.59	0.02	0.5	75.30	0.8	1.0	132.8	very weak	12.7	0.1	0.1	PM2a
4	6.48	0.35	5.5	92.70	1.1	1.2	107.9	very weak	57.2	1.2	2.0	PM4a
5	6.28	0.01	0.1	491.2	6.4	1.3	20.4	moderate	24.3	1.4	5.7	NMS1
6	7.81	0.06	0.7	159.1	24.8	15.6	62.8	weak	158.4	6.0	3.7	MK5
Residential Demolition												
1	8.20	0.35	4.3	240.2	129.8	54.0	41.6	moderate	68.8	0.6	0.8	UC9
2	7.96	0.12	1.5	304.3	92.2	30.3	32.9	moderate	57.5	13.5	23.5	UC8
3	7.60	0.11	1.4	359.0	68.4	19.1	27.9	moderate	167.0	2.1	1.3	UC5
4	7.68	0.01	0.9	221.6	35.5	16.0	45.1	moderate	115.7	4.8	4.2	UC7
5	7.52	0.07	0.9	614.3	134.8	21.9	16.3	strong	131.5	8.0	6.1	UC1
6	7.38	0.19	2.6	876.7	128.9	14.7	11.4	strong	249.7	2.6	1.0	UC3
7	7.65	0.21	2.77	259.2	46.5	17.9	38.6	moderate	174.6	3.6	2.0	G1
8	7.80	0.03	0.36	303.1	24.2	8.0	33.0	moderate	68.3	22.5	32.9	MS2
9	7.51	0.04	0.47	1138.0	834.9	73.3	8.8	strong	30.1	16.0	53.1	MK1
10	7.94	0.02	0.27	358.9	27.1	7.6	27.9	moderate	64.9	9.9	15.3	MS7
Industrial Demolition												
1	7.86	0.14	1.8	398.5	12.0	3.1	25.1	moderate	70.2	2.3	3.3	MS1b
2	7.74	0.01	0.2	354.5	34.7	9.8	28.2	moderate	1857.0	8.0	0.4	MS15a
3	8.75	0.01	0.1	168.8	0.4	0.3	59.2	weak	1183.0	73.8	6.2	MS5
4	7.83	0.06	0.7	433.7	12.7	2.9	23.1	moderate	2436.0	9.5	0.4	ORL
5	7.77	0.02	0.3	320.9	8.7	2.7	31.2	moderate	1918.0	68.1	3.6	HP11
Fly ash-Impacted												
1	7.13	0.07	1.0	539.9	10.1	1.9	18.5	strong	94.8	4.9	5.2	AS1
2	7.83	0.03	0.4	296.0	1.4	0.5	33.8	moderate	90.5	2.4	2.6	AS2
3	7.80	0.09	1.2	483.8	45.5	9.4	20.7	moderate	296.5	4.6	1.5	DA1
4	7.98	0.01	0.1	208.9	22.3	10.7	47.9	moderate	302.5	1.7	0.6	DA3
5	7.72	0.01	0.2	236.2	8.2	3.5	42.3	moderate	111.0	0.1	0.0	DA5

6.4 Electrical Conductivity

Background EC of native soils (Table 6) was between 75 µS cm^{-1} and 490 µS cm^{-1}, averaging to 125.2 µS cm^{-1}. EC of anthropogenic surface horizons ranged between 368 µS cm^{-1} and 1138 µS cm^{-1}, averaging to 355.1 µS cm^{-1}. Therefore, anthropogenic soil samples were about twice the average of the background levels indicated by native soils. The overall EC results show residential demolition sites > fly ash-impacted sites > industrial sites (Fig. 13). The calculated resistivity for each sample suggested that native soils were weakly corrosive to metals. In contrast, anthropogenic soils were moderately to strongly corrosive to metals. There were statistically significant differences between all of the geophysical properties of native vs. anthropogenic soils (Table 7 and 8).

Residential demolition sites had the highest EC values, averaging to 393 µS cm^{-1}. Thus, the values for residential demolition sites were almost three times greater than the background soil samples collected. This is most likely due to the calcareous (concrete and mortar) and ferruginous (corroded nails) microartifacts from architectural debris contain within the soil that was commonly observed at residential demolition sites. Fly ash-impacted sites and industrial sites had similar EC values averaging between 353 µS $cm^{-}1$ and 335 µS cm^{-1}respectively. Fly ash-impacted and industrial sites had EC values that were not as great as the residential demolition sites, but there is a noticeable difference that can be observed between industrial and fly ash-impacted sites and the background sites. Fly ash-impacted and industrial soils were most likely affected by the ferruginous components of coal-related and steel-making wastes.

Table 7: Mean values of electrical conductivity and magnetic susceptibility as a function of differences in land use type

	Geophysical Parameter				
Land Use Type	Electrical Conductivity ($\mu S\ cm^{-1}$)		Magnetic Susceptibility ($10^{-8}\ m^3\ kg^{-1}$)		Sample Size
Mean and Standard Deviation	Xa*	Sa	Xg	Sg	n
Native	125.2	42.6	40.0	2.7	5
Industrial	335.3	102.4	937.6	4.3	5
Residential demolition	393.0	215.6	94.6	1.9	9
Fly ash-impacted	353.0	149.7	154.9	1.8	5

*Xa, arithmetic mean; Sa, arithmetic standard deviation; Xg, geometric mean; Sg, geometric standard deviation.

Table 8: Calculated t-values for testing differences in means, and their statistical significance

Land Use Type	Electrical Conductivity				Magnetic Susceptibility			
	Parkland	Industrial	Demolished	Fly Ash-Impacted	Parkland	Industrial	Demolished	Fly Ash-Impacted
Native	--	4.240***	2.710**	3.270**	--	4.255***	2.166**	2.680**
Industrial	--	--	0.560	0.218	--	--	4.29***	2.524**
Demolished	--	--	--	0.336	--	--	--	1.405
Undemolished	--	--	--	--	--	--	--	--

*Probably significant, $p = 0.10$; **Significant, $p = 0.05$; ***Highly significant, $p = 0.01$

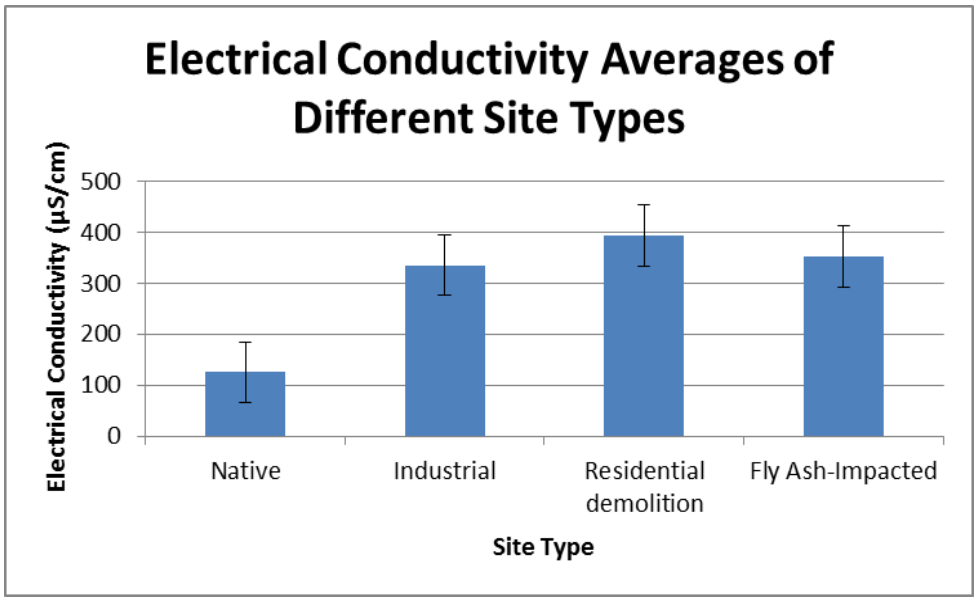

Figure 13: Electrical conductivity results from four different sites

6.5 Magnetic Susceptibility

In order to obtain mass specific susceptibility using lab methods, k values are divided by the bulk density of the sample. The bulk density of the sample is calculated by dividing the mass of the sample by the volume of the sample. The value k is $-0.9x10^{-5}$ for $10cm^3$. The value k is first divided by 1000 for unit conversion.

MS equation (Mullins, 1977):

1) $k/1000 = -0.9x10^{-8}\ m^3kg^{-1}$

2) $X = k/p$

X (mass specific susceptibility), k (volume susceptibility), p (bulk density)

Background soil samples had MS values between 24 x 10^{-8} m^3 kg^{-1} and 160 x 10^{-8} m^3 kg^{-1}, averaging to 40 x 10^{-8} m^3 kg^{-1}. Sandy parent materials in the study area were generally found to have a MS of 34 to 38 x 10^{-8} m^3 kg^{-1}. However, local glaciolacustrine sand MS ranged up to 150 x 10^{-8} m^3 kg^{-1}. This is attributed to placer deposits formed by lacustrine wave activity. These placer deposits contain slightly higher concentrations of detrital magnetite which increases MS. Clayey diamicton parent materials had a MS of 65 to 70 x 10^{-8} m^3 kg^{-1}.

Anthropogenic MS results showed industrial sites > fly ash-impacted sites > residential demolition sites (Fig. 14). Industrial sites had the greatest MS values averaging to 937.6 x 10^{-8} m^3 kg^{-1}. These results show that industrial sites had a MS value greater than 20 times of sampled background levels. MS at residential demolition sites had values between 30 x 10^{-8} m^3 kg^{-1} and 250 x 10^{-8} m^3 kg^{-1}, averaging to 94.6 x 10^{-8} m^3 kg^{-1}. Fly ash-impacted sites were between 90 m^3 x 10^{-8} kg^{-1} and 300 x 10^{-8} m^3 kg^{-1}, averaging to 154.9 x 10^{-8} m^3 kg^{-1}. MS for residential demolition sites and fly ash-impacted sites showed similar results. Though their MS values aren't as great as

the samples measured from industrial sites, their values are still two to three times greater than the background levels.

The results in Table 8 show that the differences in EC and MS between native and anthropogenic soils are statistically highly significant. No significant differences in EC were found amongst the different types of anthropogenic soils. However, industrial site soils had a significantly different MS from the other types of anthropogenic soils. The difference in MS between residential demolition and fly ash-impacted site soils was not statistically significant.

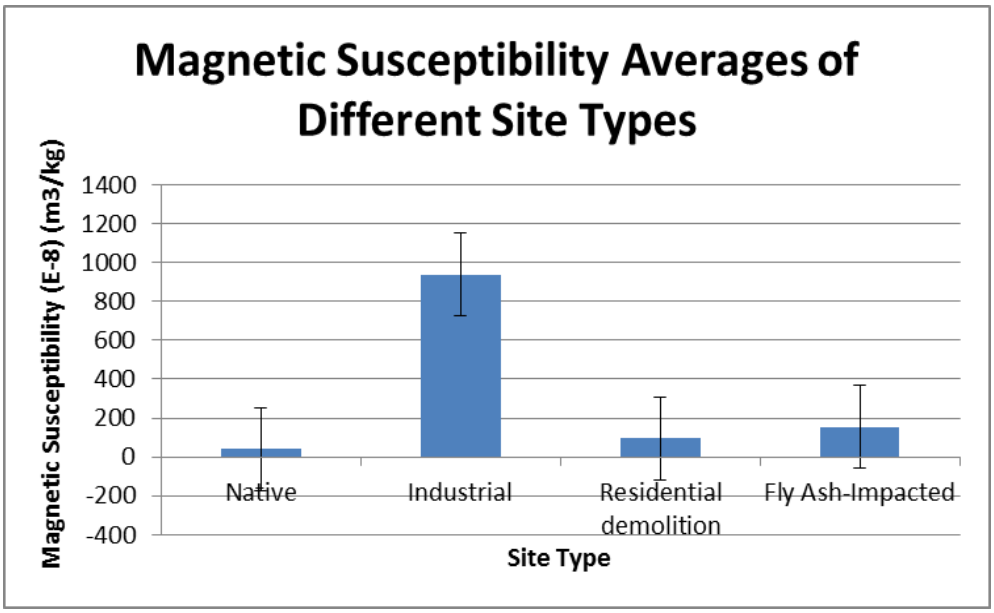

Figure 14: Magnetic susceptibility results from four different sites

Elevated levels of MS have been widely reported for anthropogenic soils in previous studies (Strzyszcz et al., 2006; Magiera et al., 2006; Yang et al., 2010, 2012). Anthropogenic soils that had the greatest impact resulted in concentrations of metallurgical wastes (Durza, 1999; Rosowiecha and Nawerocki, 2010). Fly ash-impacted soils have been previously recognized to be located at distances of 10 km or more from coal-fired power plants in other studies (Schmidt et al., 2000). The elevated MS from this study is associated with fly ash-impacted soils that

contain highly magnetic ferruginous microspheres which were seen in all three urban sites. These microspheres are known to be a by-product of coal combustion and can be seen greatly on industrial and fly ash-impacted sites (Lanteigne et al., 201; Sharonova et al., 2013). Similarly to EC measurements, magnetic microspheres and other ferruginous wastes were likely contributing to the elevated values of MS in anthropogenic soils, being most abundant in industrial site soils.

6.6 Transects

6.6.1 Introduction

Transects were made in native and anthropogenic soils. Results from anthropogenic soil transects suggest that EC and MS can be measured reasonably and precisely in a given vacant lot when the CV % of EC and MC is less than 40%. This implies that a sample can be good representative of a lot that is 10 to 20 m in size. Native soils with a CV % less than 40% suggest that native soils are easily replicable. Maps and graphs were made from transect samples taken from Kenny and Gilbo St. crossroads and Wisner and Gilbo St. crossroads. The maps and graphs show EC and MS spatial distribution from collected samples.

6.6.2 Wisner St. Transect

Wisner St. transect was sampled the east side of Detroit, about one block west from the Coleman A. Young International Airport. This sample site was composed of one transect running NW to SE on a residential demolition vacant lot (Fig. 15). A total of 7 sample points were measured and collected with a spacing of 5 m apart. This site has been previously mapped my Dr. Jeffrey Howard, as discussed in section 1.2, with a hand auger which showed a spatial distribution pattern of the artifact content.

Figure 15: Sample points of the Wisner St. transect

Wisner St. transects were gridded off in the center of one vacant lot. EC values ranged between 179.6 µS cm^{-1} and 280.7 µS cm^{-1} (Table 9 and Figure 16). Figure 16 shows that both EC and MS values are fairly consistent. MS values ranged between 797.9 m^3 g^{-1} and 209.7 x 10^{-8} m^3 g^{-1} (Table 9 and Figure 16). High EC and MS values can potentially show where and what type of large amounts of debris and waste are located from previous demolitions. The high EC and MS values were observed on the south side of the sampled transect. Overall, these high EC and MS values suggest that there is a probability of a high concentration of ferruginous (iron nails) and calcareous (concrete) MAs, i.e. architectural debris in the south east corner of the lot.

Table 9: Wisner St. transect electrical conductivity, magnetic susceptibility, and pH results

Anthropogenic Transects			
Sample	**EC ($\mu S\ cm^{-1}$)**	**MS (10^{-8}) (m3/kg)**	**pH**
Wisner St.			
A1	126	131	7.7
B1	180	210	7.7
C1	180	259	7.9
D1	204	260	7.9
E1	281	236	7.7
F1	231	247	7.9
G1	186	768	7.9
Average	198.3	301.6	7.8

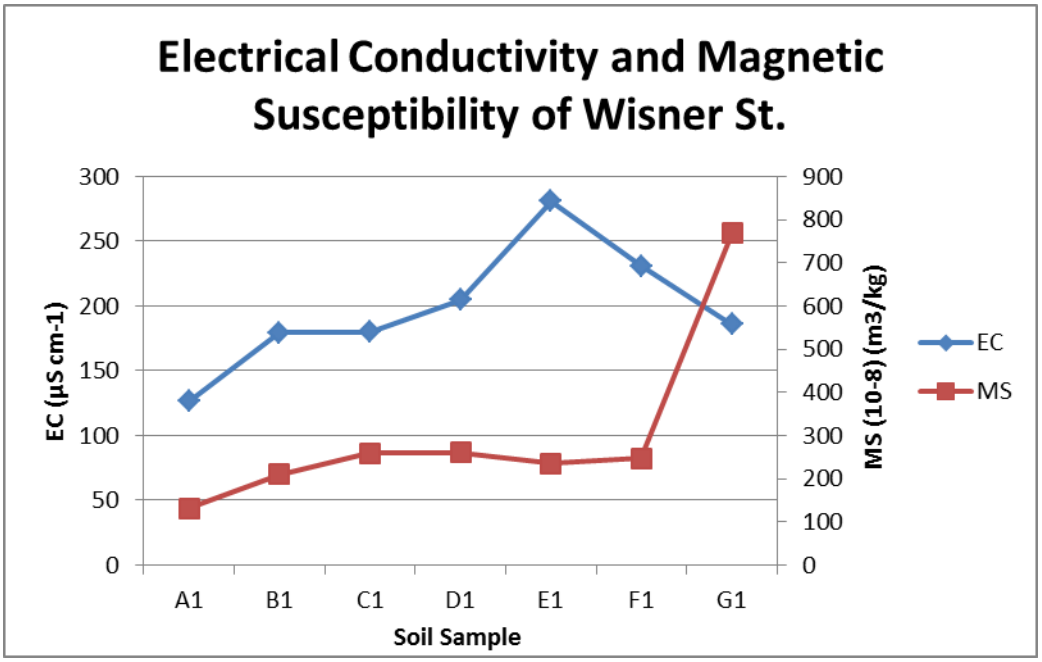

Figure 16: Electrical conductivity and magnetic susceptibility of Wisner St.

6.6.3 Kenney St. Transect

The Kenney St. transect was located on the east side of Detroit site one block from the Wisner St. transect. This sample site was composed of two transects running NW to SE straddling two vacant lots. A total of 14 sample points were measured and collected, 7 for each transect, with a spacing of 5 m apart. This site is considered as a residential demolition site with an obvious wide span of vacant land (Fig. 17).

Figure 17: Sample points from Gilbo St. transects

EC values ranged between 230 µS cm^{-1} and 608 µS cm^{-1} (Table 10 and Figure 18). Figure 19 shows that the highest EC values (left) are located on the SE side of the site. The high EC values are showing an obvious linear pattern. Low EC values started in the NW corner of the map and continued to the SW corner, making the low EC values also having a linear pattern. MS values ranged between 40.1 $m^3 g^{-1}$ and 121.7 x 10^{-8} $m^3 g^{-1}$ (Table 10 and Figure 18). Figure 19

shows the highest MS values (right) located SW and the lowest values mainly located NE. The locations of high and low MS values are heavily concentrated in one area and in result do not make the same linear pattern as the EC measurements showed. High EC and MS values suggest that there is a probability of high concentrations of ferruginous and calcareous MAs are mainly located with correspondence to where the foundation of the house once laid. The MS hot spot could also mark the location of magnetic coal combustion products.

Table 10: Kenney St. transect electrical conductivity, magnetic susceptibility, and pH results

Anthropogenic Transects			
Sample	**EC ($\mu S\ cm^{-1}$)**	**MS (10^{-8}) (m3/kg)**	**pH**
Kenney St.			
K1	230	60.6	7.8
K2	272	79.1	7.7
K3	255	60.1	7.5
K4	325	121	7.7
K5	363	89.9	7.5
K6	267	39.7	7.6
K7	304	40.1	7.7
K8	405	65.4	7.4
K9	432	48.4	7.5
K10	473	49.8	7.7
K11	543	68.3	7.6
K12	600	63.6	7.6
K13	608	59.7	7.4
K14	604	46.6	7.6
Average	406	63.8	7.6

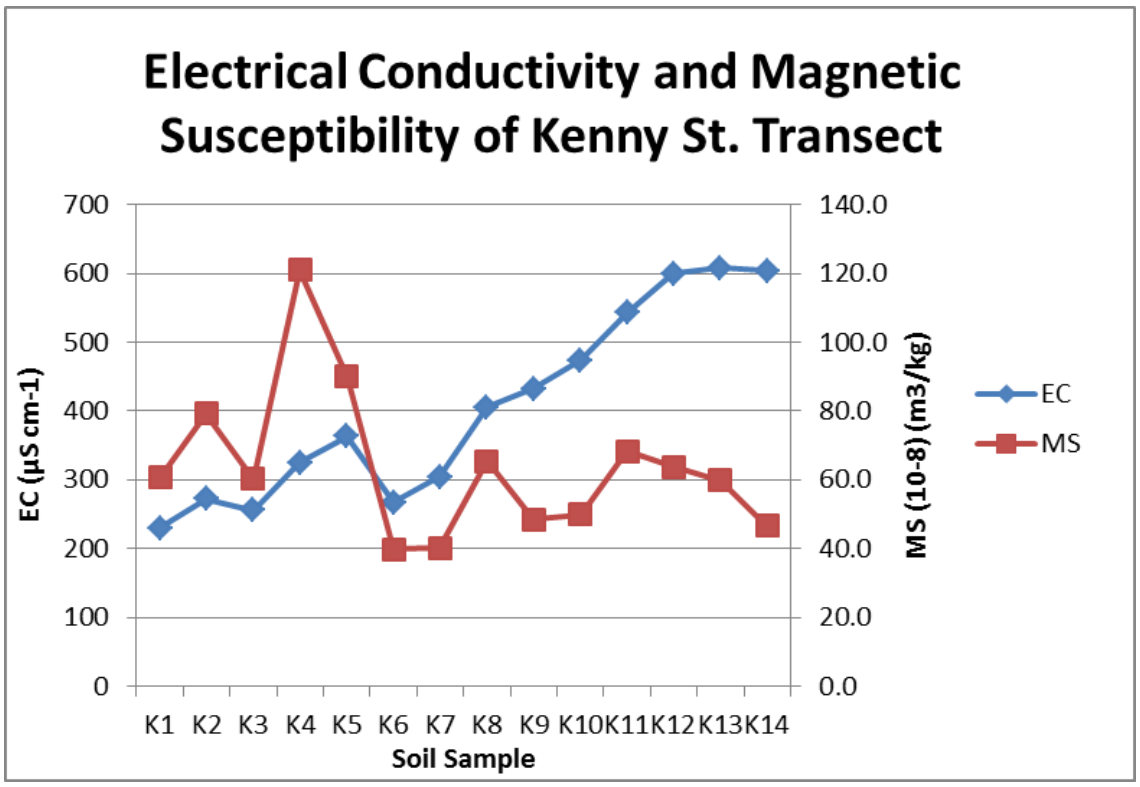

Figure 18: Electrical conductivity and magnetic susceptibility of Kenny St.

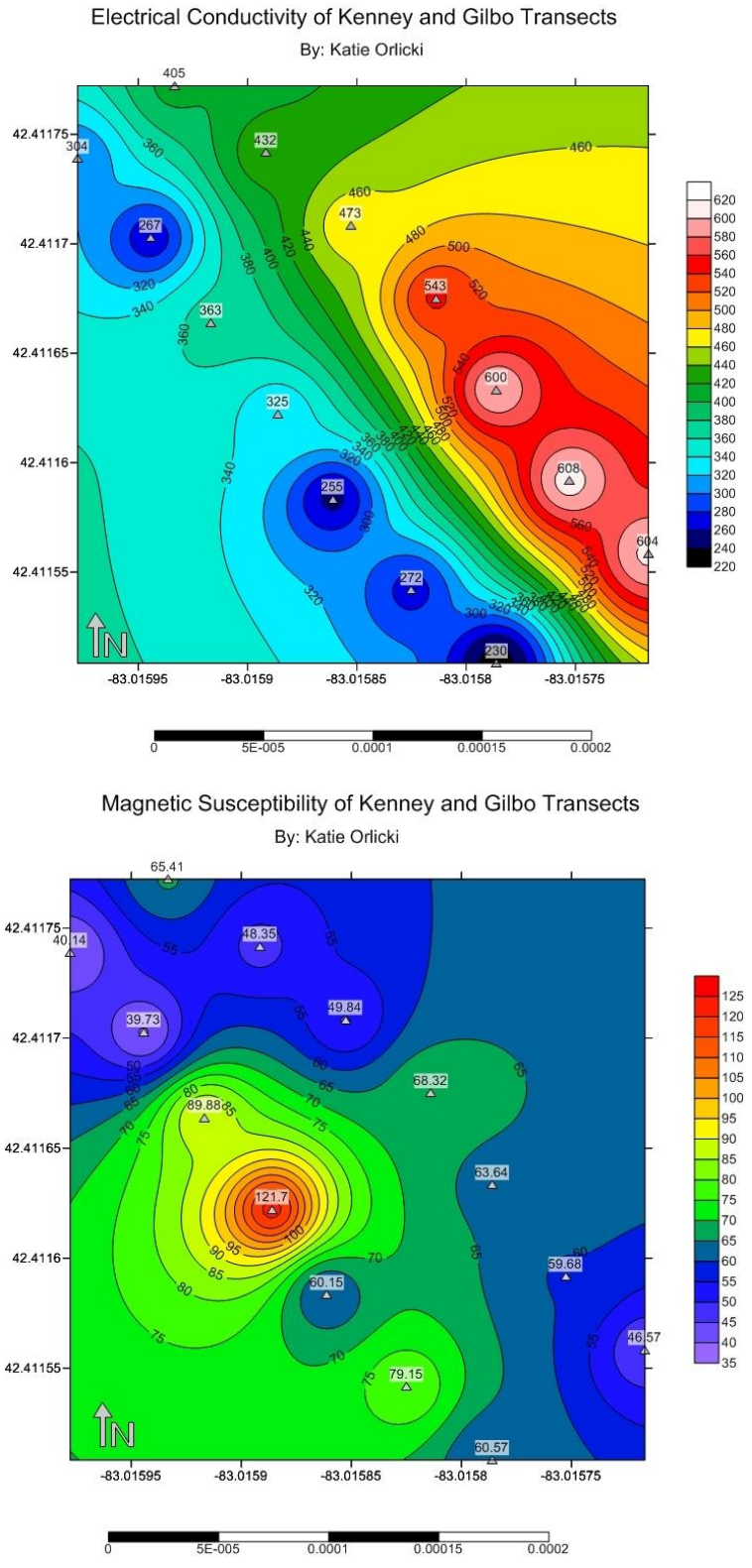

Figure 19: Map on the left is the Gilbo St. electrical conductivity transect and the map on the right is the magnetic susceptibility transect

6.6.4 Native Transects

Two native transects were sampled outside of Detroit in Warren, MI. Site 1 (PM-1A) transect consisted on 4 samples that were collected every 2 m. Measured EC ranged between 130 µS cm^{-1} and 161 µS cm^{-1} (Table 11 and Figure 20 and 21). MS values ranged between 29.0 x 10^{-8} m^3 kg^{-1} and 83.2 x 10^{-8} m^3 kg^{-1} (Table 9). Site 2 (PM-2A) showed similar results with EC ranging between 89.2 µS cm^{-1} and 120 µS cm^{-1} and MS ranging between 11.5 m^3 g^{-1} and 21.5 m^3 g^{-1} (Table 11 Figure 20 and 21). Overall, native soil transects were consistent and similar to one another. Native soil transects showed a smaller range in EC and MS values than anthropogenic transects.

Table 11: Native soil transects electrical conductivity, magnetic susceptibility, and pH results

Native Transects			
Sample	**EC (µS cm^{-1})**	**MS (10^{-8}) (m3/kg)**	**pH**
Site 1			
PM-1A-1	161	83.2	7.0
PM-1A-2	151	48.9	4.6
PM-1A-3	140	29.0	4.8
PM-1A-4	130	57.2	6.5
Average	145.5	54.6	5.7
Site 2			
PM-2A-1	120	18.2	6.5
PM-2A-2	110	11.5	6.1
PM-2A-3	99.4	21.5	6.3
PM-2A-4	89.2	19.1	6.4
Average	104.7	17.6	6.3

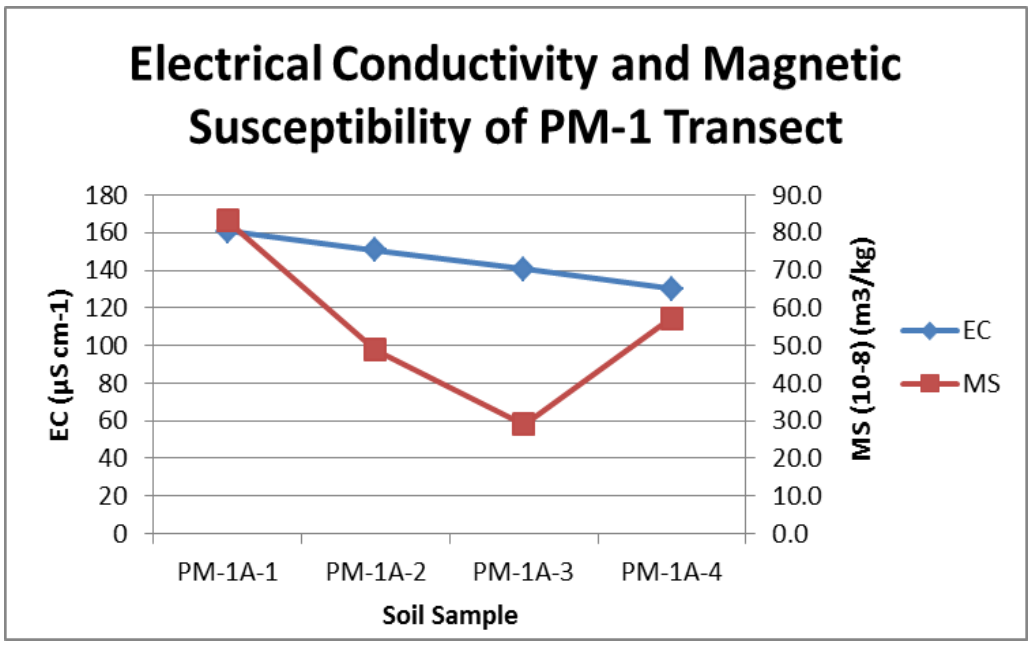

Figure 20: Electrical conductivity and magnetic susceptibility of transect PM-1

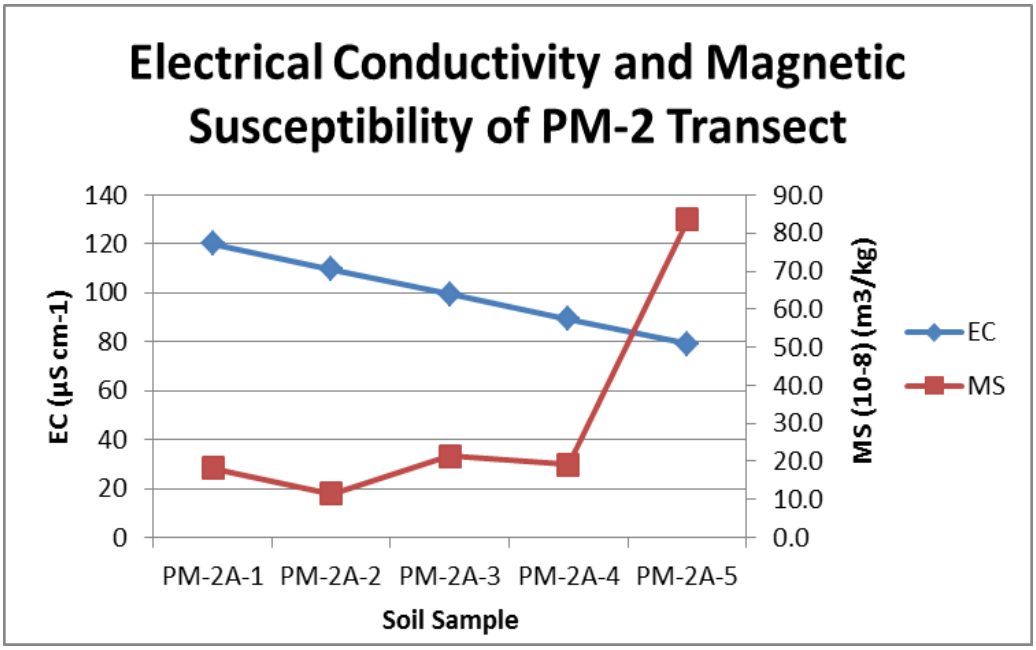

Figure 21: Electrical conductivity and magnetic susceptibility of transect PM-2

6.6.5 Overall comparison

The pH values were more variable in native soils than anthropogenic soils (Table 12). This is attributed to variations in the distribution of woodland and grassland vegetation. The EC and MS were both more variable for anthropogenic soils than for native. This was expected because anthropogenic soils are characteristically highly variable. EC showed to have a covariance of less than 40% for both anthropogenic and native transects suggesting that one sample is a strong representation over a distance of 10 to 20 m. MS showed high variability with 106.2% covariance for Wisner St. transect. Given that MS is highly sensitive to the presence of ferromagnetic minerals variability is to be expected.

Table 12: Mean, standard deviation, and covariance variation % of pH, EC, and MS for anthropogenic and native transects

Transect Site	Soil Type	pH			EC (µS cm^{-1})			MS (10^{-8} m3/kg)		
		X	S	CV%	Xa	Sa	CV%	Xg	Sg	CV%
Kenney and Gilbo St.	Anthropogenic	7.59	0.12	1.59	405.79	139.08	34.27	63.74	21.70	34.05
Wisner and Gilbo St.	Anthropogenic	7.81	0.11	1.37	198.29	48.29	24.35	198.29	210.50	106.16
PM-1A	Native	5.73	1.20	21.03	145.50	13.43	9.23	54.58	22.45	41.14
PM-2A	Native	6.16	0.40	6.45	99.52	16.25	16.33	17.58	4.28	24.37

High MS readings for Kenney and Gilbo St. (121.7 x 10^{-8} m^3 g^{-1}) were less than Wisner St (767.1 m^3 g^{-1}). Whereas, high EC values for Kenney and Gilbo St. (608 µS cm^{-1}) were greater than Wisner St. (280 µS cm^{-1}). This may be caused by the different types and percent concentration of microartifacts found within the soil. For example, high concentrations of mortar will result in higher EC values where high concentrations of nails and piping will produce high MS measurements. Overall, spatial distributions EC and MS can be determined. The transect

data suggests that, in contrast to vacant lots which have very high variability, one topsoil sample from native soils can be a moderate representation on a scale of 10 to 20 m.

6.7 Soil Profiles

6.7.1 Introduction

Anthropogenic and native soil profiles were observed and analyzed in order to identify their geophysical and chemical differences. Two profiles were excavated in Roosevelt Park, Detroit where houses used to stand when the Michigan Central Train Station was first built. The soil within the profiles were clearly disturbed and had a number of ash layers due to it most likely being a burn pit at one time. Four native soil profiles were made outside of Detroit in Dr. Jeffrey Howard's backyard and were identified as undisturbed.

The purpose of studying urban vs. native soil profiles is to observe the affect disturbed and anthropogenic soil has on EC, MS, and pH properties at different profile depths. Roosevelt Park has been excavated in previous years by Dr. Krysta Ryzewski archaeology class. The Roosevelt Park profiles being analyzed in this study took place during the fall 2012 excavation.

6.7.2 Roosevelt Park Background

Located in the center of the city, Corktown is one of the oldest remaining neighborhoods in Detroit, MI. In the 18th century European settlers established property and boundary lines by parceling the land into small individual property claims (Ryzewski, 2012). These property claims started at the edge of the Detroit River and expanded northwards and are commonly referred to as ribbon farms. By the late 1830s Corktown started to change from agricultural land to urban land. In the 1840s a large population of Irish immigrants concentrated in Corktown making it

their home (Ryzewski, 2012). In 1908 homes that once occupied Roosevelt Park (Fig. 19) started to be demolished in order to make room for the Michigan Central Train Station (Ryzewski, 2012). The purpose of Roosevelt Park was to create a grand entryway into Detroit for visitors once they exit the train station (Ryzewski, 2015).

Figure 22: Roosevelt Park before housing demolition (Ryzewski, 2012)

In 2012, an archaeological excavation took place at Roosevelt Park in order to identify the history, lifestyles, and social interactions that used to take place in this neighborhood when homes were first built. Three previously housed lots were excavated and analyzed for artifacts and soil content. However, a detailed soil profile analysis of magnetic susceptibility and electrical conductivity was done for only one lot due to time constraints and project requirements. Two profiles were analyzed, one along the East wall of the excavation site and

another along the South. Below, Figure 20 shows the location of where this excavation took place.

Figure 23: Outline of Roosevelt Park Profile showing excavation sampling point within the park

6.7.3 Excavation and anthropogenic soil profiles

Upon excavation it was clear that this site was once previously used as a trash dump and/or a privy. There were a number of ash and charcoal layers throughout the profiles along with clay, loam, and sand. A large amount of artifacts were excavated from this site such as, fully intacked glass bottles, ceramic pieces, architectural material, etc (Fig. 21). A detailed soil profile description can be seen in Figure 24 for both the East and South wall. It has been observed that despite about a century length of burial the artifacts have been very well preserved (Howard et al., 2015). Artifacts were not severely impacted by weathering due to a calcareous

soil environment and artificial compaction, which overall limited weathering effects from water and oxygen (Howard et al., 2015).

Figure 24: Artifacts found in context layers

Graphs were made to show the results of EC and MS for both the East and South wall profiles (Fig. 22 and 23). As artifacts were collected a count was done for each context layer and can be seen in Table 13. It should be noted that only artifacts that were about 3 cm in size were accounted for. Microartifacts were then analyzed through microscope work, EC, MS, and pH measurements.

Table 13: Artifact count for each context layer

	Artifacts										
Context Layer	**Glass**	**Metal (not iron)**	**Metal (iron)**	**Ceramics**	**Bone**	**Brick**	**Mortar**	**Plaster**	**Slag**	**Charcoal**	**Coal**
RP 38	210	26	306	39	60	22	0	0	0	0	0
RP 53	61	141	7	20	30	0	0	0	11	0	0
RP 63	592	67	635	127	391	6	9	0	0	0	29
RP 73	264	17	369	107	407	23	1	1	0	31	0
RP 100	0	0	7	2	19	1	0	0	0	11	0
RP 106	0	0	2	4	11	3	0	0	0	2	0

The East wall profile had high EC and MS values for the topsoil context layer, RP 38. EC results were 388 µS cm^{-1} and MS results were 208 x 10^{-8} m^3 kg^{-1} for RP 38 (Table 14). The high EC and MS values can be explained by the types of artifacts and microartifacts that were observed along with high organic content. RP 38 was composed mostly of topsoil and contained architectural debris such as nails, brick, and glass. Topsoil generally has a higher magnetic susceptibility than bedrocks and subsoils. This is due to the concentration of iron minerals in topsoil as a result form weathering of parent rock or deposited from anthropogenic sources (Clark, 2005). Topsoil MS can also be affected by vegetation fires, fermentation effects, oxidation-reduction cycles due to wetting and drying of soil (Clark, 2005). As the depth of the soil profile increased, EC and MS values slowly decreased. RP 63 had an EC value of 207 µS cm^{-1} and MS of 83 x 10^{-8} m^3 kg^{-1} (Table 14). RP 63 was composed of brown and black mottled loamy soil with charcoal debris spread throughout, most likely due to trash pit burning. A large amount of artifacts were discovered in this context layer. The artifacts ranged from architectural debris to ceramics and glass bottles. Once context layer RP 63 was broken through a sandy parent material started to be revealed. Parent material was observed in context layers RP 100 and RP 106. As the profile increased with depth the artifact concentration started to decrease. The results for pH were constant throughout the profile except in context layer RP 63. This is most likely due to the mortar line found on the surface that was revealed throughout this layer.

The East wall profile showed that EC and MS values were high for context layers that were anthropogenic and that contained a large amount of artifacts. As the profile increased with depth, the concentration of artifacts and anthropogenic soils decreased. Resulting in low EC and MS values at the lowest depth of the profile where parent soil was reached. The pH is not greatly affected by the concentration of artifacts or microartifacts found in the soil.

Table 14: East wall electrical conductivity, magnetic susceptibility, and pH results

East Wall Profile			
Context Layer	EC ($\mu S\ cm^{-1}$)	MS (10^{-8}) (m3/kg)	pH
RP 38	388	208	7.7
RP 63	207	83	6.8
RP 100	104	83	7.8
RP 106	80	80	7.8

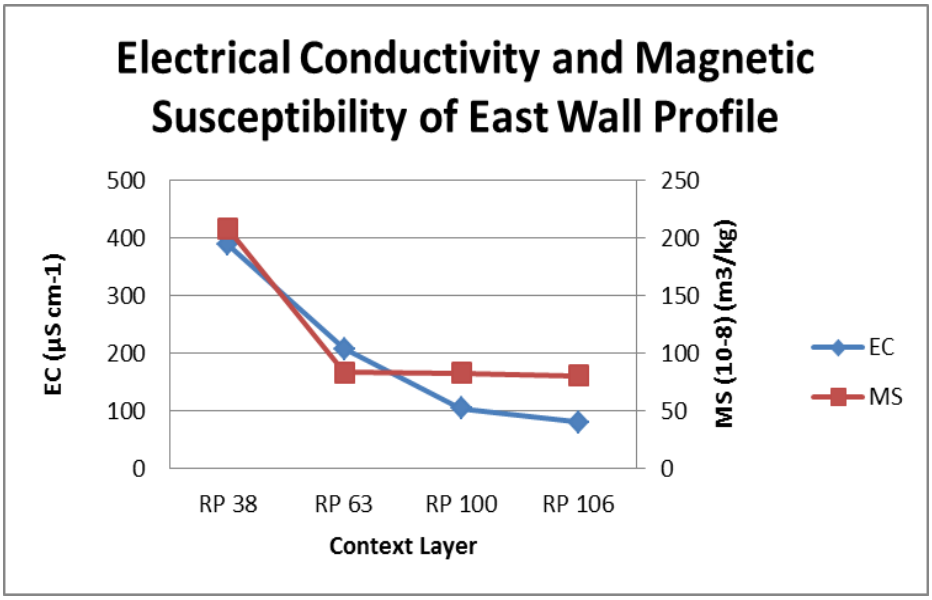

Figure 25: Electrical conductivity and magnetic susceptibility of South wall profile

The South wall profile had a greater depth that contained an increased amount of context layers. EC and MS results are very similar to the East wall profile. The topsoil context layer, RP 38, had high EC and MS values and then as the profile increased with depth, EC and MS values gradually decreased (Table 15). The pH values were constant throughout the profile, similarly to the East wall profile. The South wall profile had a significant feature that was observed, unlike the East wall where no features were found. Feature 25 was found between RP 100 and RP 106 where a parent sandy material begins to appear. Feature 25 consisted of a coarse black fill that occupied a trench where possibly a pipe once laid. Feature 25 had high EC and MS values and

spiked dramatically, it is especially noticeable because lies between two native sand context layers. This profile was able to show that not only can EC and MS identify context layers with large concentration of artifacts but it can possible identify where features are located based on their type of fill.

Table 15: South wall electrical conductivity, magnetic susceptibility, and pH results

South Wall Profile			
Context Layer	**EC (µS cm^{-1})**	**MS (10-8) (m3/kg)**	**pH**
RP 38	388	208	7.6
RP 53	212	276	7.9
RP 73	101	60	7.9
RP 100	104	83	7.8
Feature 25	625	163	8.0
RP 106	80	7	7.9

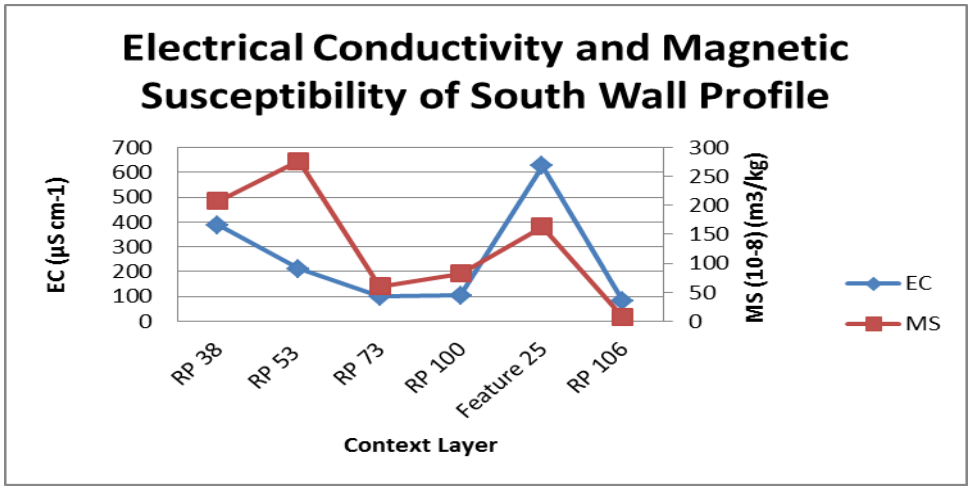

Figure 26: Electrical Conductivity and Magnetic Susceptibility of south wall profile

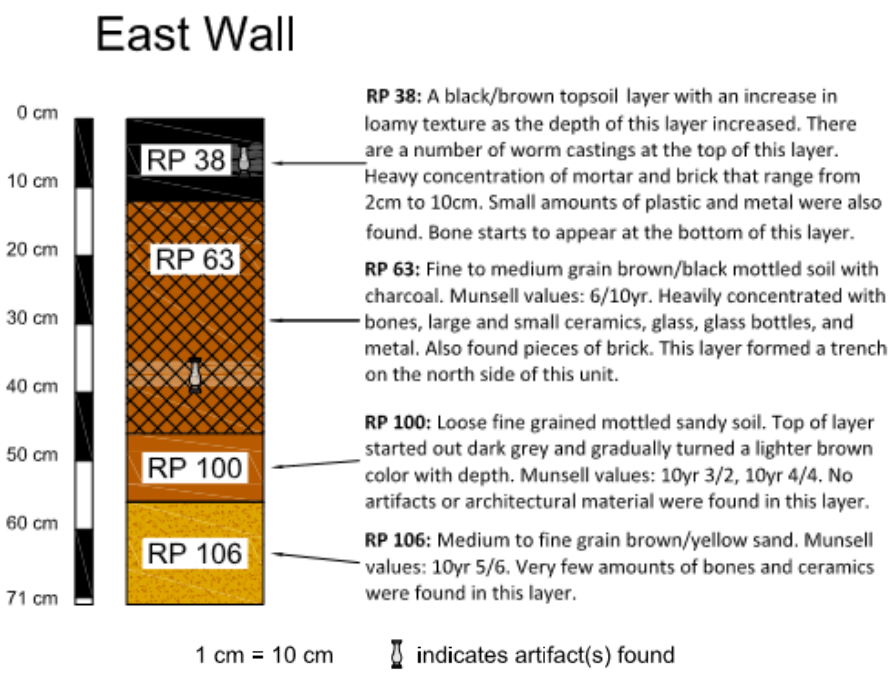

Figure 27: Profile descriptions of the East wall context layers

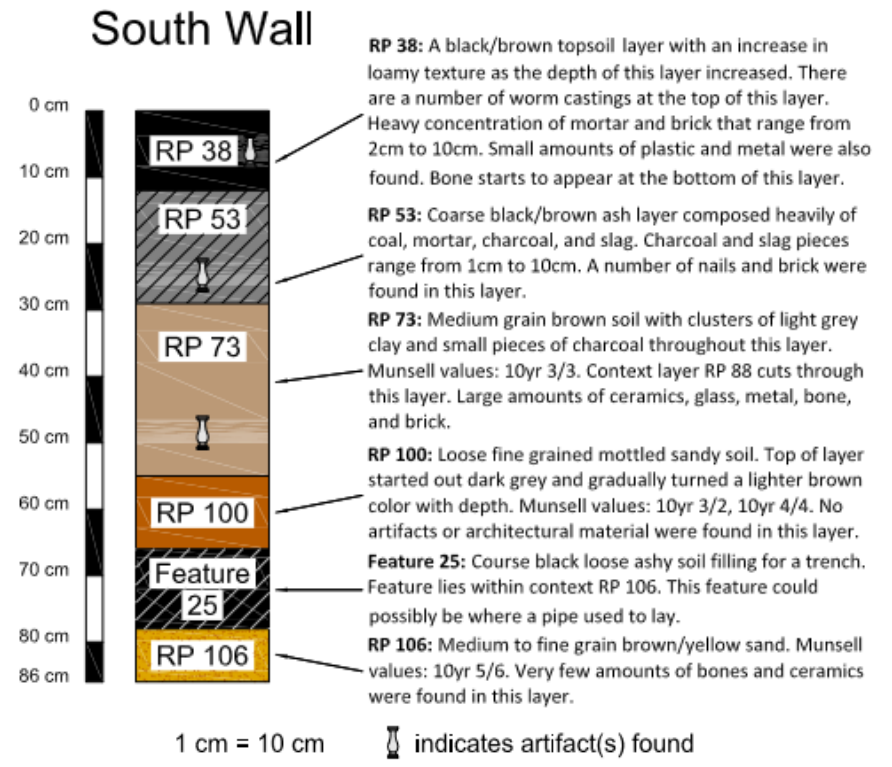

Figure 28: Profile description of the South wall context layer

6.7.4 Native Profiles

Native soil profiles were analyzed outside of the Detroit boundary in Dr. Jeffrey Howard's backyard located in Warren, MI. EC measurements ranged between 29 µS cm^{-1} and 247 µS cm^{-1}, MS ranging between 0.7 x 10^{-8} m^3 kg^{-1} and 83 m^3kg^{-1}, and pH ranging between 5.9 and 8.2. Highest EC readings were from profile PM4 at 247.1 µS cm^{-1} (Table 16). Otherwise, all other samples had EC values less than 200 µS cm^{-1}. Highest MS readings were 83 x 10^{-8} m^3 kg^{-1} and 82 m^3 kg^{-1} from profiles PM1 and PM4. All other native samples had MS values less than 80 m^3kg^{-1}. The pH values were +/- 1 from 7.0, which was expected. Overall, native soil profile readings showed similar values between one another.

The EC of the A horizons of the native soil profiles were elevated compared to the subsoil (Fig. 25). Previous studies have shown that EC is often correlated positively with cation exchange capacity (Golovko and Pozdnyakov, 2007; Doolittle and Brevik, 2014). Therefore, the amount of organic matter within the soil related to the cation exchange capacity can likely explain the observed high EC values for the topsoil. Previous studies have also observed electron transfer reactions associated with microbial nanowires from filamentous bacteria, which could affect EC values of the A horizon (Ntarlagiannis et al., 2007; Pfeffer et al., 2012). Native topsoil samples have shown lower EC values than anthropogenic topsoil. This is due to anthropogenic samples containing artifacts and being frequently disturbed. Generally, native soil profiles increased with depth the subsoils had similar EC values with an exception for profile PM4 (Fig. 25). The sudden increase of EC seen in profile PM4 is possibly due to a pedogenic carbonate that can commonly be observed in poorly drained soils (Howard et al., 2012).

Table 16: Native soil profiles electrical conductivity, magnetic suceptibilyt, and pH results

Native Soil Profiles				
Layer Number	**Sample**	**EC (µS cm^{-1})**	**MS (10^{-8}) (m3/kg)**	**pH**
Site 1				
1	PM1-A	109.5	83.2	7.0
2	PM1-B	79.6	31.8	7.0
3	PM1-C	56.0	23.6	6.6
4	PM1-D	31.1	14.7	6.0
5	PM1-E	43.5	8.9	6.4
6	PM1-F	32.7	8.5	5.9
7	PM1-G	29.0	11.5	6.0
Average		54.5	26.0	6.0
Site 2				
1	PM2-A	153.8	18.2	6.5
2	PM2-B	45.2	10.4	6.9
3	PM2-C	52.5	13.4	7.0
4	PM2-D	54.3	13.0	7.3
5	PM2-E	64.4	13.6	7.2
6	PM2-F	52.8	17.4	7.8
7	PM2-G	123.8	21.7	8.2
8	PM2-H	78.8	19.3	7.9
Average		78.2	15.9	7.4
Site 3				
1	PM4-A	103.2	82.3	7.3
2	PM4-B	86.4	59.6	7.3
3	PM4-C	64.0	36.6	7.7
4	PM4-D	149.3	29.7	8.1
5	PM4-E	247.1	28.6	8.0
Average		130.0	47.4	7.7
Site 4				
1	PM5-A	189.4	17.7	7.2
2	PM5-B	50.3	0.8	7.3
3	PM5-C	56.8	0.7	6.5
4	PM5-D	63.0	0.6	7.4
5	PM5-E	43.1	1.3	7.6
6	PM5-F	64.9	0.7	7.9
7	PM5-G	55.5	3.8	7.9
8	PM5-H	126.4	9.7	7.5
9	PM5-I	104.7	10.5	8.0

Average	83.8	5.1	8.0

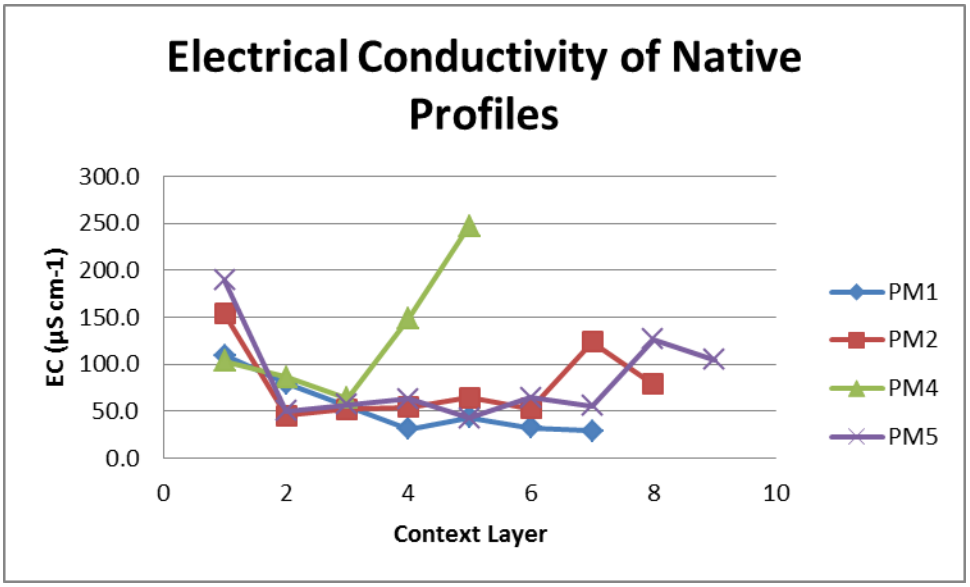

Figure 29: Electrical Conductivity results for native profiles

Similar to EC, MS values were higher for the A horizons than the subsoils (Fig. 26). This has been previously studied and determined that native topsoil is often greater with respect to underlying horizons (Mullins, 1977; Oldfield, 1991; Verosub and Roberts, 1995). This can be a result from presence of magnetite or maghemite of pedogenic origin (Maher and Taylor, 1988; Fine et al., 1989). Previous studies have also indicated that magnetotactic bacteria can also affect overall MS enhancements of the topsoil (Fassbinder et al., 1990; Oldfield, 1991). Native soil A horizons have shown a lower MS than anthropogenic soil ^A horizons, most likely due to the lack of anthropogenic particles. As the profiles increased with depth the subsoils had similar and constant MS values. The MS of the native soil profiles was overall much less than the anthropogenic profiles. This can presumably be explained by the absence of MAs and fill concentrated within the native soil profiles.

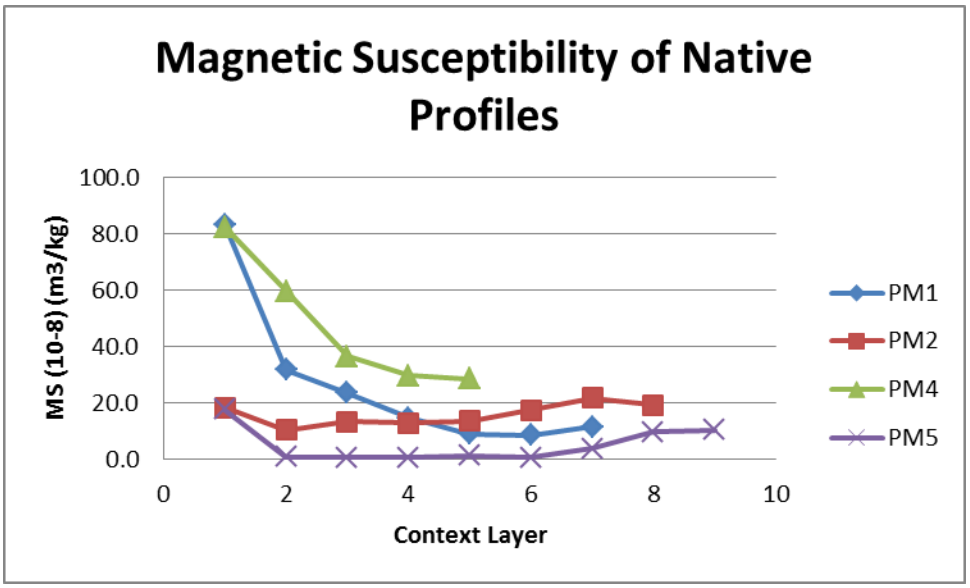

Figure 30: Magnetic Susceptibility results for native profiles

Overall, native EC and MS values were low and not as sporadic when compared to the Roosevelt Park anthropogenic profiles. Highest EC and MS values can been observed in the A horizon which can be attributed to organic, biological, and mineral makeup. Similar observations were made for anthropogenic profiles however their EC and MS readings were much greater due to the significant amount of MAs present within the soil. As the native soil profiles increased with depth the subsoils had low EC and MS values and remained consistent throughout the profile. Observed EC and MS measurements of the native soil profiles were much less than the anthropogenic soil profiles.

6.8 Maps

6.8.1 Introduction

Two maps were produced using Inverse Distance Weighting (IDW) interpolation method to map EC and MS data results with Surfer. Surfer images were then imported and overlaid into Google Earth maps. Kriging was not used to produce these maps. When using kriging, spatial

and weight distributions for the data set were largely unknown and could not be determined if the interpolation was a correct representation of the data.

6.8.2 Electrical Conductivity Map

High values for EC were concentrated heavily in residential demolition sites located in the south central part of Detroit, main burrows being Downtown, Corktown, and Midtown (Fig. 27). Areas with high EC results are represented by the color red and orange with values ranging between 1,000 µS cm^{-1} to 1,594.7 µS cm^{-1}. Intermediate EC values are represented by the color green and yellow ranging between 500 µS cm^{-1} to 900 µS cm^{-1}. These values are also heavily concentrated in the Downtown area located surrounding the hotspots. The high and intermediate values are most likely appearing in the inner part of the city because that is the oldest part of Detroit. Neighborhoods located in and near the Downtown area were developed between 1899 and 1929. Therefore, higher EC values located in the inner city are due to large amounts calcareous and ferruginous MAs being deposited from a number of demolition and rebuilding cycles.

Low EC values are represented by blue and purple with values ranging between 50 µS cm^{-1} to 400 µS cm^{-1}. These lower values are located on the East and West sides of Detroit, these areas have concentrations of younger neighborhoods in Detroit. Neighborhoods located in the younger parts of Detroit weren't developed until 1930-1960 (Fig. 29). The younger neighborhoods have gone under fewer demolition and rebuilding cycles than the inner city, therefore gaining less demolition debris in the same period of time. Low EC values can also be observed outside of the city's border where native soils were collected.

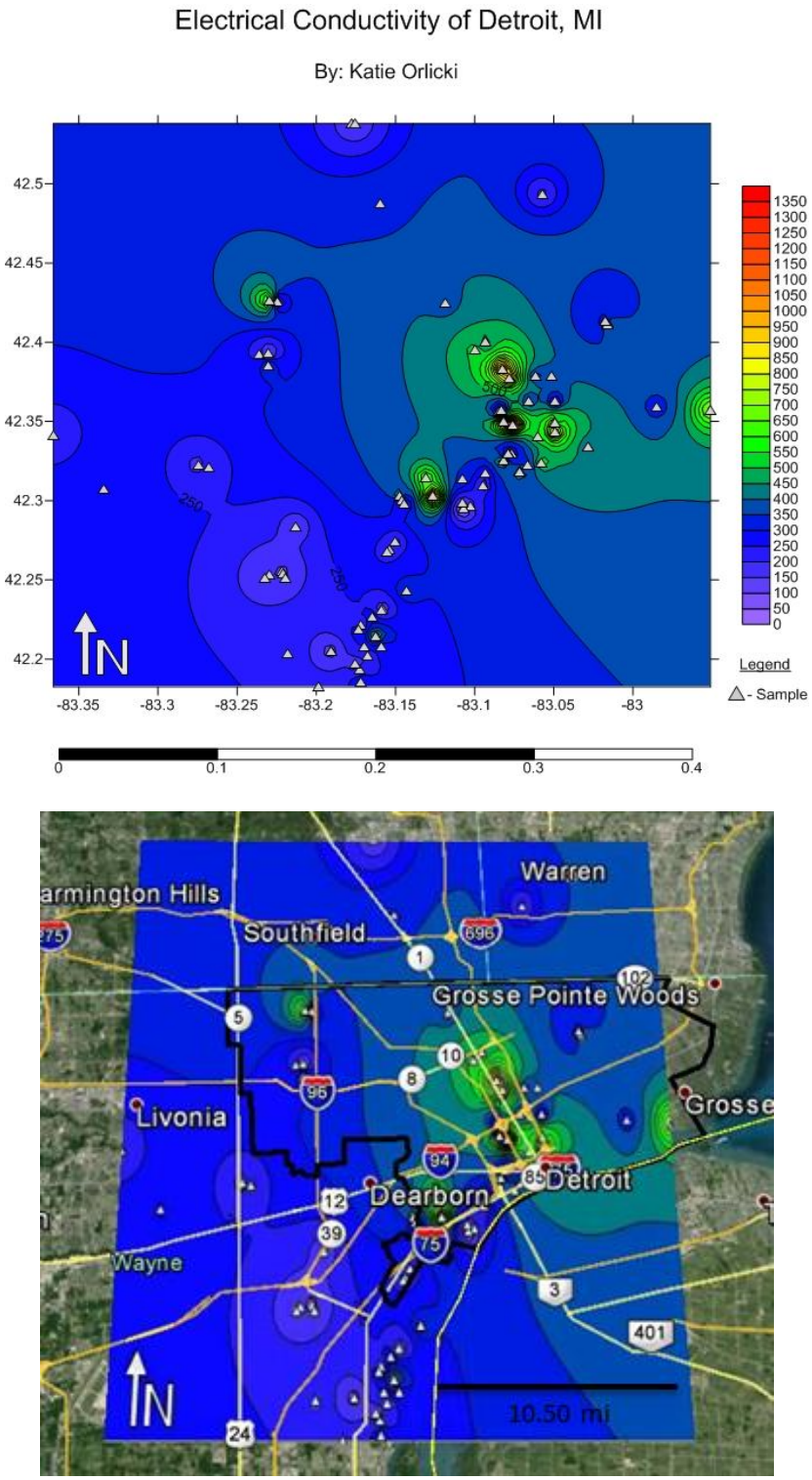

Figure 31: Map of Electrical Conductivity of Detroit, MI. Map on the top is the original surfer contour map where the map on the bottom is the contour map overlaid onto Google Earth

6.8.3 Magnetic Susceptibility Map

High MS values were heavily concentrated in industrial sites located in and around Downtown Detroit (Fig. 28). High values are represented by the colors red and orange which range between 1,400 x 10^{-8} m^3 kg^{-1} to 1,900 x 10^{-8} m^3 kg^{-1}. Intermediate values are represented by the colors yellow and green and range between 700 x 10^{-8} m^3 kg^{-1} to 1300 x 10^{-8} m^3 kg^{-1}, which can also be seen in the Downtown area of Detroit. High MS values are a result from large amounts of ferruginous waste being deposited from combustion, smelting, and other human activity. These types of waste are seen greatly around industrial sites which are heavily concentrated in the Downtown area along the Detroit River and railroad tracks. Industries located near the MS hotspots include, but are not limit to, Seven Sisters, Uniroyal, The River Rouge, and the Russel Industrial plant.

Low MS values are represented color blue and purple ranging between 0 x 10^{-8} m^3 kg^{-1} and 500 x 10^{-8} m^3 kg^{-1}. It is possible that these values are outlining where potential fly ash-impacted sites are located. The dark purple contour lines of the MS map are located near Zug Island and Olympic Steel (south), Packard Plant (east), Ford Motor Company in Highland Park (north), and the River Rouge Plant (west). However, more samples need to be taken in order to clearly identify if fly ash is possible to map.

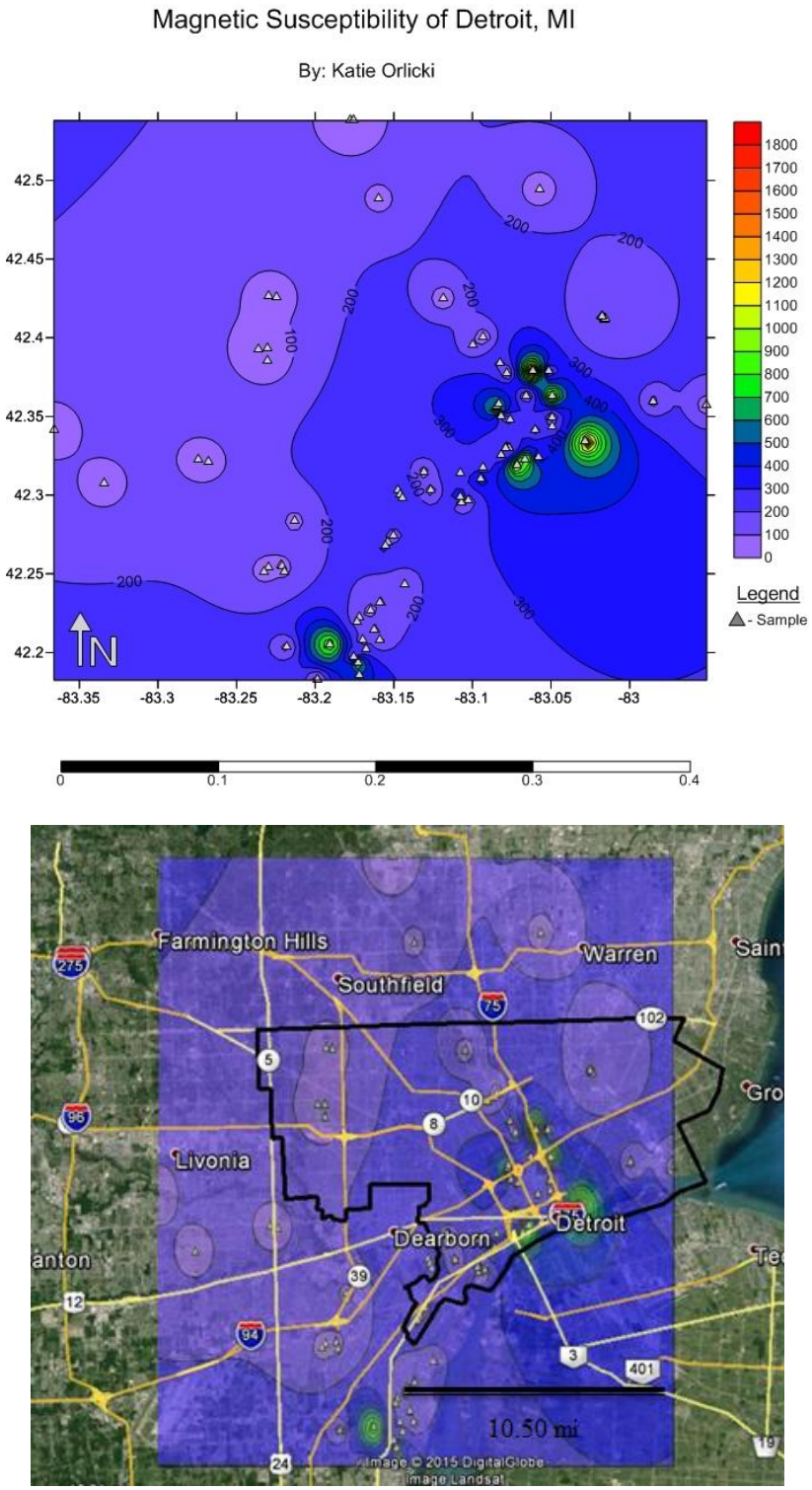

Figure 32: Map of Magnetic Susceptibility of Detroit, MI. Map on the top is the original surfer contour map where the map on the bottom is the contour map overlaid onto Google Earth

6.8.4 Age of Detroit, MI

Houses located in the inner part of Detroit were built in 1899 or earlier, around the same time the Detroit Automotive Company was founded. When the car industry roared between 1940 and 1950 a number of factories and industries were built. In the 1950s Detroit's population greatly increased making it the fifth largest city in the nation (Hyde, 1980). Factories and industries were built in an area where means of transporation for goods and services were easily accessible. Downtown Detroit is closely located to the Detroit river and the railroad system, making these two methods of transportation an excellent source for transporting any goods and services. Houses and neighborhoods were then quickly built to accomidate the workers of the automobile industry. Homes were first built close to the plants in the Downtown area and then expanding outward to the outer part of Detroit. As the borderlines of Detroit started to expand so did the neighborhoods. The auto industry then started to expand outside of city and put up offices in the suburbs and rural areas. Detroit then started to lose many manufactruing jobs (Hyde, 1980).

Houses on the outside of Downtown are considerably younger and built between 1930 and 1960 (Fig. 29). Overtime the Downtown area has increased the conceation of demoltion debris and industrial waste. As induestries crumbled and individuals lost their jobs, many left Detroit to find new beginnings elsewhere which meant leaving their homes and company buildings behind. Below, Figure 29 shows development ages of the city.

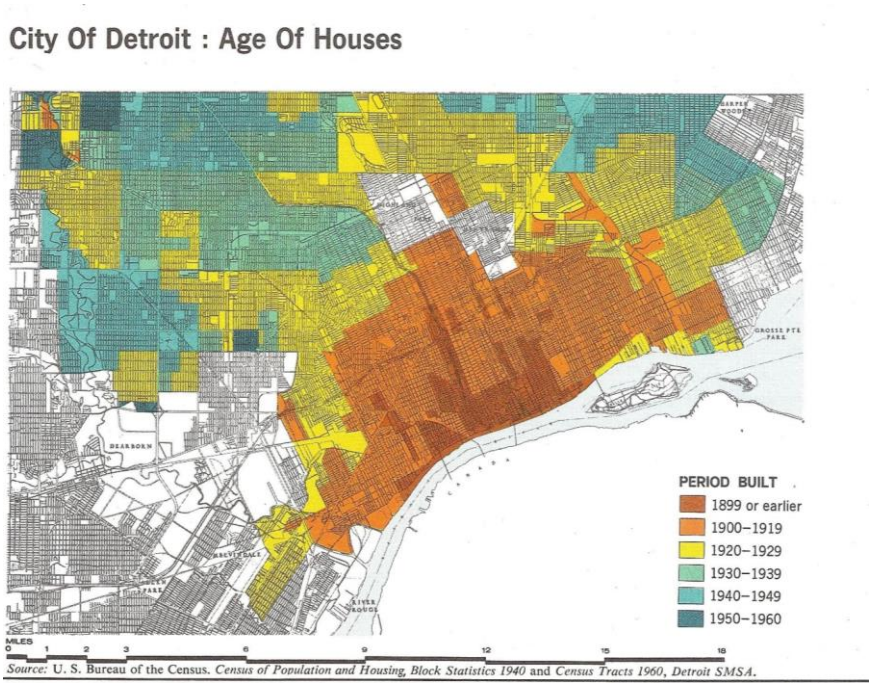

Figure 33: Age of burrow developments in Detroit, MI (Doxiadis, 1967)

Overall, high values for EC and MS were influenced by time, concentration of MAs, and previous land use history. Both high EC and MS values were located in the oldest part of the city where large amounts of fill can be observed. High EC values were located in older neighborhoods where housing demolition has taken place or awaiting for demolition to begin. High EC values are a result from large concentrations of calcarious and ferruginous MAs mainly from architectural debris. High MS values were located by older industrial sites where combustion and smelting often took place which produced large amounts of ferruginous and carbonacious MAs such as steel slag, ferruginous microspheres, and charcoal. Low EC and MS values can be obersevered outside of the inner city where soils have not been heavily disturbed.

CHAPTER 7

FUTURE WORK

A better understanding is needed of MAs and their effects on soils and public health. Many MAs studied were deposited during the demolition process but microparticles, such as ferruginous microspheres form from fly ash, can easily be airborne and transported elsewhere. The process of deposition and transport of these MAs should be further studied in order to understand their dispersal within the soil relevant to human interaction. Vacant land is in a continuous need of repurposing and therefore safety precautions when dealing with anthropogenic soils needs to be further identified. This study has shown that anthropogenic soils with high amounts of architectural debris and industrial waste can be recognized and classified. However, it is unclear how much of this waste and debris can affect the overall health of the public and other soils.

More soil samples need to be taken throughout the city of Detroit, specifically on the East and West sides. This study had a high sampling concentration throughout the center of Detroit but lacked samples towards the outer part of the city. To properly us EC and MS as a mapping technique more samples need to be collected and analyzed. A field crew has been assembled for additional fieldwork in summer and fall 2015 in order to collect more samples. Samples are to be collected on the east and west side of Detroit going through residential demolition, industrial, and fly ash-impacted sites. During this process EC, MS, and pH measurements should be measured in the field as well as in the lab. EC and MS field probes were obtained at the end of this study and will be used by the summer and fall 2015 field crew. The samples and data collected during the fall and summer 2015 mapping project are not included in this study based on time constraints.

CHAPTER 8

SUMMARY AND CONCLUSION

An assemblage of reference artifacts helped identify MAs within the collected soil samples. MAs with in the collected soil samples were identified successfully using optical microscopy, XRD, SEM, and EDAX. These MAs were then found possible to be classified into subgroups of carbonaceous, calcareous, siliceous, ferruginous, and miscellaneous based on their overall composition, pH, EC, and MS analysis. These MA subgroups were then identifiable with specific types of waste (coal) and debris (architectural) and can therefore represent a function of previous land use history.

Artifacts were found in variable proportions at all three urban sites (residential demolition, industrial, fly ash-impacted) that were studied. There were substantial differences in the chemical and geophysical properties of reference artifacts that represented building waste materials, coal-related wastes, industrial wastes, and archaeological materials. Analysis of reference artifacts suggests that the elevated pH of anthropogenic soils were caused by calcareous building material wastes mostly found in residential demolition sites, these artifacts mainly being wood, glass, concrete, mortar, and brick. Elevated EC was a result from both calcareous and ferruginous wastes mostly from architectural debris found in residential demolition sites. Elevated MS values were attributed to ferromagnetic materials such as corroded iron and metalliferous slag, which were mostly observed at industrial sites. It was then determined that overall a very low concentration of MAs is needed in order to observe a significant geophysical and chemical change in the soil in which they are contained in. Thus, revealing that MAs have unique geophysical and chemical signatures.

The A horizons of anthropogenic soils in Detroit were found to be distinguishable from native soils based on their EC and MS results. Anthropogenic soils had a pH greater than 7.0, EC greater than 150 µS cm^{-1}, and MS greater than 150 x 10^{-8} m^3 kg^{-1}. Background levels of native soils were often considerably less with averages of 6.95 for pH, 100.5 µS cm^{-1} for EC, and 42.1 x 10^{-8} m^3 kg^{-1} for MS. Overall, MS and EC results were able to be mapped when using Surfer and IDW interpolation method. Once MS and EC values were mapped, high MS and EC values were observed in the inner part of the city where industrial buildings and neighborhoods have been established for a longer period of time. High EC values were specifically observed in neighborhoods located near the Downtown area and high MS results were definitely shown Downtown as well, near the Detroit River and railroad system. Sampled transects and profiles showed spatial variability with depth and distance for both native and anthropogenic soils. Results suggested that anthropogenic soils are highly variably, whereas one soil sample is an overall good representation of a plot of native soils that is 10 to 20 m in size.

APPENDIX A

FULL DATA SET

7.1 Electrical Conductivity of Soil Samples

Table 17: Complete data set of all soil samples

Sample Site			Trial 1					Trial 2				
Sample	**GPS N**	**GPS W**	**EC a** ($\mu S\ cm^{-1}$)	**EC b** ($\mu S\ cm^{-1}$)	**EC c** ($\mu S\ cm^{-1}$)	**EC avg** ($\mu S\ cm^{-1}$)	**pH**	**EC a** ($\mu S\ cm^{-1}$)	**EC b** ($\mu S\ cm^{-1}$)	**EC c** ($\mu S\ cm^{-1}$)	**EC avg** ($\mu S\ cm^{-1}$)	**pH**
K1	42.4115	-83.0157	153.8	157.7	159.7	157.1	7.7	269.0	268.0	268.0	268.3	7.7
K2	42.4115	-83.0158	217.0	221.0	225.0	221.0	7.7	303.0	303.0	303.0	303.0	7.6
K3	42.4115	-83.0158	193.3	219.0	205.0	205.8	7.5	263.0	272.1	273.2	269.4	7.5
K4	42.4115	-83.0158	194.9	190.5	204.0	196.5	7.6	326.0	329.0	335.0	330.0	7.6
K5	42.4116	-83.0159	176.8	180.7	184.4	180.6	7.4	296.0	297.0	298.0	297.0	7.5
K6	42.4117	-83.0159	282	281	281.0	281.3	7.5	251.0	252.0	253.0	252.0	7.6
K7	42.1173	-83.0159	232	233	234.0	233.0	7.7	377.0	374.0	375.0	375.3	7.6
K8	42.4117	-83. 0159	422	423	425	423.3	7.4	387.0	386.0	386.0	386.3	7.3
K9	42.4117	-83.0158	453	454	454	453.7	7.4	410.0	411.0	410.0	410.3	7.5
K10	42.4117	-83.0158	512	515	516	514.3	7.6	505.0	245.0	546.0	432.0	7.6
K11	42.4116	-83.0158	559	559	560	559.3	7.6	525.0	527.0	527.0	526.3	7.6
K12	42.4116	-83.0157	595	596	602	597.7	7.6	601.0	601.0	603.0	601.7	7.6
K13	42.4115	-83.0157	608	606	609	607.7	7.4	635.0	595.0	596.0	608.7	7.3
K14	42.4115	-83.0157	638	645	645	642.7	7.5	586.0	554.0	555.0	565.0	7.5
A1	42.4132	-83.0176	113.5	116.4	116.1	115.3	7.6	135.9	138.0	138.0	137.3	7.7
B1	42.4132	-83.0176	163.6	164.7	171.6	166.6	7.7	189.3	194.2	194.3	192.6	7.6
C1	42.4131	-83.0176	193.7	194.5	195.4	194.5	7.8	165.9	165.6	165.2	165.6	7.8
D1	42.4131	-83.0175	232	233	234	233.0	7.8	175.5	176.0	176.4	176.0	7.8
E1	42.4131	-83.0175	238	239	240	239.0	7.7	322.0	321.0	324.0	322.3	7.7
F1	42.4131	-83.0175	225	234	234	231.0	7.8	229.0	231.0	231.0	230.3	7.8
G1	42.4131	-83.0175	167.9	168.6	169.5	168.7	7.8	203.0	203.0	204.0	203.3	7.8
MK1	42.3029	-83.1261	565.0	539.0	540.0	548.0	7.8	1750.0	1723.0	1713.0	1728.7	7.8
MK4	42.3145	-83.1306	605.0	635.0	646.0	628.7	8.1	771.0	771.0	772.0	771.3	8.1
MK5	42.3176	-83.0929	133.1	143.3	148.5	141.6	7.3	174.5	177.8	177.4	176.6	7.3
2UC-01	42.3493	-83.0499	719	740	755	738.0	7.4	1054.0	1053.0	1053.0	1053.3	7.4
2UC-02	42.3435	-83.0496	1182	1214	1234	1210.0	7.4	988.0	983.0	986.0	985.7	7.4
2UC-03	42.3307	-83.0779	208	208	211	209.0	6.9	484.0	478.0	478.0	480.0	6.9
2UC-04	42.3834	-83.0823	1095	1252	1366	1237.7	7.0	577.0	1191.0	1068.0	945.3	7.0
2UC-05	42.3478	-83.0756	1823	1868	1897	1862.7	7.2	1386.0	1380.0	1378.0	1381.3	7.2
2UC-06	42.3498	-83.0814	1703	1749	1774	1742.0	7.2	1395.0	1394.0	1397.0	1395.3	7.2
2UC-07	42.3257	-83.0816	1105	862	1176	1047.7	7.2	851.0	851.0	846.0	849.3	7.2

2UC-08	42.3774	-83.0778	691	758	734	727.7	7.3	1107.0	1106.0	1107.0	1106.7	7.4
2UC-09	42.3786	-83.0515	278	280	280	279.3	7.8	361.0	361.0	360.0	360.7	7.8
HP-11	42.3786	-83.0615	334	368	279	327.0	7.7	309.0	308.0	308.0	308.3	7.7
MS-EPA-1	42.4255	-83.2248	105.1	107.3	108.3	106.9	7.8	115.6	119.3	119.2	118.0	7.8
MS-EPA-2	42.4263	-83.2298	569	568	613	583.3	7.4	799.0	796.0	797.0	797.3	7.4
MS-EPA-4	42.3927	-83.2361	166.4	171.3	179	172.2	7.5	276.0	280.0	280.0	278.7	7.4
MS-EPA-5	42.3855	-83.2304	320	316	374	336.7	7.3	370.0	370.0	370.0	370.0	7.3
MS-EPA-6	42.3932	-83.2306	80	79.6	86.8	82.1	7.7	126.0	126.0	126.0	126.0	7.7
MS-01	42.3341	-83.0286	474	485	498	485.7	7.6	382.0	381.0	380.0	381.0	7.5
MS-02	42.3595	-82.9853	283	286	289	286.0	7.8	320.0	320.0	321.0	320.3	7.7
MS-03	42.3573	-82.9509	210	213	215	212.7	6.9	712.0	711.0	711.0	711.3	6.9
MS-04	42.3408	-83.0599	270	264	274	269.3	7.1	1401.0	1408.0	1409.0	1406.0	7.1
MS-05	42.3629	-83.0492	161.6	179.5	164.3	168.5	8.7	168.0	170.5	168.7	169.1	8.7
MS-06	42.3631	-83.0656	250	233	263	248.7	7.9	317.0	320.0	320.0	319.0	7.9
MS-07	42.3627	-83.0656	374	378	382	378.0	7.9	337.0	342.0	340.0	339.7	7.9
MS-08-A	42.3141	-83.1078	331	381	417	376.3	7.5	370.0	369.0	369.0	369.3	7.5
MS-08-B	42.3141	-83.1078	107.7	107.2	111.8	108.9	7.6	115.7	116.1	116.2	116.0	7.6
MS-09	42.2967	-83.1024	110.6	115.4	120.7	115.6	7.8	227.0	226.0	225.0	226.0	7.7
MS-10-A	42.2953	-83.1068	23.7	25.3	26.3	25.1	7.8	26.7	26.6	26.3	26.5	7.9
MS-10-B	42.2953	-83.1068	19.22	19.4	19.43	19.4	7.7	45.1	44.7	44.7	44.8	7.7
MS-11-A	42.3190	-83.0716	263	201	187.8	217.3	7.7	220.0	219.0	219.0	219.3	7.7
MS-11-B	42.3188	-83.0718	228	229	228	228.3	6.5	87.0	136.0	136.1	119.7	6.5
MS-11-C	42.3185	-83.0716	1013	1068	1020	1033.7	7.4	695.0	969.0	697.0	787.0	7.4
MS-12	42.2986	-83.1079	100.8	106.6	105.5	104.3	7.7	180.1	180.2	182.2	180.8	7.7
MS-13	42.3098	-83.0944	72.2	72.7	72.7	72.5	7.7	152.4	152.4	152.4	152.4	7.8
MS-14	42.3227	-83.0666	298	259	281	279.3	7.9	243.0	242.0	240.0	241.7	7.9
MS-15-A	42.3558	-83.0842	276	279	294	283.0	7.7	379.0	379.0	379.0	379.0	7.7
MS-15-B	42.3563	-83.0845	82.5	79.9	80.8	81.1	8.1	150.1	149.2	148.9	149.4	8.1
MS-16	42.3575	-83.0833	142.3	144.5	147.7	144.8	7.8	4.84 mS	4.84 mS	4.84mS	4.84mS	7.7
AS-01	42.3952	-83.0997	406	538	654	532.7	7.1	487.0	485.0	483.0	485.0	7.2
AS-02-A	42.4002	-83.0931	76.5	74.9	78.6	76.7	7.8	1102.0	1099.0	1095.0	1098.7	7.8
AS-02-C	42.4002	-83.0931	257	294	334	295.0	7.4	292.0	299.0	300.0	297.0	7.5
NMS-01	42.4248	-83.1184	135.7	137.6	130.8	134.7	6.2	490.0	487.0	483.0	486.7	6.2
NMS-02	42.5380	-83.1778	156.6	155.7	158.9	157.1	7.2	190.2	190.2	192.1	190.8	7.2
A1-RY3	42.4879	-83.1593	327	388	273	329.3	6.0	317.0	317.0	317.0	317.0	5.9
DA-1	42.3033	-83.1474	515	517	516	516.0	7.7	451.0	451.0	453.0	451.7	7.8
DA-2	42.3003	-83.1460	176.1	179.5	180.5	178.7	7.7	193.9	194.0	194.7	194.2	7.7
DA-3	42.2979	-83.1445	222	226	226	224.7	7.9	191.7	193.6	193.9	193.1	7.9

DA-4	42.2742	-83.1499	177.3	177.5	177.7	177.5	7.9	178.4	178.1	178.6	178.4	7.6
DA-5	42.2695	-83.1541	229	231	231	230.3	7.7	242.0	242.0	242.0	242.0	7.7
DA-6	42.2676	-83.1554	230	248	248	242.0	7.6	208.0	219.0	220.0	215.7	7.4
ORL	42.3338	-83.0280	431	431	412	424.7	7.7	443.0	442.0	443.0	442.7	7.8
PM-1A-1	42.5085	-83.0515	103.7	102.3	101.9	102.6	6.9	116.2	116.2	116.6	116.3	7.0
PM-1A-2	42.5085	-83.0515	74.8	74.7	74.6	74.7	4.6	76.3	75.7	75.5	75.8	4.5
PM-1A-3	42.5085	-83.0515	73.6	73.8	73.9	73.8	4.7	77.3	77.3	77.4	77.3	4.7
PM-1A-4	42.5085	-83.0516	93.9	93.4	93.3	93.5	6.7	92.2	91.9	91.5	91.9	6.2
PM-2A-1	42.5384	-83.1737	166.1	155.9	157.8	159.9	6.4	153.7	155.6	133.4	147.6	6.5
PM-2A-2	42.5384	-83.1738	123.6	114.3	115.3	117.7	6.1	115.1	97.4	123.8	112.1	6.1
PM-2A-3	42.5384	-83.1738	123	122.3	124.2	123.2	6.3	122.4	120.1	122.4	121.6	6.3
PM-2A-4	42.5384	-83.1738	46.2	45.8	43.3	45.1	6.0	70.0	61.1	63.4	64.8	6.8
PM-2A-5	42.5384	-83.1738	125.4	105.1	104.4	111.6	5.4	138.1	120.3	119.2	125.9	5.6
PM-1B	42.5085	-83.0515	68.4	67.2	67.3	67.6	7.1	96.5	90.0	88.0	91.5	6.7
PM-1C	42.5085	-83.0515	55.8	55.8	55.7	55.8	6.6	56.2	56.2	56.3	56.2	6.5
PM-1D	42.5085	-83.0515	30.6	30.7	30.7	30.7	5.9	31.6	31.5	31.4	31.5	5.9
PM-1E	42.5085	-83.0515	43.7	43.8	43.8	43.8	6.4	43.2	43.1	43.1	43.1	6.3
PM-1F	42.5085	-83.0515	32.1	32.1	32.2	32.1	5.6	33.2	33.1	33.2	33.2	6.0
PM-1G	42.5085	-83.0515	28.7	28.6	28.6	28.6	5.9	29.3	29.4	29.4	29.4	5.9
PM-2B	42.5384	-83.1737	38.3	57	40.9	45.4	6.4	44.9	45.0	45.2	45.0	7.2
PM-2C	42.5384	-83.1737	44.5	48.2	55.8	49.5	6.8	55.3	55.4	55.6	55.4	7.1
PM-2D	42.5384	-83.1737	44.3	61.6	56.5	54.1	6.8	54.2	54.3	54.7	54.4	7.8
PM-2E	42.5384	-83.1737	46.6	51.6	51.1	49.8	7.2	78.6	79.0	79.4	79.0	7.1
PM-2F	42.5384	-83.1737	50.3	51.5	51.5	51.1	7.6	54.5	54.5	54.5	54.5	7.90
PM-2G	42.5384	-83.1737	105.2	104.9	104.8	105.0	8.1	142.5	142.6	142.7	142.6	8.1
PM-2H	42.5384	-83.1737	74.9	76.1	76.4	75.8	7.9	81.6	81.9	82.0	81.8	7.9
PM-5A	42.4937	-83.0583	208	212	212	210.7	7.1	168.4	167.6	168.2	168.1	7.2
PM-5B	42.4937	-83.0583	48.2	48.2	48.2	48.2	7.2	52.2	52.4	52.5	52.4	7.3
PM-5C	42.4937	-83.0583	61.5	61.9	62.8	62.1	6.5	51.2	51.6	52.0	51.6	6.5
PM-5D	42.4937	-83.0583	62	60.2	60.2	60.8	7.3	65.0	65.1	65.3	65.1	7.4
PM-5E	42.4937	-83.0583	41.6	41.8	42	41.8	7.5	44.1	44.4	44.6	44.4	7.6
PM-5F	42.4937	-83.0583	60.6	63.9	65.7	63.4	7.6	66.7	66.3	65.9	66.3	8.0
PM-5G	42.4937	-83.0583	55.2	55.4	55.5	55.4	7.8	55.6	55.6	55.8	55.7	8.0
PM-5H	42.4937	-83.0583	109	109.7	109.5	109.4	7.6	142.5	143.5	144.0	143.3	7.4
PM-5I	42.4937	-83.0583	112	111.7	111.7	111.8	8.0	97.6	97.3	97.7	97.5	8.0
PM-4A-1	42.50012	-83.4655	97.4	97.9	98.1	97.8	7.4	107.7	108.9	109.0	108.5	7.2
PM-4A-2	42.50012	-83.4655	129.8	129.9	130.1	129.9	6.9	106.9	107.1	107.1	107.0	6.9
PM-4A-3	42.50012	-83.4656	128.1	128.2	128.8	128.4	7.5	114.8	115.5	116.1	115.5	7.2

PM-4A-4	42.50012	-83.4656	84.5	84.6	85	84.7	7.7	68.4	68.5	68.6	68.5	7.0
PM-4A-5	42.50012	-83.4656	74.9	75.9	76.1	75.6	7.2	70.9	72.0	72.0	71.6	7.2
PM4B	42.50012	-83.4655	88	87.9	87.8	87.9	7.3	84.2	84.5	86.0	84.9	7.2
PM4C	42.50012	-83.4655	71.1	68.3	67.1	68.8	7.7	60.1	58.8	58.7	59.2	7.6
PM4D	42.50012	-83.4655	142.1	140.9	141.7	141.6	8.2	156.8	156.9	157.1	156.9	8.0
PM4E	42.50012	-83.4655	170.2	172.4	172.9	171.8	8.0	319.0	323.0	325.0	322.3	8.0

7.2 Electrical Conductivity of Roosevelt Park Soil Samples

Table 18: Electrical Conductivity of Roosevelt Park Soil Samples

Sample Site			Trial 1					Trail 2				
Sample	**GPS N**	**GPS W**	**EC a** ($\mu S\ cm^{-1}$)	**EC b** ($\mu S\ cm^{-1}$)	**EC c** ($\mu S\ cm^{-1}$)	**EC avg** ($\mu S\ cm^{-1}$)	**pH**	**EC a** ($\mu S\ cm^{-1}$)	**EC b** ($\mu S\ cm^{-1}$)	**EC c** ($\mu S\ cm^{-1}$)	**EC avg** ($\mu S\ cm^{-1}$)	**pH**
Transects												
1A	42.3300	-83.076	322	320	320	320.7	7.4	241	240	240	240.3	7.3
1B	42.3300	-83.076	240	240	240	240.0	7.7	250	249	249	249.3	7.5
1C	42.3300	-83.076	249	256	261	255.3	7.4	317	317	304	312.7	7.4
1D	42.3300	-83.076	313	315	316	314.7	7.5	237	237	237	237.0	7.5
1E	42.3300	-83.076	265	263	263	263.7	7.5	254	263	262	259.7	7.9
1F	42.3300	-83.076	263	263	263	263.0	6.9	300	299	299	299.3	7.6
1G	42.3300	-83.076	225	226	228	226.3	7.7	284	286	306	292.0	7.5
2A	42.3298	-83.079	128.6	129.5	130.3	129.5	7.6	109.1	110.5	110.9	110.2	7.5
2B	42.3298	-83.079	239	246	245	243.3	7.5	312	312	312	312.0	7.5
2C	42.3298	-83.079	228	224	224	225.3	7.5	416	415	415	415.3	7.4
2D	42.3298	-83.079	184.2	185.4	186	185.2	7.4	203	204	205	204.0	7.4
2E	42.3298	-83.078	245	245	242	244.0	7.6	383	381	381	381.7	7.3
2F	42.3298	-83.078	258	186.5	185.4	210.0	7.7	239	241	242	240.7	7.7
Profiles												
RP38 Topsoil	42.3298	-83.076	305	304	304	304.3	7.4	366	366	367	366.3	7.7
RP38 Topsoil	42.3298	-83.076	511	511	512	511.3	7.6	529	528	527	528.0	7.6
RP38 Topsoil	42.3298	-83.076	271	272	272	271.7	7.6	282	283	283	282.7	7.7
RP50 Ash	42.3298	-83.076	208	209	210	209.0	8.0	204	204	204	204.0	8.0
RP53	42.3298	-83.076	203	205	206	204.7	7.8	221	219	220	220.0	7.9
RP63	42.3298	-83.076	190.7	194.6	198	194.4	6.8	210	210	210	210.0	6.7
RP63 Mortar	42.3298	-83.076	131.2	135.7	137.2	134.7	8.0	185.7	186.7	187.9	186.8	7.6
RP64	42.3298	-83.076	224	223	224	223.7	7.9	222	222	222	222.0	8.1
RP73 A	42.3298	-83.076	105.7	103	102.5	103.7	7.9	106.8	107.7	108.1	107.5	7.9
RP73 B	42.3298	-83.076	90.3	90.7	92.5	91.2	7.8	95.4	102.8	102.5	100.2	7.8
RP73 B Paper	42.3298	-83.076	123.6	123.1	123.6	123.4	7.8	113.7	114.2	114.1	114.0	7.8
RP87 Ash	42.3298	-83.076	157.3	157.7	157.4	157.5	7.8	144.8	146.6	147.9	146.4	8.0
RP100	42.3298	-83.076	102	103.2	103.1	102.8	7.8	105.1	105.1	105.2	105.1	7.7
RP106	42.3298	-83.076	79.8	80.1	80.1	80.0	7.8	80.1	80.5	80.6	80.4	7.7
RP 106 /Feature 25	42.3298	-83.076	787	732	732	750.3	8.1	508	509	511	509.3	7.8
RP107	42.3298	-83.076	69.3	69.3	69.6	69.4	7.8	62	62.4	62.3	62.2	7.8

Lot 4, STP1	42.3298	-83.076	236	237	237	236.7	7.9	231	231	231	231.0	7.9
RP81	42.3298	-83.076	76.2	77	77.1	76.8	7.6	86.1	86.2	86.2	86.2	7.7

7.3 Magnetic Susceptibility of Soil Samples

Table 19: Magnetic Susceptibility of Soil Samples

Sample Site			Trial 1				Trial 2			
Sample	GPS N	GPS W	Weight S (g)	Bulk Density (g/cm3)	MS (10^{-5})	K (10-8) (m3/kg)	Weight S (g)	Bulk Density (g/cm3)	MS (10^{-5})	K (10^{-8}) (m3/kg)
K1	42.4115	-83.0158	8.43	0.84	48	57.0	7.63	0.76	49	64.2
K2	42.4115	-83.0158	7.34	0.73	55	74.9	7.20	0.72	60	83.4
K3	42.4116	-83.0159	7.80	0.78	51	65.4	8.20	0.82	45	54.9
K4	42.4116	-83.0159	10.08	1.01	133	131.9	9.79	0.98	109	111.4
K5	42.4117	-83.0159	13.00	1.30	75	57.7	8.19	0.82	100	122.1
K6	42.4117	-83.0159	7.47	0.75	27	36.1	8.08	0.81	35	43.3
K7	42.4117	-83.0160	7.28	0.73	28	38.5	7.17	0.72	30	41.8
K8	42.4118	-83.0159	8.90	0.89	64	71.9	8.82	0.88	52	59.0
K9	42.4117	-83.0159	8.75	0.88	43	49.1	8.41	0.84	40	47.6
K10	42.4117	-83.0159	9.36	0.94	48	51.3	9.30	0.93	45	48.4
K11	42.4117	-83.0158	8.82	0.88	63	71.4	9.04	0.90	59	65.2
K12	42.4116	-83.0158	9.49	0.95	57	60.1	9.52	0.95	64	67.2
K13	42.4116	-83.0158	8.55	0.86	54	63.2	8.72	0.87	49	56.2
K14	42.4116	-83.0157	9.20	0.92	41	44.6	9.47	0.95	46	48.6
A1	42.4132	-83.0176	10.94	1.09	135	123.4	11.54	1.15	161	139.5
B1	42.4132	-83.0176	10.05	1.00	213	212.0	10.03	1.00	208	207.4
C1	42.4132	-83.0176	9.70	0.97	264	272.0	10.26	1.03	253	246.7
D1	42.4132	-83.0176	10.10	1.01	281	278.3	10.02	1.00	242	241.5
E1	42.4131	-83.0176	7.94	0.79	182	229.2	8.27	0.83	200	241.8
F1	42.4131	-83.0176	9.26	0.93	230	248.3	9.22	0.92	226	245.2
G1	42.4131	-83.0175	10.38	1.04	780	751.7	10.22	1.02	801	784.0
MK1	42.3029	-83.1261	12.33	1.23	51	41.4	12.25	1.23	23	18.8
MK4	42.3146	-83.1306	11.22	1.12	45	40.1	11.22	1.12	48	42.8
MK5	42.3176	-83.0930	10.39	1.04	169	162.6	10.64	1.06	164	154.2
2UC-01	42.3493	-83.0500	11.37	1.14	156	137.2	11.36	1.14	143	125.8
2UC-02	42.3435	-83.0496	10.60	1.06	182	171.7	10.37	1.04	192	185.1
2UC-03	42.3307	-83.0779	9.75	0.98	245	251.2	9.82	0.98	243	247.5
2UC-04	42.3834	-83.0824	9.01	0.90	90	99.9	8.87	0.89	83	93.5
2UC-05	42.3479	-83.0757	10.33	1.03	174	168.5	10.27	1.03	170	165.5
2UC-06	42.3498	-83.0815	9.73	0.97	103	105.8	10.88	1.09	104	95.6
2UC-07	42.3257	-83.0817	10.69	1.07	120	112.3	10.41	1.04	124	119.1
2UC-08	42.3774	-83.0778	12.09	1.21	58	48.0	12.08	1.21	81	67.1
2UC-09	42.3787	-83.0515	12.58	1.26	86	68.4	12.58	1.26	87	69.2
HP-11	42.3786	-83.0614	10.05	1.00	1879	1870.1	9.57	0.96	1882	1966.4
MS-EPA-1	42.4255	-83.2248	9.50	0.95	49	51.6	10.04	1.00	37	36.9

MS-EPA-2	42.4263	-83.2299	10.58	1.06	57	53.9	10.69	1.07	58	54.3
MS-EPA-4	42.3927	-83.2361	10.70	1.07	34	31.8	10.50	1.05	41	39.1
MS-EPA-5	42.3856	-83.2304	9.76	0.98	23	23.6	10.08	1.01	24	23.8
MS-EPA-6	42.3932	-83.2306	10.00	1.00	21	21.0	10.57	1.06	35	33.1
MS-01	42.3341	-83.0286	10.94	1.09	75	68.5	10.87	1.09	78	71.8
MS-02	42.3595	-82.9854	10.29	1.03	54	52.5	10.09	1.01	85	84.2
MS-03	42.3574	-82.9510	10.72	1.07	57	53.2	10.17	1.02	54	53.1
MS-04	42.3409	-83.0600	10.78	1.08	122	113.2	10.56	1.06	125	118.4
MS-05	42.3630	-83.0493	10.43	1.04	1288	1235.1	10.04	1.00	1135	1130.8
MS-06	42.3632	-83.0656	11.11	1.11	124	111.6	11.32	1.13	94	83.1
MS-07	42.3628	-83.0657	10.71	1.07	62	57.9	10.71	1.07	77	71.9
MS-08-A	42.3142	-83.1078	9.87	0.99	229	232.0	9.87	0.99	220	222.8
MS-08-B	42.3142	-83.1078	11.38	1.14	562	493.9	12.01	1.20	604	502.8
MS-09	42.2967	-83.1025	11.50	1.15	126	109.6	11.78	1.18	122	103.6
MS-10-A	42.2954	-83.1069	15.52	1.55	87	56.1	15.56	1.56	90	57.8
MS-10-B	42.2954	-83.1069	15.80	1.58	136	86.1	15.51	1.55	143	92.2
MS-11-A	42.3191	-83.0716	10.68	1.07	577	540.0	11.69	1.17	695	594.7
MS-11-B	42.3188	-83.0718	10.39	1.04	1596	1536.6	10.37	1.04	1633	1575.0
MS-11-C	42.3186	-83.0716	8.53	0.85	959	1123.7	8.99	0.90	1072	1192.4
MS-12	42.2987	-83.1080	9.15	0.91	540	590.2	8.81	0.88	496	563.2
MS-13	42.3099	-83.0944	11.46	1.15	16	14.0	11.44	1.14	1125	983.8
MS-14	42.3228	-83.0667	8.69	0.87	1122	1291.2	8.71	0.87	1058	1214.6
MS-15-A	42.3558	-83.0843	10.24	1.02	1908	1862.9	10.15	1.01	1879	1851.5
MS-15-B	42.3563	-83.0846	13.92	1.39	127	91.2	13.81	1.38	140	101.4
MS-16	42.3575	-83.0834	7.14	0.71	444	621.9	8.46	0.85	102	120.6
AS-01	42.3952	-83.0998	11.50	1.15	105	91.3	11.49	1.15	113	98.3
AS-02-A	42.4003	-83.0932	11.10	1.11	11	9.9	11.18	1.12	8	7.2
NMS-01	42.4249	-83.1184	8.69	0.87	22	25.3	9.85	0.98	23	23.4
NMS-02	42.5380	-83.1779	8.50	0.85	18	21.2	7.16	0.72	14	19.6
A1-RY3	42.4880	-83.1594	11.37	1.14	72	63.3	12.27	1.23	87	70.9
ORL	42.3339	-83.0280	8.03	0.80	1952	2429.7	8.27	0.83	2020	2443.2
DA-1	42.3033	-83.1475	8.11	0.81	243	299.7	8.15	0.81	239	293.3
DA-2	42.3004	-83.1460	8.25	0.82	230	278.9	8.24	0.82	224	271.8
DA-3	42.2979	-83.1446	7.37	0.74	222	301.3	7.15	0.71	217	303.6
DA-4	42.2743	-83.1499	7.54	0.75	131	173.7	8.56	0.86	143	167.1
DA-5	42.2696	-83.1541	8.20	0.82	91	111.0	7.75	0.77	86	111.0
DA-6	42.2676	-83.1555	6.48	0.65	256	394.9	6.61	0.66	265	401.1
PM-1A-1	42.50857	-83.0515	10.46	1.05	91	87.0	10.32	1.03	82	79.5

PM-1A-2	42.50857	-83.0515	9.50	0.95	44	46.3	9.72	0.97	50	51.5
PM-1A-3	42.50857	-83.0516	12.07	1.21	36	29.8	11.69	1.17	33	28.2
PM-1A-4	42.5384	-83.1737	9.93	0.99	56	56.4	9.99	1.00	58	58.0
PM-1B	42.5384	-83.1738	13.32	1.33	36	27.0	12.33	1.23	45	36.5
PM-1C	42.5384	-83.1738	14.54	1.45	32	22.0	13.92	1.39	35	25.1
PM-1D	42.5384	-83.1738	15.16	1.52	21	13.9	14.79	1.48	23	15.5
PM-1E	42.5384	-83.1738	15.18	1.52	13	8.6	15.09	1.51	14	9.3
PM-1F	42.50857	-83.0515	14.65	1.47	12	8.2	13.64	1.36	12	8.8
PM-1G	42.50857	-83.0515	13.64	1.36	16	11.7	13.39	1.34	15	11.2
PM-2A-1	42.5378	-83.1754	7.13	0.71	13	18.2	7.14	0.71	13	18.2
PM-2A-2	42.50857	-83.0515	9.86	0.99	11	11.2	9.23	0.92	11	11.9
PM-2A-3	42.50857	-83.0515	5.98	0.60	12	20.1	6.56	0.66	15	22.9
PM-2A-4	42.50857	-83.0515	6.55	0.65	13	19.9	6.00	0.60	11	18.3
PM-2A-5	42.5384	-83.1737	6.50	0.65	54	83.0	6.90	0.69	58	84.1
PM-2B	42.5384	-83.1737	11.87	1.19	13	11.0	12.16	1.22	12	9.9
PM-2C	42.5384	-83.1737	11.22	1.12	17	15.1	12.01	1.20	14	11.7
PM-2D	42.5384	-83.051	11.04	1.10	15	13.6	11.33	1.13	14	12.4
PM-2E	42.5384	-83.051	11.57	1.16	16	13.8	12.01	1.20	16	13.3
PM-2F	42.5384	-83.051	12.04	1.20	21	17.4	12.26	1.23	22	17.4
PM-2G	42.5384	-83.051	11.18	1.12	25	22.4	11.85	1.18	25	21.1
PM-2H	42.4937	-83.051	12.04	1.20	23	19.1	11.80	1.18	23	19.5
PM-5A	42.4937	-83.058	7.61	0.76	13	17.1	8.78	0.88	16	18.2
PM-5B	42.4937	-83.058	12.73	1.27	1	0.8	11.93	1.19	1	0.8
PM-5C	42.4937	-83.058	15.32	1.53	1	0.7	15.42	1.54	1	0.6
PM-5D	42.4937	-83.058	15.98	1.60	1	0.6	15.55	1.56	1	0.6
PM-5E	42.4937	-83.058	15.96	1.60	2	1.3	15.85	1.59	2	1.3
PM-5F	42.4937	-83.058	15.26	1.53	1	0.7	15.39	1.54	1	0.6
PM-5G	42.4937	-83.058	15.24	1.52	7	4.6	13.69	1.37	4	2.9
PM-5H	42.4937	-83.058	10.50	1.05	10	9.5	10.12	1.01	10	9.9
PM-5I-A	42.4937	-83.058	9.71	0.97	10	10.3	10.31	1.03	11	10.7
PM-4A-1	42.50012	-83.465	10.61	1.06	81	76.3	10.64	1.06	94	88.4
PM-4A-2	42.5001	-83.465	11.06	1.11	101	91.3	11.10	1.11	105	94.6
PM-4A-3	42.50012	-83.465	11.19	1.12	125	111.7	11.46	1.15	136	118.6
PM-4A-4	42.5001	-83.465	11.80	1.18	173	146.6	11.54	1.15	169	146.5
PM-4A-5	42.5001	-83.465	11.90	1.19	181	152.1	12.02	1.20	218	181.3
PM4B	42.50012	-83.465	12.07	1.21	72	59.6	11.73	1.17	70	59.7
PM4C	42.50012	-83.465	10.40	1.04	38	36.5	9.81	0.98	36	36.7
PM4D	42.50012	-83.465	10.47	1.05	28	26.7	10.71	1.07	35	32.7

PM4E	42.50012	-83.465	10.11	1.01	30	29.7	10.52	1.05	29	27.6
14-MA-1	42.3225	-83.2744	11.43	1.14	55	48.1	11.85	1.18	61	51.5
14-MA-2	42.2553	-83.2214	10.09	1.01	80	79.3	10.59	1.06	82	77.4
14-MA-3	42.2544	-83.2211	9.86	0.99	96	97.3	10.61	1.06	80	75.4
14-MA-4	42.2511	-83.2194	9.84	0.98	84	85.3	9.85	0.99	98	99.5
14-MA-5	42.2033	-83.2183	7.90	0.79	52	65.8	8.05	0.80	47	58.4
14-MA-6	42.2536	-83.2294	10.92	1.09	72	65.9	10.27	1.03	68	66.2
14-MA-7	42.2514	-83.2328	9.26	0.93	62	67.0	9.87	0.99	70	71.0
14-MA-8	42.2833	-83.2131	9.92	0.99	64	64.5	9.92	0.99	63	63.5
14-MA-9	42.3072	-83.3342	10.15	1.01	42	41.4	9.63	0.96	42	43.6
14-MA-10	42.3414	-83.3661	10.58	1.06	43	40.6	10.58	1.06	42	39.7
14-MA-11	42.2142	-83.1619	9.56	0.96	143	149.6	10.08	1.01	152	150.9
14-MA-11B	42.2144	-83.1622	11.09	1.11	151	136.1	11.23	1.12	148	131.8
14-MA-12	42.2050	-83.1908	10.19	1.02	1195	1173.3	10.61	1.06	1295	1221.0
14-MA-12B	42.2050	-83.1908	11.19	1.12	1570	1402.7	10.22	1.02	1285	1257.9
14-MA-13	42.2050	-83.1908	9.69	0.97	118	121.7	9.45	0.95	108	114.2
14-MA-14	42.2317	-83.1583	9.78	0.98	80	81.8	10.99	1.10	89	81.0
14-MA-15	42.2314	-83.1586	10.30	1.03	109	105.8	9.48	0.95	107	112.9
14-MA-16	42.2336	-83.1581	7.68	0.77	144	187.4	8.02	0.80	145	180.7
14-MA-18	42.1825	-83.1989	11.00	1.10	27	24.6	10.54	1.05	23	21.8
14-MA-20	42.3211	-83.2678	10.17	1.02	55	54.1	10.67	1.07	57	53.4
14-MA-25	42.2081	-83.1589	10.62	1.06	51	48.0	11.98	1.20	66	55.1
14-MA-29	42.3243	-83.0576	8.19	0.82	125	152.6	8.51	0.85	140	164.6
14-MA-30	42.3490	-83.0493	9.74	0.97	95	97.5	10.21	1.02	98	96.0
14-MA-31	42.2265	-83.1649	9.45	0.94	43	45.5	9.50	0.95	37	38.9
14-MA-34	42.2434	-83.1433	6.60	0.66	90	136.5	6.69	0.67	73	109.1
14-MA-36	42.2021	-83.1677	10.01	1.00	258	257.7	9.77	0.98	250	255.8
14-MA-37	42.1857	-83.1717	9.63	0.96	470	487.8	9.85	0.98	507	514.9
14-MA-38	42.1933	-83.1726	8.88	0.89	784	883.1	8.48	0.85	679	800.5
14-MA-39	42.2079	-83.1700	8.80	0.88	104	118.1	9.09	0.91	109	119.9
14-MA-41	42.2220	-83.1718	10.90	1.09	44	40.4	10.90	1.09	43	39.4
14-MA-42	42.2200	-83.17	9.34	0.93	205	219.4	9.79	0.98	168	171.7

7.4 Magnetic Susceptibility of Roosevelt Park Soil Samples

Table 20: Magnetic Susceptibility of Roosevelt Park Soil Samples

Sample Site			Trial 1				Trail 2			
Sample	GPS N	GPS W	Weight S (g)	Bulk Density (g/cm3)	k MS (10^{-5})	X (m3/kg)	Weight S (g)	Bulk Density (g/cm3)	k MS (10^{-5})	X (m3/kg)
Transects										
1A	42.3300	-83.0768	9.74	0.97	147	151.0	9.61	0.96	143	148.9
1B	42.3300	-83.0767	8.46	0.85	141	166.7	8.09	0.81	140	173.1
1C	42.3300	-83.0766	7.51	0.75	121	161.1	7.60	0.76	113	148.7
1D	42.3300	-83.0766	7.99	0.80	155	194.1	7.81	0.78	144	184.3
1E	42.3300	-83.0765	8.03	0.80	140	174.3	8.36	0.84	150	179.4
1F	42.3300	-83.0764	9.46	0.95	243	256.9	8.19	0.82	132	161.1
1G	42.3300	-83.0769	7.40	0.74	131	177.1	7.56	0.76	130	172.0
2A	42.3298	-83.0792	7.30	0.73	210	287.8	7.30	0.73	137	187.6
2B	42.3298	-83.0791	8.85	0.89	168	189.7	8.00	0.80	164	205.0
2C	42.3298	-83.0791	7.55	0.76	132	174.7	8.25	0.82	151	183.0
2D	42.3299	-83.0790	6.36	0.64	130	204.3	6.86	0.69	136	198.2
2E	42.3299	-83.0790	7.78	0.78	189	243.0	8.05	0.80	189	234.9
2F	42.3299	-83.0789	7.09	0.71	197	277.8	7.337	0.7337	199	271.2
Profiles										
RP38 Topsoil	42.3298	-83.0765	8.31	0.83	167	200.9	11.19	1.12	175	156.5
RP38 Topsoil	42.3298	-83.0764	6.08	0.61	187	307.6	9.23	0.92	186	201.5
RP38 Topsoil	42.3298	-83.0765	8.23	0.82	156	189.5	7.93	0.79	151	190.4
RP50 Ash	42.3298	-83.0764	8.99	0.90	235	261.5	8.72	0.87	274	314.1
RP53	42.3298	-83.0764	8.39	0.84	228	271.7	7.87	0.79	221	280.9
RP63	42.3298	-83.0765	10.72	1.07	88	82.1	10.67	1.07	90	84.4
RP63 Mortar	42.3298	-83.0765	10.40	1.04	121	116.4	10.46	1.05	105	100.4
RP64	42.3298	-83.0765	11.53	1.15	146	126.7	11.55	1.16	143	123.8
RP73 A	42.3298	-83.0764	9.69	0.97	83	85.6	9.39	0.94	82	87.3
RP73 B	42.3298	-83.0764	10.23	1.02	32	31.3	10.55	1.05	39	37.0
RP73 B Paper	42.3298	-83.0765	9.25	0.93	66	71.3	9.07	0.91	76	83.8
RP87 Ash	42.3298	-83.0764	7.55	0.75	220	291.5	6.81	0.68	176	258.6
RP100	42.3298	-83.0764	9.28	0.93	76	81.9	9.23	0.92	77	83.4
RP106	42.3298	-83.0765	13.18	1.32	7	5.3	13.46	1.35	12	8.9
RP 106/Feature 25	42.3298	-83.0765	11.16	1.12	175	156.8	11.14	1.11	189	169.6
RP107	42.3298	-83.0765	11.58	1.16	12	10.4	11.58	1.16	12	10.4
RP Ash , N	42.3299	-83.0764	11.90	1.19	190	159.6	12.25	1.23	187	152.6

Lot 4, STP 1	42.3299	-83.0764	9.15	0.91	169	184.8	9.02	0.90	176	195.1
RP81	42.32981	-83.0765	11.26	1.12627	23	20.4	11.19	1.12	15	13.4

REFERENCES

Ahmad, S., Iqbal, Y., Ghani, F., 2008. Phase and Microstructure of Brick-Clay Soil and Fired Clay-Bricks From Some Areas in Peshawar Pakistan. Jour. Pakist. Mater. Soc. 2, 33-39 pp.

Asami, K., Kikuchi, M., 2002. Characterization of rust layers on weathering steels air-exposed for a long period. Materials Trans. 43, 2818-2825 pp.

Aydin, A. 2015. "Observing Urban Soil Pollution Using Magnetic Susceptibility." International Journal of Environmental Research. 295 pp.

Barbosa, R., and Overstree., C. 2009. What is soil electrical conductivity? LSU AgCenter Research and Extension.

Bay, J. W., 1938. Glacial history of the streams of southeastern Michigan. Cranbrook Inst. Sci. Bull. 12, 68 pp. (map scale: ~1:200,000).

Berna, F., Matthews, A., and Weiner, S., 2004. Solubilities of bone mineral from archaeological sites: the recrystallization window. Journal of Archaeological Science. Volume 31, Issue 7, 867-882 pp.

Bityukova, L., Scholger, R., and Birke, M. 1998. Magnetic susceptibility as indicator of environmental pollution of soils in Tallinn. Phys. Chem. Earth (A): 829-835 pp.

Brodowski, S., Amelung, W., Haumaier, L., Abetz, C., Zech, W., 2005. Morphological and chemical properties of black carbon in physical soil fractions as revealed by scanning electron microscopy and energy dispersive x-ray spectroscopy. Geoderma 128, 116-129 pp.

Burger, H., Sheehan, A., Jones, C. 2006. Introduction to applied geophysics. W. W. Norton & Company Inc.

Burton, C.M., 1922. The city of Detroit Michigan, 1701-1922 (v. 1). S.J. Clark Pub., Deroit, 854 pp.

Carroll, Z. L., and Oliver, M. A., 2005. Exploring the spatial relations between soil physical properties and apparent electrical conductivity 128, 354-374 pp.

Clark, A. J. Magnetic Susceptibility in Archaeological Pospecting. Bartington Instruments (2005).

Cornelissen, G., Gustafsson, O., Bucheli, T.D, Jonker, M.T.O., Koelmans, A.A., van Noort, P.C.M., 2005. Extensive sorption of organic compounds to carbon black, coal, and kerogen in sediments and soils: Mechanisms and consequences for distribution, bioaccumulation, and biodegradation. Environ. Sci. Tech. 39, 6881-6895 pp.

Corwin, D. L., and Lesch, S. M., 2005. Apparent soil electrical conductivity measurements in agriculture. Computers Electronics Agric. 46, 11-43 pp.

Cultrone, G., Sebastian, E., Elert, K., de la Torre, M. J., Cazalla, O., Rodriguez–Navarro, C., 2004. Influence of mineralogy and firing temperature on the porosity of bricks: Journal of the European Ceramic Society 24, 547–564 pp.

Cultrone, G., Sebastian, E., de la Torre, M.J., 2005. Mineralogical and physical behavior of solid bricks with additives: Construction and Building Materials 19, 39-48 pp.

Doolittle, J.A., Brevik, E.C., 2014. The use of electromagnetic induction techniques in soils studies. Geoderma 223-225, 33-45 pp.

Doolittle, J., Chibirka, J., Muniz, E., and Shaw, R., 2013. Using EMI and P-XRF to characterize the magnetic properties and the concentration of metals in soils formed over different lithologies. Soil Horizons 54, 1-10 pp.

Doxiadis, Ca., 1967. Emergence and growth of an urban region: Developing urban Detroit area. Deteroit Edison Co. 408 pp.

Dubay, B.R., 2012. Urban soil genesis, weathering of waste building materials, and bioavailability of lead in a chronosequence at former demolition sites, Detroit, Michigan. M.S. thesis, Dept. of Geology, Wayne State University, Detroit, MI, 107 pp.

Durza, O 1999. Heavy metals contamination and magnetic susceptibility around metallurgical plant. Phys. Chem. Earth (A).

Elias, V., 2000. Corrosion/degradation of soil reinforcements for mechanically stabilized earth walls and reinforced soil slopes. U.S. Dept. of Transp. Federal Highway Admin. Pub. FHWA-NHI-00-044, 94 pp.

Fassbinder, J. W. E., Stanjek, H., and Vali, H., 1990. Occurrence of magnetic bacteria in soil. Nature 343, 161-163 pp.

Fleming, A. H., Drake, A.A., and McCartan, L., 1994. Geologic map of the Washington West quadrangle, District of Columbia, Montgomery and Prince George's Counties, Maryland, and Arlington and Fairfax Counties, Virginia. USGS Geological quadrangle map GQ-1748, Scale 1:24,000.

Forbes, M.S., Raison, R.J., Skjemstad, J.O., 2006. Formation, transformation and transport of black carbon (charcoal) in terrestrial and aquatic systems. Sci. Total Env. 370, 190-206 pp.

Fine, P., Singer, M. J., La Ven, R., Verosub, K., and Southard, R. J., 1989. Role of pedogenesis in distribution of magnetic susceptibility in two California chronosequences. Geoderma 44, 287-306 pp.

Fisher, G.L., Chang, D.P.Y., Brummer, M.,1976. Fly ash collected from electrostatic precipitators: Microcrystalline structures and the mystery of the spheres. Science 192, 553-555 pp.

Fredericci, C.; Zanotto, E.D.; Ziemath, E.C., 2000. Crystallization mechanism and properties of a blast furnace slag glass. Journal of Non-Crystalline Solids 273, 64–75 pp.

Friedman, S. P., 2005. Soil properties affecting apparent electrical conductivity: a review. Computers Electron. Agric. 46, 45-70 pp.

Gladysheva, M. A., Ivanov, A. V., and Stroganova, M. N., 2007. Detection of technogenically contaminated soil areas based on their magnetic susceptibility. Eurasian Jour. Soil Sci. 40, 215-222 pp.

Grant, W. H., 1969. Abrasion pH, an index of chemical weathering. Clays Clay Min. 17, 151-155 pp.

Gray, R.J., 1991. Some petrographic applications to coal, coke and carbons. Org. Geochem. 17, 535-555 pp.

Huiming Li, Xin Qian, Haitao Wei, Ruibin Zhang, Yang Yang, Zhe Lie, Wei Hu, Hailong Goa, and Yulei Wang. 2014. Magnetic properties as proxies for the evaluation of heavy metal contamination in urban street dusts of Nanjing, southeast China. Geophysical Journal International.

Hyde, C.K., 1980. Detroit: An industrial history guide. Detroit Historical Society, Detroit, MI.

Howard, J.L. 2010, Late Pleistocene glaciolacustrine sedimentation and paleogeography of southeastern Michigan, USA. Sedim. Geol. 223, 126-142 pp.

Howard, J.L., Olszewska. D., 2011. Pedogenesis, geochemical forms of heavy metals, and artifact weathering in an urban soil chronosequence, Detroit, Michigan. Envir. Poll. 159, 754-761 pp.

Howard, J.L., Dubay, B.R., Daniels, W. L., 2013a. Artifact weathering, anthropogenic microparticles, and lead contamination in urban soils at former demolition sites, Detroit, Michigan. Envir. Poll. 179: 1-12 pp.

Howard, J.L., Putnam, S., Moorhead, S., Schooch, R., 2013c (unpub.), Preliminary Quaternary geologic map of the Detroit, Michigan quadrangle. Scale: 1:24,000.

Howard, J.L., Ryzewski, K., Dubay, B.R., Killion, W., 2014. Artifact preservation and post-depositional site-formation processes in an urban setting: a geoarchaeological study of 19th century neightborhood in Detroit, Michigan, USA. Journal of Archaeological Science 53: 178-189 pp.

Howard, J.L., Shuster, W.D. 2014. Experimental order 1 soil survey of vacant urban land, Detroit, Michigan, USA. Catena 126: 220-230 pp.

Hu, X. F., Su, Y., Ye, R., Li, X. Q., and Zhang, G. L., 2007. Magnetic properties of the urban soils in Shanghai and their environmental implications. Catena 70, 428-436 pp.

ICCP (International Committee for Coal and Organic Petrology), 1998. The new vitrinite classification (ICCP System 1994). Fuel 77, 349-358 pp.

Isaaks, E. and Srivastave, M. 1989. An introduction to applied geostatistics. New York: Oxford University Press, Inc.

Kapper, K.L., Anesin, D., Donadini, F., Angelucci, D.E., Cavulli, F., Pedrotti, A., Hirt, A.M., 2014. Linking site formation processes to magnetic properties. Rock and archaeomagnetic analysis of the combustion levels at Riparo Gaban (Italy). Jour. Archaeol. Sci. 41, 836-855 pp.

Karato, S. I., and Wang, D., 2013. Electrical conductivity of minerals and rocks. In: Karato, S. I. (Ed.), Physics and chemistry of the deep Earth, Wiley, New York, pp. 145-182 pp.

Klein, C., and Dutrow, B., 2007. Manual of mineral science (23rd ed.), Wiley, Hoboken, NJ, 675 pp.

Kontny,A., and Dietl, C., 2002. Relationship between contact metamorphism and magnetite formation and destruction in a pluton's aureole, White-Inyo Range, easterm California. Geol. Soc. Am. Bull. 114, 1438-1451 pp.

Kosmatka, S.H., Kerkoff, B., Panerese, W.C., 2002. Design and control of concrete mixtures. 14th ed., Skokie, IL., Portland Cement Assoc., 358 pp.

Kriaa, A., Hajji, M., Jamoussi, F., and Hamzaoui, A. H., 2014. Electrical conductivity of 1:1 and 2:1 clay minerals. Surface Eng. Appl. Electrochem. 50, 84-94 pp.

Lam, Tima. "4817: Life in Michigan's Most Polluted Zip Code." *Detroit Free Press* 22 June 2010.

Lane, D.S., 2004. Petrographic methods of examining hardened concrete: A petrographic manual. U.S. Dept. of Transp. Pub. FHWA-HRT-04-150, 324 pp.

Lanteigne, S., Schindler, M., McDonald, A.M., Skeries, K., Abdu, Y., Mantha, N.M., Murayama, M., Hawthrone, F.C., Hochella, M. F., Jr., 2012. Mineralogy and weathering of smelter-derived spherical particles in soils: Implications for the mobility of Ni and Cu in the surficial environment. Water Air Soil Pollut. 223, 3619-3641 pp.

Larson, J. D., 1977. Soil survey of Wayne County area, Michigan. U.S. Gov. Printing Office, 83 pp.

Livingston, R.A., Stutzman, P.E., Schumann, I., 1998. Quantitative x-ray diffraction analysis of handmolded brick. In: Baer, N. S., Fritz, S., and Livingston, R. A. (Eds.), Conservation of historic brick structures. Donhead Pub. Ltd., Shafesbury, UK., 105-116 pp.

Lu, S.G., Wang, H.Y., Guo, J.L., 2011. Magnetic enhancement of urban roadside soils as a proxy of degree of pollution by traffic-related activities. Environ. Earth Sci. 64, 359-371 pp.

Lund, E. D., Christy, C. D., Drummond, P. E. 1999. Practical applications of soil electrical conductivity mapping. Veris Technologies.

Maher, B. A., and Taylor, R. M., 1988. Formation of ultrafine-grained magnetite in soils. Nature 336, 368-370 pp.

Marshall, A. 1998. Visualizing burnt areas: Patterns of magnetic susceptibility at Guiting Power 1 Round Barros. Arch Prosp. 159-177 pp.

Matthews, A., 1976. Magnetite formation by the reduction of hematite with iron under hydrothermal conditions. Am. Min. 61, 927-932 pp.

McGill, J.T., 1964. Growing importance of urban geology. USGS Circular 487, 4 pp.

Moffatt, I., Wallis, L.A., Hounslow, M.W., Niland, K., Domett, K., Trevorrow, G., 2010. Geophysical prospection for late Holocene burials in coastal environments: Possibilities and problems from a pilot study in south Australia. Geoarchaeology 25, 645-665 pp.

Mozola, A. J., 1969. Geology for land and ground-water development in Wayne County, Michigan. Michigan Geological Survey Report of Investigations, 3, Michigan Departmetn of Natural Resoures, Lansing, Michigan, 25 p.

Mukherjee, S., 2011. Applied mineralogy – applications in industry and environment. Springer, Dordrecht, 575 pp.

Mullins, M. S. Tite and C. 1971. Enhancement of magnetic susceptibility of soils in archaeological sites. Archaeometry. 209-219 pp.

Mullins, C. E., 1977. Magnetic susceptibility of the soil and its significance in soil science – A review. Jour. Soil Sci. 28, 223-246 pp.

Nearing, G. S., Tuller, M., Jones, S. B., Heinse, R., and Meding, M. S., 2013. Electromagnetic induction for mapping textural contrasts of mine tailings deposits. Jour. of Applied Geophy. 89, 11-20 pp.

Oldfield, F., 1991. Environmental magnetism – A personal perspective: Quat. Sci. Rev. 10, 73-85 pp.

Neff, D., Dillman, P., Bellot-Gurlet, L., Beranger, G., 2005. Corrosion of iron archaeological artefacts in soil: characterization of the corrosion system. Corros. Sci. 47, 515-535 pp.

Ntarlagiannis, D., Atekwana, E. A., Hill, E. A., and Gorby, Y., 2007. Microbial nannowires: Is the subsurface "hardwired"? Geophy. Res. Lett. 34, L17305.

Petrakis, L., Grandy, D.W., 1980. Coal analysis, characterization and petrography. Jour. Chem. Ed. 57, 689-694 pp.

Pfeffer, C., Larsen, S., Song, J., Dong, M., Besenbacher, F., Meyer, R. L., Kjeldse, K. U., Schreiber, L., Gorby, Y. A., El-Naggar, M. Y., Leung, K. M., Schramm, A., Risgaard-Petersen, N., and Nielsen, L. P., 2012. Filamentous bacteria transport electrons over centimetre distances. Nature 491, 218-221 pp.

Piatak, N. M., and Seal, R. R., II, 2012. Mineralogy and environmental geochemistry of historic iron slag, Hopewell Furnace National Historic Site, Pennsylvania, USA. Appl. Geochem. 27, 623-643 pp.

Pozdnyakov, Golovko, L., and Anatoly I. 2007. Electrical geophysical methods in agriculture. Progress of Information Technology in Agriculture.

Prinkgle, Jamie, Giubertoni, Matteo, Cassidy, Migetl, Wisniewski, Kristopher, Hansen, James, Linford, Neil, Daniels, Rebecca. 2015. The use of magnetic susceptibility as a forensic search tool. Forensic Science International. 31-42 pp.

Proctor, D.M., Fehling, K.A., Shay, E.C., Wittenborn, J. L., Green, J.J., Avent, C., Bigham, R.D., Connolly, M., Lee, B., Shepker, T.O., Zak, M.A., 2000. Physical and chemical characteristics of blast furnace, basic oxygen furnace, and electric arc furnace steel industry slags. Envir. Sci. Tech. 34, 1576-1582 pp.

Rapp, G., 2009. Archaeomineralogy. Springer, Dordrecht.

Rhoades, J. D., Manteghi, N. A., Shouse, P. J., and Alves, W., J., 1989. Soil electrical conductivity and soil salinity: New formulations and calibrations. Soil Sci. Soc. Am. Jour. 53: 433-439 pp.

Rosenbaum, M.S., McMillan, A.A., Powell, J.H., Cooper, A.H., Culshaw, M.G., Northmore, K.J., 2003, Classification of artificial (man-made) ground: Eng. Geol. 69, 399-409 pp.

Rutherford, D.W., Wershaw, R.L., Cox, L.G., 2005. Changes in composition and porosity occurring during the thermal degradation of wood and wood components. USGS Special Inv. Rept. 2004-5292, 79 pp.

Ryzewski, Krysta, 2015. No home for the "ordinary gamut": A historical archaeology of community displacement and the creation of Detroit, City Beautiful. Journal of Social Archaeology. 1-24 pp.

Ryzewski, Krysta, 2012. Roosevelt park archaeological excavation report. Wayne State University, field report. Unpublished.

Santini, T. L., Fey, M. V., and Smirk, M. N., 2013. Evaluation of soil analytical methods for the characterization of alkaline Technosols: I. Moisture content, pH, and electricalconductivity. Jour. Soils Seds. 13:1141soils.

Schaefer, M. V., 2010. Spectroscopic evidence for interfacial Fe (II)-Fe(III) electron transfer in clay minerals. M.S. Civil Environ. Eng., Univ. of Iowa.

Scherzer, W, H., 1916. Detroit Folio. Geologic atlas of the United States, U. S. Geol. Surv. Folio, 205, 162 pp.

Schmidt, A., Yarnold, R., Hill, M., and Ashmore, M., 2005. Magnetic susceptibility as proxy for heavy metal pollution: a site study. Jour. Geochem. Explor. 85, 109-117 pp.

Sharonova, O. M., Anshits, N.N., Anshits, A. G., 2013. Composition and morphology of narrowly sized ferrospheres isolated from various types of fly ash. Inorg. Mat. 49, 586-594 pp.

Singh, V., Pande, P.C., Jain, D.K., 2010. Text Book of Botany: Structure Development and Reproduction in Angiosperms; Rastogi Publications, 220 pp.

Smith, R.D., Campbell, J.A., Nielson, K.K., 1979. Concentration dependence upon particle size of volatized trace elements in fly ash. Envir. Sci. Tech. 13, 553-558 pp.

Soil Survey Staff, 2014. Keys to Soil Taxonomy (12th ed.). USDA-NRCS, U.S. Govt. Print. Office, Washington, DC.

Stevens, R. E., and Carron, M. K., 1948. Simple field test for distinguishing minerals by abrasion pH. Am. Min. 33, 31-49 pp.

Strzyszcz, Z., Magiera, T., and Rachwal, M., 2006. Application of soil magnetometry for identification of technogenic anomalies in trace metal and iron contents: a case study in the Katowice Forest district: Polish Jour. Environ. Studies 15, 176-184 pp.

Suarez-Ruiz, I., 2012. Organic petrology: An overview. In: Al-Juboury, A. (Ed.), Petrology – New perspectives and applications, Intech Pub., Shanghai, 199-224 pp.

Telford, W.M., Geldart, L.P., Sheriff, R.E., 1990. Applied geophysics (2nd ed.), Cambridge Univ. Press, 283-292 pp.

Van Oss, H.G., 2005. Background facts and issues concerning cement and cement data. U. S. Geological Survey Open File Report 2005-1152, 44 pp.

Waanders, F. B., Vinken, E., Mans, A., and Mulaba-Bafubiandi, A. F., 2003. Iron minerals in coal, weathered coal and coal ash – SEM and Mossbauer results. Hyperfine Interactions 148/149, 21–29 pp.

Ward, C. R., 2002. Analysis and significance of mineral matter in coal seams. Int. Jour. Coal Geol. 50, 135-168 pp.

Ward, C.R., French, D., 2005. Relation between coal and fly ash mineralogy, based on quantitative x-ray diffraction methods. Proc. World of Coal Ash Conf., Lexington, KY, 14 pp.

Weiner, Stephen, 2010. Microarchaeology beyond the visible archaeological record. Cambridge University Press.

Wightman, W.E., Jalinoos, E.F., Sirles, P., Hanna, K.,. 2003. Application of Geophysical Methods to Highway Related Problems. Federal Highway Administration, Central Federal Lands Highway Division, Lakewood, CO, Publication No. FHWA-IF-04-02.

Wilimzig, M., and Bock, E., 1996. Attack of mortar by bacteria and fungi. In: Heitz, E., Flemming, H. C., and Sand, W. (Eds.), Microbially-influenced corrosion of materials. Berlin, Springer-Verlag, 311-323 pp.

Wu, Y., Hubbard, S., Williams, Kenneth., Ajo-Franklin, Jonathan., 2010. On the complex conductivity signatures of calcite precipitation. Journal of Geophysical Research. Volume 115, Issue G2.

Yang, T., Liu, Q., Li, H., Zeng, Q., Chan, L., . 2010a. Anthropogenic magnetic particles and heavy metals in the road dust: Magnetic identification and its implications. Atmos. Envir. 44, 1175-1185 pp.

Yang, Y., Mahler, B.J., Van Metre, P.C., Ligouis, B., Werth, C. J., 2010b. Potential contributions of asphalt and coal tar to black carbon quantification in urban dust, soils, and sediments. Geochim. Cosmo. Acta 74, 6830-6840 pp.

Yildirim, I. Z., Prezzi, M., 2011. Chemical, mineralogical, and morphological properties of steel slag. Adv. Civil Eng. Article 463638, 13 pp.

ABSTRACT

EFFECTS OF ANTHROPOGENIC PARTICLES ON THE CHEMICAL AND GEOPHYSICAL PROPERTIES OF URBAN SOILS, DETROIT, MICHIGAN

by

KATHARINE ORLICKI

December 2015

Advisor: Dr. Jeffery L. Howard

Major: Geology

Degree: Master of Science

There is a great need in many cities for a better quality of urban soil maps. This is due to the increasing interest in repurposing vacant land for urban redevelopment, agriculture, and green infrastructure. Mapping vacant urban land in Detroit can be very difficult because anthropogenic soils were often highly variable and frequently contained demolition debris (such as brick), making it difficult to use a hand auger. This study was undertaken in Detroit, MI to create a more efficient way to map urban soils based on their geophysical and chemical properties. This will make the mapping process faster, less labor intensive, and therefore more cost effective.

Optical and chemical criteria for the identification and classification of microartifacts (MAs) were made from a set of reference artifacts of a known origin. These MAs were then observed and tested in urban topsoil samples from sites in Detroit, Michigan that represent three different land use types (residential demolition, fly ash-impacted, and industrial). Optical analyses, SEM, EDAX, and XRD showed that reference MAs may be classified into five basic compositional types (carbonaceous, calcareous, siliceous, ferruginous and miscellaneous).

Reference MAs were generally distinguishable using optical microscopy by color, luster, fracture and microtexture. MAs that were more difficult to classify were further differentiable when using SEM, EDAX, and XRD.

MAs were found in all of the anthropogenic soils studied, but were highly variable. All three study sites had concentrations coal-related wastes were the most common types of MAs observed and often included coal, ash (microspheres, microagglomerate), cinders, and burnt shale. MAs derived from waste building materials such as brick, mortar, and glass, were typically found on residential demolition sites. Manufacturing waste MAs, which included iron-making slag and coked coal were commonly observed on industrial sites. Fly ash-impacted sites were composed of only microspheres and microagglomerate that were concentrated within the soils by airborne deposition, making it widespread. These results support the hypothesis that MA assemblages of distinct composition vary with land use. Therefore, it seems likely that magnetic susceptibility surveying and other geophysical methods will prove effective for mapping anthropogenic soils on vacant urban land.

Anthropogenic soils and MAs were assessed for pH, electrical conductivity (EC), and magnetic susceptibility (MS). The A horizons of urban soils at residential demolition, industrial-impacted, and fly ash-impacted sites were found to be distinguishable from those of native soils. Anthropogenic soils were higher by one pH unit or more than the background level, had an EC value two to three times the background level, and had MS measurements up to 20 times greater than the background level. The analysis of reference artifacts suggested that the elevated pH of anthropogenic soils was caused by calcareous building material wastes, the elevated EC were the result of both calcareous and ferruginous wastes, and elevated MS were attributable to ferromagnetic materials. Anthropogenic soils collected at residential demolition sites were

differentiable by EC, whereas those at collected form industrial sites were distinguishable using MS. Therefore, anthropogenic soils and native soils have a unique chemical and geophysical signature which can be highly dependent on the concentration of MAs. This suggests that EC and MS surveying methods may be used to remotely sense and map urban soils more effectively than using traditional methods alone.

AUTOBIOGRAPHICAL STATEMENT

I was born and raised in Grosse Pointe, Michigan along with my younger sister Hannah Orlicki. I graduated from Grosse Pointe South High School in 2008 and began my undergraduate degree at Wayne State University that fall. I was undecided about my academic interests throughout my first year of undergrad. Gradually my curiosity for science and active hands on learning lead me to geology. I earned a Bachelor's of Science in Geology in the fall of 2012 and started my graduate studies in the fall of 2013.

Throughout my graduate studies I have been able to work on a number of different projects that were outside of my research, my favorite one being an archaeology excavation in Roosevelt Park. During this project I was able to use my background in geology in a whole new way than I did in my undergraduate years. I very much enjoyed learning the history of a local area and comparing that to soil and artifact findings.

My graduate years also provided me with more knowledge and work experience in the lab and field. Outside of my research studies I had the opportunity to work with Akrulogic Inc. as a Field Operator in Dearborn, MI where air samples were being taken. I'm excited to see what new doors open for me after achieving my degree.